

STRUCTURAL AND FUNCTIONAL STUDIES OF
CYTOCHROME bc_1 COMPLEX FROM
RHODOBACTER SPHAEROIDES

By

HUA TIAN

Bachelor of Science

Nankai University

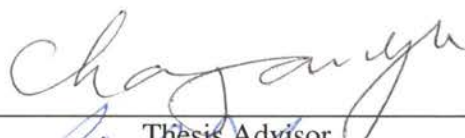
Tianjin, P.R.China

1993

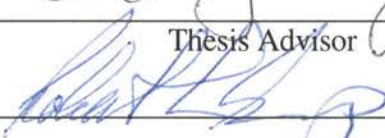
Submitted to the Faculty of the
Graduate College of the
Oklahoma State University
in partial fulfillment of
the requirements for
the Degree of
DOCTOR OF PHILOSOPHY
December, 1999

STRUCTURAL AND FUNCTIONAL STUDIES OF
CYTOCHROME bc_1 COMPLEX FROM
RHODOBACTER SPHAEROIDES

Thesis Approved:



Thesis Advisor











Dean of the Graduate College

ACKNOWLEDGEMENTS

I wish to express my sincere gratitude to Dr. Chang-An Yu for his guidance, support and encouragement throughout my graduate program. My sincere appreciation extends to my graduate committee members: Dr. Linda Yu, Dr. Richard Essenberg, Dr. Olin Spivey, and Dr. Robert Burnap, for their suggestions and assistance.

I would also like to thank Dr. Anatoly Kachurin for his suggestions and assistance, Drs. Dayan He, Li Zhang and Di Xia and Fu-Ming Chen for their help in this study.

Finally I am deeply grateful to my parents, Guangxin and Daijia for their inspiration and encouragement, and my husband, Xudong Yang, for his support and patience,

TABLE OF CONTENTS

Chapter	Page
I. INTRODUCTION.....	1
General introduction.....	2
The catalytic mechanism of the cytochrome bc_1 complex: protonmotive Q-cycle.....	8
Structural analysis of the cytochrome of bc_1 complex by X-ray.....	14
Functional indication from the structural analysis of cytochrome bc_1 complex.....	38
Other catalytic function of bc_1 complex.....	44
References.....	50
II. THE INVOLVEMENT OF SERINE 175 AND ALANINE 185 of CYTOCHROME b OF <i>RHODOBACTER SPHAEROIDES</i> CYTOCHROME bc_1 COMPLEX IN INTERACTION WITH IRON-SULFUR PROTEIN	
Abstract.....	58
Introduction.....	59
Experimental procedures.....	61
Results and discussion.....	65
References.....	84
III. FLEXIBILITY OF THE NECK REGION OF RIESKE IRON-SULFUR PROTEIN IS FUNCTIONAL IMPORTANT IN THE CYTOCHROME bc_1 COMPLEX	
Abstract.....	88
Introduction.....	89
Experimental procedures.....	94
Results and discussion.....	98
References.....	112
IV. EVIDENCE FOR THE HEAD DOMAIN MOVEMENT OF RIESKE IRON- SULFUR PROTEIN IN ELECTRON TRANSFER REACTION OF THE CYTOCHROME bc_1 COMPLEX	
Abstract.....	116
Introduction.....	117
Experimental procedures.....	120
Results and discussion.....	124
References.....	140
V. DISCUSSION	

General discussion.....	142
The paradox about the interaction of the head domain of ISP with Q _o site of cytochrome <i>b</i> and its position relative to <i>b</i> and <i>c</i> ₁ subunits.....	146
The paradox about stigmatellin induced redox potential increase of ISP.....	151
The paradox about the chemsity of quinol oxidation at the Q _o pocket.....	154
Conclusion.....	158

LIST OF TABLES

	page
CHAPTER II	
I. Characterization of the S155C, S175C, and A185C cytochrome <i>b</i> mutations.....	66
II. The effect of NEM on the cytochrome <i>bc</i> ₁ complexes from complement, S175C, and A185C cells.....	73
CHAPTER III	
I. Characterization of ISP neck mutant.....	101
CHAPTER IV	
I. Characterization of ISP neck cysteines (s) mutants.....	126
II. The effect of β -ME, NEM and PCMB on the cytochrome <i>bc</i> ₁ complex in chromatophore and ICM membrane.....	130

LIST OF FIGURES

CHAPTER I	Page
1. The sites of electron transfer that form NADH and FADH ₂ in glycolysis and the citric acid cycle.....	3
2. Schematic representation of electron transfer chains.....	5
3. The protonmotive Q cycle mechanism	9
4. 'Scheme of squares' presentation of ubiquinone intermediates.....	13
5. Structural overview of the cytochrome <i>bc</i> ₁ complex from bovine heart mitochondria.....	16
6. Ribbon diagram of cytochrome <i>b</i> subunit.....	18
7. Structure of selected inhibitors of <i>bc</i> ₁ complex.....	21
8. Q _i site of cytochrome <i>b</i> subunit.....	23
9. Q _o site of cytochrome <i>b</i> subunit.....	25
10. Comparison of structures of cytochrome <i>c</i> and <i>c</i> ₁	29
11. Ribbon diagram of the ISP head domain (ISF).....	31
12. Structure of the "Rieske" [2Fe-2S] cluster.....	34
13. Effects of inhibitor binding on the anomalous, electron electron density peak of the [2Fe-2S] cluster.....	36
14. Cytochrome <i>bc</i> ₁ complex exists as a dimer and function as a dimer.....	39
15. Different positions of ISP head domains in different crystal forms.....	41
 CHAPTER II	
1. Reaction scheme for treatment of sealed and detergent-disrupted (opened) chromatophores with NEM for topological mapping.....	70
2. Radioactivity distribution among subunits of the cytochrome <i>bc</i> ₁ complexes from complement, S175C, and A185C treated with [³ H]-NEM.....	72

3.	The EPR spectra of <i>b</i> cytochromes in purified <i>bc</i> ₁ complexes of complement and cytochrome <i>b</i> A185C mutant with and without NEM treatment	75
4.	The EPR spectra of the Rieske [2Fe-2S] cluster in the cytochrome <i>bc</i> ₁ complexes of complement and cytochrome <i>b</i> A185C mutant with and without NEM treatment.....	77
5.	Gel pattern of pH sucrose gradient fractions of the alkaline-treated cytochrome <i>bc</i> ₁ complex.....	80
6.	[³ H]NEM distribution among subunits of the iron-sulfur protein (ISP)-depleted <i>bc</i> ₁ subcomplexes.....	81
7.	³ H radioactivity distribution in an HPLC chromatogram of Arg-C-digested, [³ H]NEM-labeled cytochrome <i>c</i> ₁ protein.....	82

CHAPTER III

1.	Sequence alignment of amino-terminal portions of Rieske iron-sulfur proteins from different species.....	92
2.	Local environment of ISP neck region.....	93
3.	Western blot analysis of chromatophore membranes from mutant and wild-type complement strains.....	103
4.	EPR spectra of the [2Fe-2S] cluster of Rieske iron-sulfur protein in chromatophore membranes from the complement, Δ ADV, and ALA-PLP and in ICM from the complement and ADV-PPP.....	106
5.	SDS-polyacrylamide gel electrophoresis of purified His ₆ -tagged <i>bc</i> ₁ complexes.....	107
6.	Arrhenius plots of the cytochrome <i>bc</i> ₁ complex of the ALA-PLP mutant and complement chromatophore membranes.....	110

CHAPTER IV

1.	Western blot analysis of the cytochrome <i>bc</i> ₁ complexes in mutant and chromatophore membranes.....	127
2.	EPR spectra of the [2Fe-2S] cluster of the Rieske iron sulfur protein in mutant and complement membranes.....	128
3.	The effect of dodecylmaltoside concentration on the activity and the solubilization efficiency of <i>bc</i> ₁ complex from membranes of the double cysteine-substituted mutants and the complement cells.....	135
4.	SDS-PAGE of purified His ₆ -tagged <i>bc</i> ₁ complexes.....	137

CHAPTER V

1. The architecture of ef loop of cytochrome *b*: staging area of ISP and cytochrome *c*₁..... 144

NOMENCLATURE

[2Fe-2S] cluster	iron-sulfur cluster of Rieske iron-sulfur protein
b_L	low potential cytochrome <i>b</i>
b_H	high potential cytochrome <i>b</i>
β -ME	β -mercaptoethanol
DTT	dithiothreitol
DM	dodecylmaltoside
<i>E. coli</i>	Escherichia coli
E_{m7}	redox midpoint potential at pH 7.0
EPR	electron paramagnetic resonance
HPLC	high pressure liquid chromatography
ICM	intra-cytoplasmic membrane (s)
ISP	Rieske iron-sulfur protein
ISF	water soluble domain of iron-sulfur protein
kb	kilobase pair
MOA-stilbene	(<i>E</i>)- β -methoxyacrylate stilbene
NEM	<i>N</i> -ethylmaleimide
NTA	nitrilotriacetic acid
PCMB	<i>p</i> -chloromercuribenzoic acid
PAGE	polyacrylamide gel electrophoresis
Q	ubiquinone
QH ₂	ubiquinol
Q _o	ubiquinol oxidation site

Q_i	ubiquinone reduction site
Q_2H_2	2,3-dimethoxy-5-methyl-6-geranyl-1,4-benzoquinol
$Q_oC_{10}BrH_2$	2,3-dimethoxy-5-methyl-6-(10-bromodecyl)-1,4-benzoquinol
UHDBT	5-n-undecyl-6-hydroxy-4,7-dioxobenzothiazole

CHAPTER I

INTRODUCTION

I. General introduction

II. The catalytic mechanism of the bc_1 complex: protonmotive Q-cycle

III. Structural analysis of the cytochrome of bc_1 complex by X-ray diffraction

A. Structure overview

B. Cytochrome b subunit

1. Heme and heme ligands
2. Inhibitor and inhibitor binding sites
3. Conformational changes induced by inhibitors binding

C. Cytochrome c_1 subunit

D. Iron-sulfur Protein

1. The pH dependence of the redox potential of ISP
2. ISP subunit in bovine tetragonal cytochrome bc_1 crystal
3. Conformational changes in ISP induced by Q_o inhibitor binding
4. The docking interface between ISP head domain and cytochrome b and ISP

IV. Functional indication from the structural analysis of cytochrome bc_1 complex

A. Cytochrome bc_1 complex exists as a functional dimer

B. ISP head domain movement is required for bc_1 catalysis

C. Two transient quinone binding sites may exist during quinol oxidation at Q_o site

V. Other catalytic function of bc_1 complex

A. Generation of superoxide anion at Q_o site

B. Role of supernumerary subunits in the assembled complex

VI. References

I. General introduction

Energy conservation in all organisms occurs principally via the synthesis of ATP from ADP and inorganic phosphate. There are three distinct methods for synthesizing ATP (1): substrate-level phosphorylation, oxidative phosphorylation (respiratory chain) and photosynthetic (or photo) phosphorylation. Each method involves one or more oxidation-reduction reactions, but the way in which these exergonic reactions are coupled to the endergonic condensation of ADP and phosphate is fundamentally different for the substrate-level phosphorylation as compared to the other two processes. Some types of substrate level phosphorylation entail the oxidation of an organic substrate (e.g. pyruvate) by an appropriate endogenous oxidant such as NAD^+ to generate a non-phosphorylated intermediate with a high free energy of hydrolysis (1). This subsequently undergoes a phosphate substitution to yield an energy-rich acyl phosphate (such as acetyl-phosphate) which finally donates a phosphoryl group ($-\text{PO}_3^{2-}$) to ADP to form ATP. Substrate-level phosphorylation is thus a scalar (spatially-directionless) series of reactions in which the chemical group transfer is catalyzed by essentially soluble cytoplasmic enzymes via the sequential stoichiometric formation of covalent intermediates. It most commonly occurs in the early stages of carbohydrate metabolism, and is responsible for only a small fraction of total ATP synthesized by cells carrying out respiration (1). In contrast, oxidative and photosynthetic phosphorylations are membrane-bound vectorial processes, which occur via a series of sequential oxidation-reduction reactions that involve several types of spatially-organized redox carriers (the respiratory chain and photosynthetic electron transfer system). Both processes act to generate a proton (H^+) concentration gradient across the membrane. Discharge of this membrane gradient is enzymatically coupled to the formation of ATP (1).

For aerobic organisms, the ultimate energy source comes from the combustion of food materials, such as sugars, proteins and fat, into a more oxidized form and ultimately into CO_2 and H_2O . The 12 electron pairs removed from oxidation of glucose are not

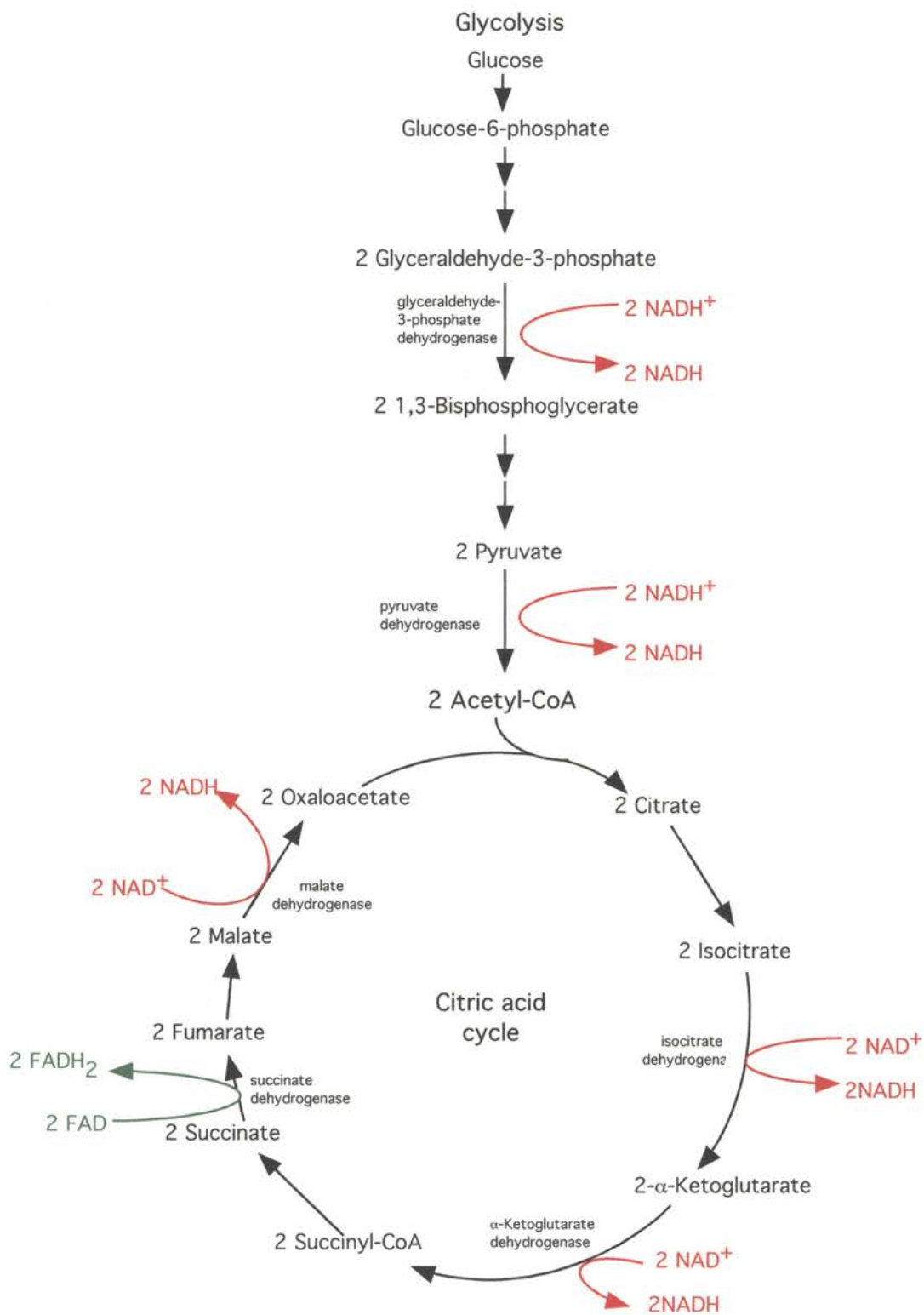


Figure 1. The sites of electron transfer that form NADH and FADH₂ in glycolysis and the citric acid cycle.

directly transferred to O_2 (2). Rather, as shown in figure 1, they are transferred to the coenzymes NAD^+ and FAD to form $10 NADH + 2 FADH_2$. In other words, the free energy from glucose is transformed into NADH and $FADH_2$ molecules. The electrons then pass into the electron-transport chain where, through reoxidation of NADH and $FADH_2$, they participate in a sequential oxidation-reduction of over 10 redox centers before reducing O_2 to H_2O . During these electron transfer processes, protons are expelled from the mitochondrion. The free energy stored in the resulting pH gradient drives the synthesis of ATP. Most of the mitochondria inner membrane electron transport chain accommodates four enzyme complexes (3). Each complex consists of several protein subunits that are associated with a variety of redox active prosthetic groups with successively increasing redox potentials. The arrangement of these complexes and the agents that transfer electron between them are illustrated in figure 2A. Complex I and Complex II function as dehydrogenases that transfer electrons from NADH (-0.315V) and succinate (0.03V) to ubiquinone (+0.10V) (2). Quinone is a universal electron carrier in the biological system (4). It freely diffuses through the membrane because of the hydrophobic nature of the isoprenoid tail. Most respiratory chain dehydrogenases transfer reducing equivalents to ubiquinone (in mitochondria), menaquinone (in fermentative bacteria) or plastoquinone (in plant) (5). Oxidation of quinol by molecular oxygen is then catalyzed by the sequential action of complex III (bc_1 complex) which oxidizes ubiquinol and reduces cytochrome c , and complex IV (cytochrome c oxidase) which oxidizes cytochrome c and reduces oxygen to water. Cytochrome c is a peripheral membrane protein that alternately binds to cytochrome bc_1 complex and cytochrome c oxidase; therefore it functions to shuttle electrons between them (2).

For photosynthetic organisms, ATP is generated by the cyclic or non cyclic electron transfer pathways at the expense of solar energy (2). In contrast to plant and cyanobacteria, which generate their reducing equivalents by light-driven oxidation of

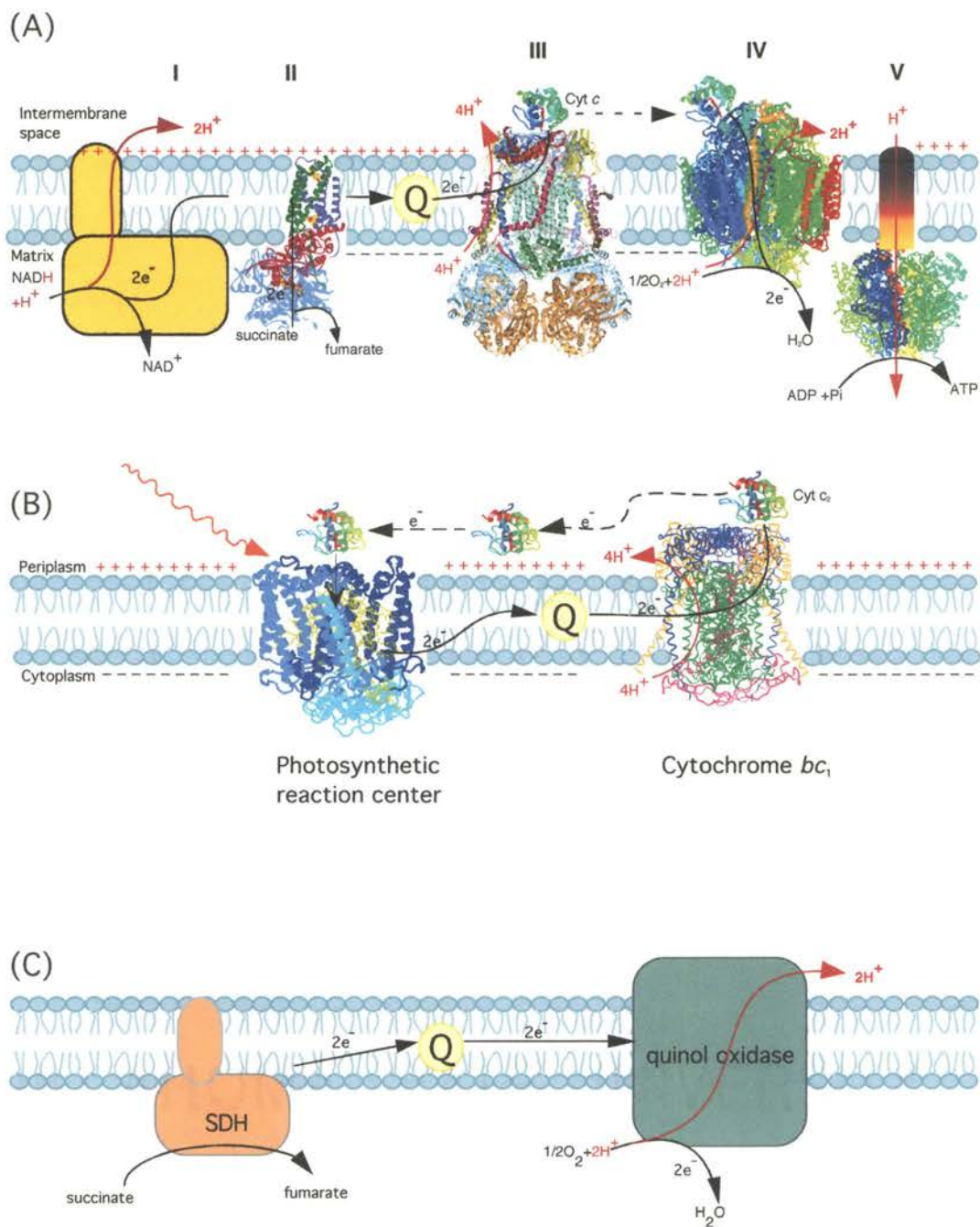


Figure 2. Schematic representation of electron transfer chain. (A) mitochondria respiratory chain; (B) Photosynthetic bacteria cyclic electron transfer pathway; (C) *Rb. sphaeroides* bc_1 -independent respiratory chain.

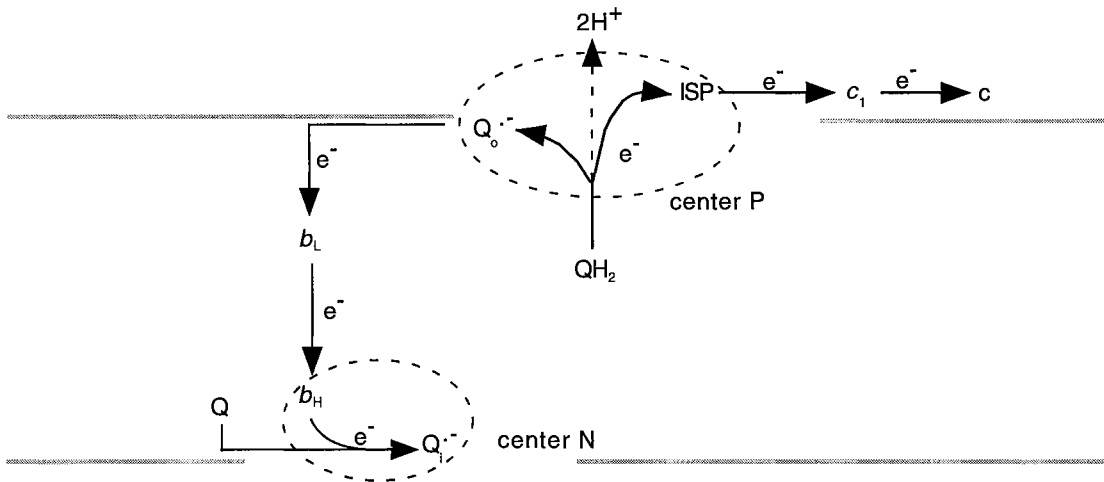
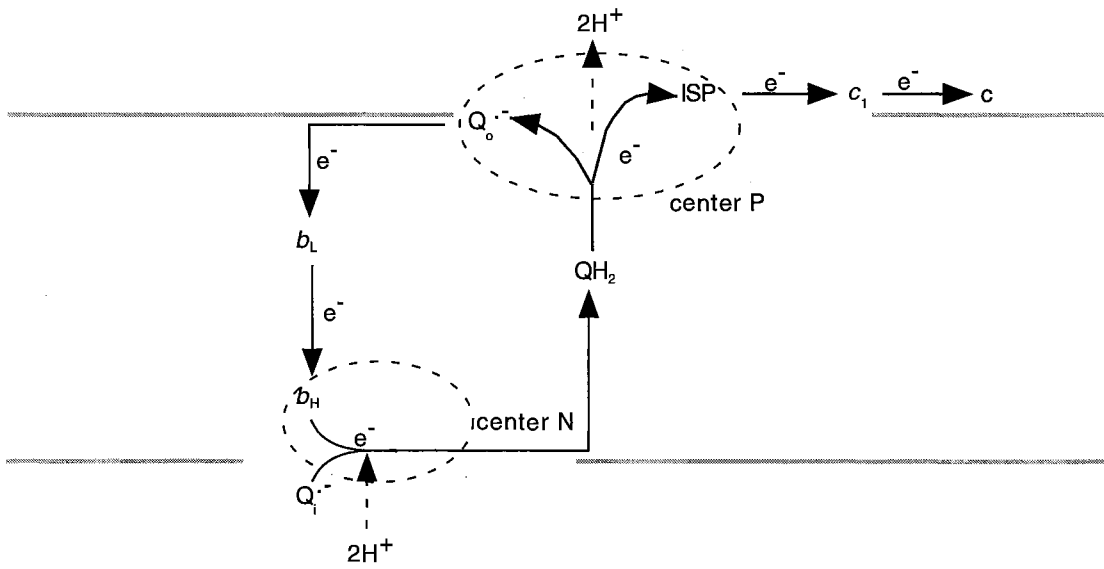
H₂O, photosynthetic bacteria rely on the environment for the reducing equivalents supply, such as H₂S, S, S₂O₃²⁻, H₂, and many organic compounds. *Rhodobacter sphaeroides* is an anoxygenic phototrophic bacterium. The photosynthesis in this type of bacteria depends on the oxygen-deficient conditions, because synthesis of the photosynthetic pigments bacteriochlorophyll is repressed by oxygen. As a consequence, the ecological niches of anoxygenic phototrophic bacteria are anoxic parts of waters and sediments, which receive light of sufficient quantity and quality to allow phototrophic development (6). When *R. sphaeroides* grows photosynthetically, the light energy is captured by the cyclic electron transfer pathway and stored in the proton gradient across the membrane. The dissipation of the pH gradient across the membrane through the ATPase drives the synthesis of ATP, a process known as photophosphorylation. The cyclic electron transfer pathway consists of two enzyme complexes (Figure 2B): photosynthetic reaction center and cytochrome *bc*₁ complex. Bacteriochlorophyll P870 in reaction center consecutively absorbs two photons and liberates two electrons to ubiquinone bound at Q_A site and subsequently transferred to Q at Q_B site. Reduced ubiquinol at Q_B site upon protonation is released from the reaction center and diffuses through the membrane to cytochrome *bc*₁ complex which oxidizes it to ubiquinone with concomitant liberation of its protons to the external medium. The return of the electrons to P870 is accomplished via peripheral membrane protein cytochrome *c*₂ which shuttles electrons between cytochrome *bc*₁ complex and reaction center. The whole process results in no net oxidation-reduction. Rather, it functions to translocate the cytoplasmic protons acquired by ubiquinol across the plasma membrane. The mechanisms of ubiquinol oxidation and proton translocation are essentially identical to those in mitochondrial complex III. Photosynthetic bacteria use photophosphorylation generated ATP to drive their various endergonic processes; thus *bc*₁ complex is an essential enzyme for cell anaerobic photosynthetic growth. However, the laboratory adapted *R. sphaeroides* can also undergo respiratory growth when the environmental oxygen tension is high (6). Repression of the photosynthetic apparatus by

oxygen is accompanied by an increase in content of oxidases and hence in the respiratory capacity, thus allowing these facultative phototrophs to conserve energy via oxidative phosphorylation. Among the multiple respiratory pathways, the quinol oxidase branch is independent of the cytochrome bc_1 complex (Figure 2C), allowing respiratory growth of bc_1 -deficient mutants which are photosynthesis-deficient (Ps^-) (3).

As we have discussed above, cytochrome bc_1 complex is a key component of mitochondrial and bacterial respiratory chains. The bc_1 complex and its homologue, the b_6f complex, also play a central role in photosynthetic electron transfer in phototrophic bacteria, algae and higher plants (3). This family of enzymes catalyzes two-electron transfer from their substrate ubiquinol to a one-electron acceptor cytochrome c (c_2 in bacteria). The reaction is coupled to the translocation of protons across the inner mitochondria or bacteria plasma membrane to generate a transmembrane proton electrochemical gradient. All the bc_1 complexes share a common set of four redox prosthetic groups (3): a high potential Rieske [2Fe-2S] cluster, a c -type cytochrome, a high potential b-type cytochrome (b_H or b_{562}), and a low potential b-type cytochrome (b_L or b_{565}). These groups are housed in three protein subunits: the Rieske Iron Sulfur protein (ISP), the cytochrome c_1 and the diheme cytochrome b . Cytochrome b is a transmembrane protein in which the two heme groups form an electrical circuit across the membrane, with the low-potential b_{565} heme near the positive side of the membrane and the higher-potential b_{562} heme near the negative side of the membrane (7). Cytochrome c_1 and ISP each has a transmembrane anchor. The majority of ISP and cytochrome c_1 subunits including their redox prosthetic groups are located on electropositive surface of the membrane(7). Although mitochondrial bc_1 complex contains up to 8 additional subunits which lack prosthetic groups and are called supernumerary subunits, the role of these supernumerary subunits is believed to be structural rather than catalytic because no significant functional differences have been found from the bacteria enzyme in which only the three redox proteins are present (7).

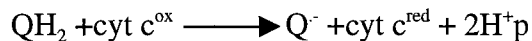
Bacterial bc_1 complexes, in particular those from the facultative phototrophs of *Rhodobacter* species, constitute attractive model systems for studying the catalytic core of the more elaborate mitochondrial complexes. *Rhodobacter sphaeroides* provides several experimental advantages that complement those offered by other organisms, such as yeast or bovine: (i) Structural simplicity. The bc_1 complex from *Rhodobacter sphaeroides* contains only four subunits (cytochrome *b*, cytochrome c_1 , ISP and subunit IV). The three catalytic subunits are homologous to their mitochondrial counterparts. (ii) Readily applicable molecular engineering protocols. In eukaryotic systems, such as yeast, the cytochrome *b* gene is encoded in the mitochondria and is inconvenient for site-directed mutagenesis. In *Rb. sphaeroides*, the three catalytic subunits of bc_1 complex are encoded by genes organized in an *fbcFBC* operon(8). Cytochrome bc_1 complex is readily overexpressed in chromosomal deletion strain BC17 (lacking *fbcFBC* operon) by a plasmid carrying the genes complementing them *in trans*. Such genetic system has been used extensively to study site-directed mutants as well as spontaneous mutants resistant to bc_1 inhibitors, and proven to be extremely valuable (9). In previous years, combined genetic and biochemical approaches have defined the nature of the amino acid residues liganding the prosthetic groups, the location of inhibitor binding domains in cytochrome *b*, and the functional roles of various residues of cytochrome bc_1 complex (10). (iii) biochemical and biophysical methods are still applicable to the mutated bc_1 complex that can not support photosynthetic growth of the cell. The presence of quinol oxidase allows the cell to survive on a cytochrome bc_1 -independent branch of respiratory chains. Therefore, mutants overexpressing defective bc_1 complex are able to grow under semi-aerobic dark growth condition. Intracytoplasmic membrane (ICM) with defective bc_1 complexes is induced under this growth condition and can be readily analyzed by EPR or other biochemical methods to assess the basis of the defect.

II. The catalytic mechanism of the bc_1 complex: protonmotive Q-cycle

Q cycle: Step 1**Q cycle: Step 2**Figure 3. The protonmotive Q cycle .

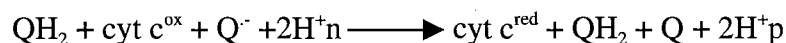
The bc_1 complex transfers electrons from ubiquinol to cytochrome c . The electron transfer from ubiquinol in the bc_1 complex includes a putative difficulty: ubiquinol is a two-electron donor, whereas all prosthetic groups of the bc_1 complex are one-electron carriers. It was first postulated by Wikstrom and Berden (11) that the electron transfer pathway through the bc_1 complex is not a linear chain, but a branched pathway in which the two electrons from ubiquinol diverge upon QH_2 oxidation, one reducing cytochrome b and the other cytochrome c_1 . This idea led to Mitchell's formulation of the Q-cycle mechanism (12).

There are two key features of Q-cycle mechanism: (1) the postulate of two separate quinone (Q) sites in cytochrome b subunits, which are located on opposite sides of the membrane; the ubiquinol oxidation center, called Q_o site or center P, on the positive side of the membrane, the ubiquinone reduction center, Q_i site or center N on the negative side of the membrane. (2) at the Q_o site, two electrons from the ubiquinol (QH_2) are transferred to two different acceptors, one to the [2Fe-2S] cluster ($E_{m,7} = 0.29V$)(13) and the other one to heme b_L ($E_{m,7} = -0.02V$)(14). Q-cycle can be explained as two continuous turnovers, depicted in figure 3. In the first turnover, the substrate ubiquinol molecule comes in and binds to the Q_o site in cytochrome b . The bc_1 complex then oxidizes it by a concerted reaction in which the first electron from ubiquinol is transferred to the [2Fe-2S] cluster of the iron-sulfur protein to form a ubisemiquinone, which immediately reduces the low potential heme b_L . This two-electron oxidation of ubiquinol releases two protons at the positive surface of the membrane, and is catalyzed by a reaction site referred to as center P. The electron that was transferred to the ISP is then transferred to cytochrome c_1 and then to cytochrome c . The second electron from ubiquinol, transferred from ubisemiquinone at center P to low potential heme b_L , recycles through the bc_1 complex from b_L to b_H then reduces a tightly bound ubiquinone at center N to form a stable ubisemiquinone. The result of the first step is displayed in the equation below:

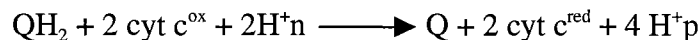


One electron is transferred to cytochrome *c*, two protons are released to the outer, positive side of the membrane and one molecule of ubiquinol is converted to ubisemiquinone at center N.

In the second turnover, a second molecule of ubiquinol is oxidized by transferring one electron to iron-sulfur protein then to cytochrome *c*₁, and the second electron on the resulting Q⁻ again is transferred to heme *b*_L, and then to heme *b*_H. Oxidation of the ubiquinol releases additional two protons at the outer surface of the membrane. However, during the second turn over of the Q cycle, the heme *b*_H reduces the ubisemiquinone, which was formed in the first turn over, to ubiquinol with the uptake of two protons from the negative side of the membrane. The reaction catalyzed by the second step of the Q cycle is:



During one complete Q cycle, two molecules of ubiquinol are oxidized to ubiquinone at center P, but one molecule of ubiquinol is regenerated at center N. The ISP, cytochrome *c*₁ and the two hemes of cytochrome *b* are reduced and reoxidized twice. The high potential *b*_H heme reduces ubiquinone to ubisemiquinone during the first turn over, and reduces the ubisemiquinone to ubiquinol during the second half of the cycle. By summing the two reactions above, one can see that as one molecule of ubiquinol is oxidized to ubiquinone, two molecules of cytochrome *c* are reduced, two protons are consumed on the negative side of the membrane, and four protons are deposited on the positive side of the membrane:



The Q cycle mechanism is supported by many experimental observations:

- a) There are two sets of inhibitors that bind to Q_i and Q_o sites (15). One set of inhibitors, including myxothiazol, UHDBT, and stigmatellin, block the oxidation of

quinol and bind at or near the Q_o site. The other set of inhibitors, including antimycin and HQNO, bind to the Q_i site of the enzyme and block quinone reduction.

- b) A stable ubisemiquinone was detected in isolated mitochondrial bc_1 complex and the EPR signal from this semiquinone was eliminated upon addition of antimycin (16), an inhibitor with higher affinity for Q_i site than ubiquinone or ubisemiquinone.
- c) A pulse of oxygen induces oxidation of cytochrome c and c_1 , which is accompanied by a transient reduction of cytochrome b . Rapid oxidation of the c -type cytochromes and ISP accelerates ubiquinol oxidation, leading to a transient increase in Q^- , the reductant for cytochrome b . Antimycin blocks reoxidation of b_H , enhancing the oxidant-induced reduction (17).
- d) A transient, unstable ubisemiquinone was detected by de Vires and coworkers (18) during oxidant-induced reduction of cytochrome b of mitochondrial cytochrome bc_1 complex, and the EPR signal from this semiquinone was not eliminated by antimycin. However, the existence of this unstable semiquinone species was recently questioned by Rich and coworkers (19) since no Q_o site inhibitor-sensitive semiquinone signal was detected under the same oxidant-induced condition. Wang and Crofts (20) also failed to detect an antimycin sensitive semiquinone signal in bacterial chromatophore membrane.
- e) The ejection of two protons across the membrane per one electron transfer is observed in cytochrome bc_1 complexes from many sources (21).

Although Q cycle hypothesis can explain those experimental observations listed above very well, it does not include important steps for the ubiquinol oxidation reaction:

- a) The bifurcated electron transfer mechanism at center P. The ubiquinol oxidation at center P by two different acceptors is the unique feature of the cytochrome bc_1 complex. The redox potential difference between acceptors [2Fe-2S] ($E_{m,7}=290\text{mV}$) and heme b_L ($E_{m,7}=-20\text{mV}$) is over 300mV. What prevents both of the electrons to flow into the

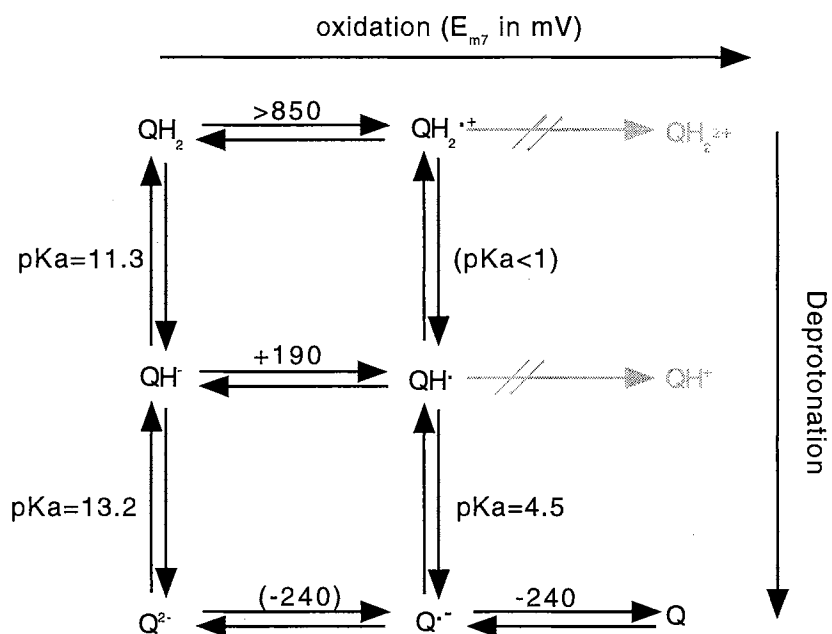
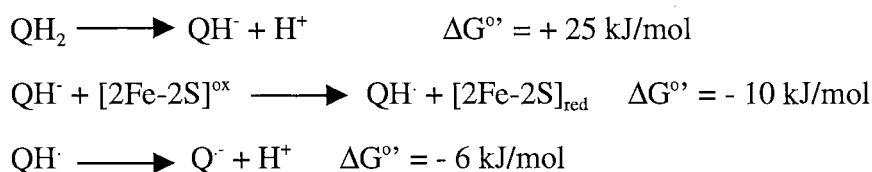


Figure 4. 'Scheme of squares' presentation of ubiquinone intermediates. E_{m7} and pK_a values are based on the physical constants of biological quinone in 80% ethanol. Values in parentheses are calculated to complete the respective 'square'

thermodynamically much more favorable pathway (the [2Fe-2S]) is still under investigation.

b) The actual chemistry taking place at center P. What is the first step for quinol oxidation? The two hydrogen atom redox change of Q/QH₂ must be considered in terms of individual one electron and one-proton transfers, and hence allow many possible routes of redox equilibration. These routes are generally represented as the “scheme of squares” in Figure 4. The possible sequence for quinol oxidation is proposed (22):



It is not possible to assign definitive values to the operative physical constants of the biological quinones because of their amphipathic nature. The standard free energy change were calculated based on the physical properties of ubiquinone in 80% ethanol and could be altered significantly by change of environment and by binding to specific sites on proteins during reaction. Meanwhile, there is no effective way to separate those steps experimentally. There are still many controversial issues remaining to be addressed.

III. Structural analysis of the cytochrome *bc*₁ complex by X-ray diffraction.

As Q cycle gained acceptance, attention focused on elucidating the structure of the cytochrome *bc*₁ complex as it relates to the mechanism. Previous knowledge of the structure of the complex is based on electron microscopy of membrane crystals as well as a number of other approaches. The secondary structure of cytochrome *b* subunit was predicted by empirical algorithms and the topology of the connecting loops was explored by alkaline phosphatase fusion protein technique (23). Chapter II of this dissertation described the use of chemical modifications on the amino acid residues localized at the membrane surface or interior to further confirm the eight-transmembrane helices

model of cytochrome *b*, as well as the existence of a ninth, extramembranous amphipathic helix between helix C and helix D. The location of Q_o and Q_i sites on cytochrome *b* have been defined by spontaneous and site-directed point mutations, which confer resistance to inhibitors that block Q cycle reactions at these sites, and neighboring relationships between the helices have been deduced from intragenic complementations (revertants) (24). The distance of the redox prosthetic groups from the membrane surface was studied by EPR using specific spectroscopic probes (25). The combined genetic and biochemical approaches have also revealed the nature of the amino acid residues liganding the prosthetic groups and attributed specific structural or functional roles to various residues of the bc_1 complex (10).

The first three dimensional structure of bovine cytochrome bc_1 complex was reported by Xia et.al in 1997 (26). Since then additional crystallographic structures for this enzyme have become available from two other groups (27-28). These structural analyses have directly consolidated a huge volume of biochemistry data obtained through rather indirect methods as mentioned above. More importantly, they also added atomic scale precision to our knowledge about bc_1 complex's structural details and raised new issues about its mechanism of function.

III.A. Structural overview:

The bovine $I4_122$ tetragonal crystals of mitochondrial cytochrome bc_1 complex diffracted x-rays to 2.9 Å. An overall view of the cytochrome bc_1 complex from the form viewed parallel to the membrane is presented in figure 5. The structure is pear-shaped with a maximal diameter of 130 Å and a height of 155 Å, similar to the dimensions observed by electron microscopic studies. The bc_1 complex exists as a closely interacting dimer, suggesting that the dimer is a functional unit. Subunit core II and cytochrome *b* contribute major dimer interactions across the two-fold symmetry axis. Subunit 6 interacts with core I and core II of the other monomer.

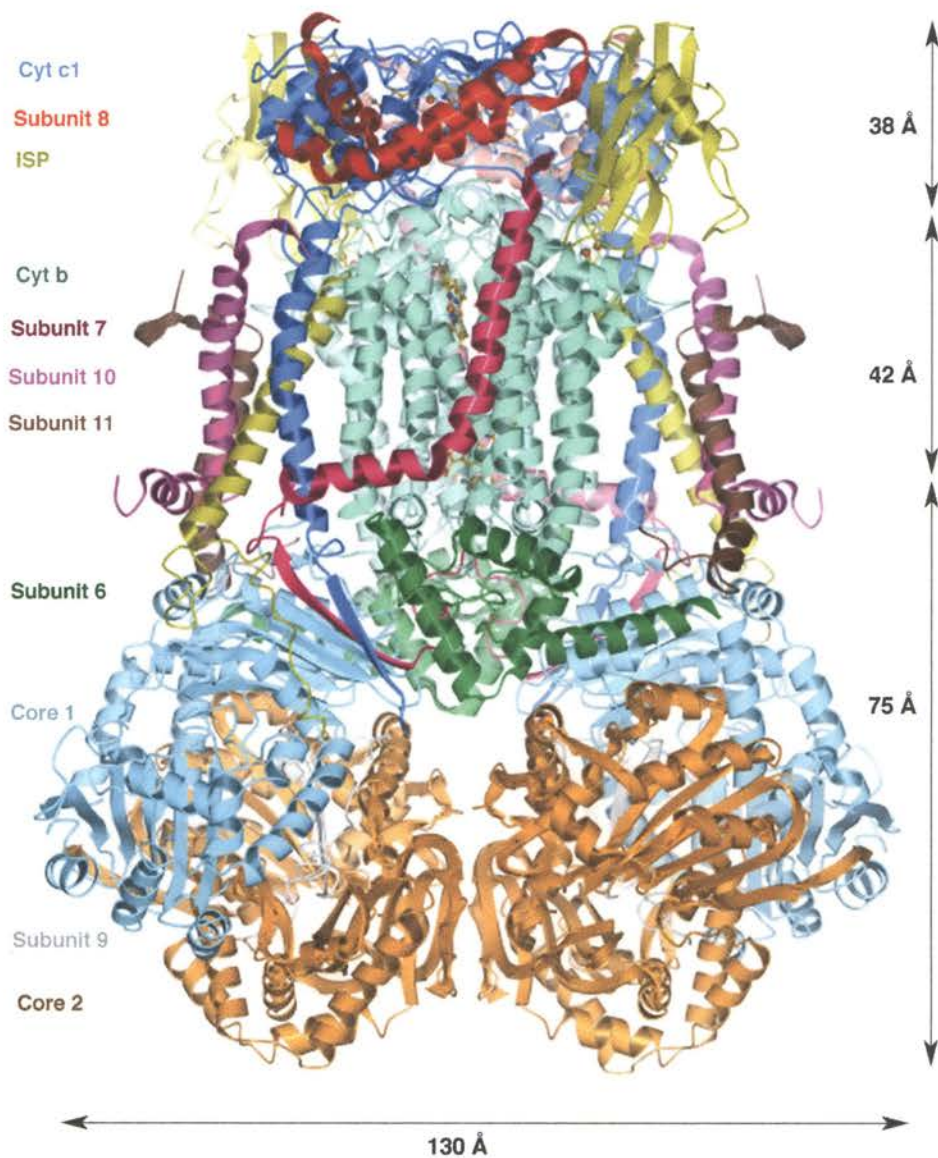


Figure 5. Structure overview of cytochrome bc_1 complex from bovine heart mitochondria. The molecule can be divided into three regions from the top to bottom: the inter-membrane space region, membrane-spanning region and the matrix region. The dimensions for each region of the molecule and the color code for each subunit are indicated.

The cytochrome bc_1 complex can be divided into three regions, the inter-membrane space region, the trans-membrane helix region and the matrix region. The inter-membrane space region comprises the functional domain of cytochrome c_1 , ISP and subunit 8, extending 38 Å into the cytoplasm from the membrane surface. The transmembrane helix region is about 42 Å thick with thirteen transmembrane helices in each monomer. Most part of cytochrome b is located within the membrane. Eight membrane spanning helices belong to this subunit. Subunits 7, 10, 11 each have a transmembrane helix. ISP and cytochrome c_1 each have a transmembrane anchor in their N-terminal and C-terminal respectively. Two symmetry related large cavities are found in the membrane spanning region, which are made of the transmembrane helices D, C, F and H in one monomer and helices D' and E' from the other monomer of cytochrome b , and the transmembrane helices of cytochrome c_1 , ISP, subunit 10 and 11 (Figure 14A). More than half of the molecular mass is located in the matrix region of the molecule, extending from the trans-membrane helix region by 75 Å. This region consists of core 1, core 2, subunit 6, and part of subunit 7 and subunit 9.

IIIB. Cytochrome b subunit:

Both the N and C-termini of cytochrome b subunit are located in the mitochondrial matrix. The eight transmembrane helices of the cytochrome b subunit are approximately where predicted from hydrophathy analysis of the primary sequence (29) and from mutagenesis studies (30). They associate into two groups, with helices A, B, C, D, and E in one group and helices F, G, and H in the other (Figure 6).

IIIB-1 heme and heme ligands:

Heme irons are located by anomalous difference density map. When the X-ray wavelength used in the data collection was shifted to the absorption edge of the iron atoms in the crystals, the anomalous scattering effect increased, although the noise remained unchanged, which indicated that the signals indeed come from the iron atoms in the bc_1 crystal. Two of the peaks are located in the transmembrane region, one near the



Figure 6. Ribbon diagram of cytochrome *b* subunit. The eight transmembrane helices are labeled sequentially, A through H. Loops are labeled according to the two helices they connect. The hemes, shown in red stick models, are bound to helices B and D.

matrix surface and one near the intermembrane space surface. On the basis of biochemical and biophysical data, the two peaks are assigned to the heme irons of b_L and b_H , with b_L being closer to the P side and b_H to the N side. The distance between heme irons is illustrated in figure 14C. The distance of 21 Å (iron to iron) between the two b -type hemes inside the membrane is in good agreement with the prediction of 22 Å derived from the distance between the putative heme ligands in the primary sequence and from the spin relaxation of b_H and b_L in electron paramagnetic resonance studies (25). One interesting observation is that the distance between two b_L heme irons is also 21 Å, which may allow rapid electron transfer between them. The two b -type hemes are bound within the four-helix bundle made by helices A, B, C and D. The axial ligands of both hemes are histidines, as predicted (31): His83 and His182 for b_L and His97 and His196 for b_H . These histidines, located in transmembrane helices B and D, are absolutely invariant in the sequences of b -type cytochromes from more than 900 different species. One of the propionate acids on the heme b_H protoporphyrin IX ring is stabilized by salt-bridging with Arg100. Substitutions of this residue with A and Q affect assembly of bc_1 complex. Similar type of substitution by replacing Arg with Lys results in a lower E_m for b_H . The propionate side chains in heme b_L are also stabilized by either electrostatic interaction or hydrogen bonding. The functional role of the amino acid residues surrounding the heme propionate side chains is still under investigation. The preliminary result indicated that the conserved residues Arg80 and Tyr81 play important roles in stabilizing heme b_L . Mutation of those residues destabilizes the overall enzyme stability and a loss of bc_1 activity was observed during detergent extraction, although enzyme activity in the membrane is close to wild type. The perturbed conformation of heme b_L was evidenced by its modified EPR gz signal detected in the mutant chromatophore membrane(32). Modified EPR signal of heme b_L was also observed in mutants G146V and G146A (33). Glycine 146 is one of the four invariant glycine residues of cytochrome

b. The three-dimensional structure of bovine bc_1 complex reveals the close proximity of Gly146 to heme b_L .

IIIB-2. Inhibitor binding sites:

One of the major observations that lead to the Q cycle hypothesis is that there are two types of inhibitors, namely Q_i and Q_o site inhibitors (15). Q_i site inhibitors, including antimycin, diuron, HQNO and funiculosin, block reduced b_H reoxidation by displacement of a tightly bound ubiquinone at the Q_i site. Q_o site inhibitors, including stigmatellin, UHDBT and MOA-stilbene, block ubiquinol oxidation by ISP and heme b_L .

All Q_i site inhibitors do not share common structure motifs. The most commonly used Q_i site inhibitor is antimycin, which bears no structure similarity to the natural substrate ubiquinone (Figure 7). Antimycin binding results in a spectral red shift of heme b_H (34).

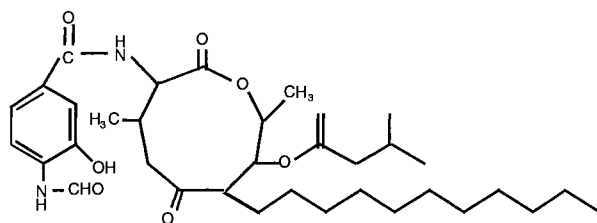
Q_o site inhibitors can be classified further on the basis of common structure motifs (35) (figure 7):

1. 2-Hydroxy-1,4-benzoquinone derivatives. These inhibitors resemble the substrate ubiquinol but contain an additional 2-hydroxy group. UHDBT is representative of this type of inhibitors. Binding of UHDBT induces EPR spectrum change as well as increases ISP redox potential.

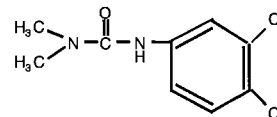
2. Stigmatellins, i.e., chromone derivatives. These components bind to ISP and shift EPR spectrum of reduced [2Fe-2S] cluster. This change is also accompanied by over 200 mV increase in the midpoint potential of ISP. In addition, they also induce a spectral change mostly of heme b_L , indicating the interaction of this type of inhibitors with heme b_L .

3. MOA inhibitors. These inhibitors all contain the E- β -methoxyacrylate group, which resembles part of the ubiquinone structure. The inhibitors have an aromatic side chain attached in the α -position (MOA-stilbene) or in the β -position (myxothiazol). They bind to cytochrome *b*, inducing a red shift of the α and γ bands of heme b_L .

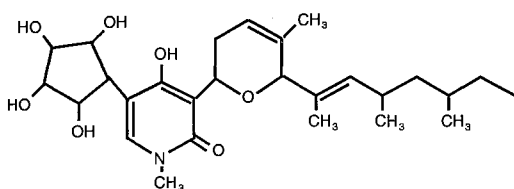
Inhibitors of quinone reduction (Qi site inhibitors)



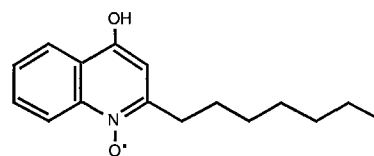
Antimycin A



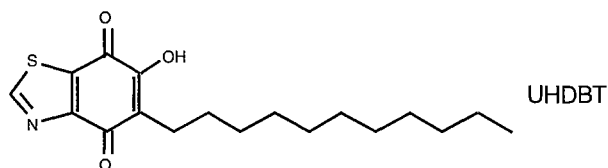
Diuron



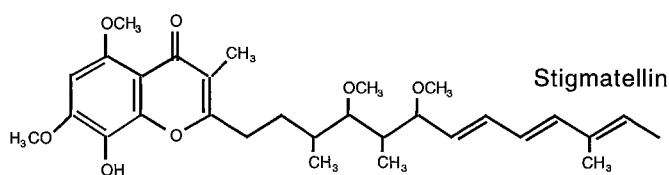
Funiculosin

HQNO
(heptylhydroxyquinoline-N-oxide)

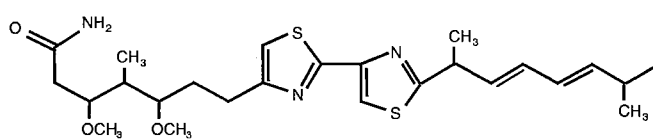
Inhibitors of quinol oxidation (Qo site inhibitors)



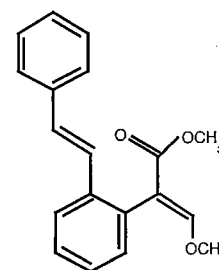
UHDBT



Stigmatellin



Myxothiazol



MOA-stilbene

Figure 7. Structure of selected inhibitors of bc_1 complex.

The two quinone binding sites function independently, i.e., cytochrome *b* is reducible through either the Q_o site or the Q_i site. Therefore, cytochrome *b* can still be reduced by ubiquinol if either a Q_o or Q_i site inhibitor is added even though steady-state electron transfer through the bc_1 complex is blocked. Only simultaneous addition of Q_o and Q_i site inhibitors leads to an inhibition of *b* reduction (double kill). The separation of the Q_o and Q_i reaction sites is also indicated by the fact that the inhibitors have large effects on the spectra of the heme which is close to the respective binding site and only minor spectral effects on the distant heme (35).

The structure analysis of the bc_1 complex co-crystallized with inhibitors allows us, for the first time, to see where in relation to the catalytic sites the residues known to affect catalysis or inhibitor binding are situated. The crystallization behavior of the bc_1 complex mixed with inhibitors was similar to that of the native protein; the crystals were isomorphous with the native ones, and the X-ray diffraction data obtained from these crystals were of comparable quality.

Structural analysis of the Q_i site (figure 8):

A strong positive density for antimycin A near heme b_H shows up in the difference-density maps between inhibitor bound and native crystals. As predicted from spontaneous and site directed inhibitor resistant mutational studies, the Q_i site lies between the N-terminal part of helix A, E and the C-terminal part of helix D, and is capped by amphipathic helix a and the de-loop. Binding of antimycin A resulted in an extended negative electron density in this volume, which represents a ubiquinone molecule bound in the native crystal but displaced by antimycin A. The volume of the Q_i site is larger than needed in order to accommodate either the substrate or antimycin. These two occupants are found in different, but overlapping volumes, with antimycin located deeper in the pocket and closer to heme b_H . The speculative quinone binding model based on the electron density map was recently established, with the benzoquinone ring near the matrix surface and the alkyl side chain extended towards the center of the

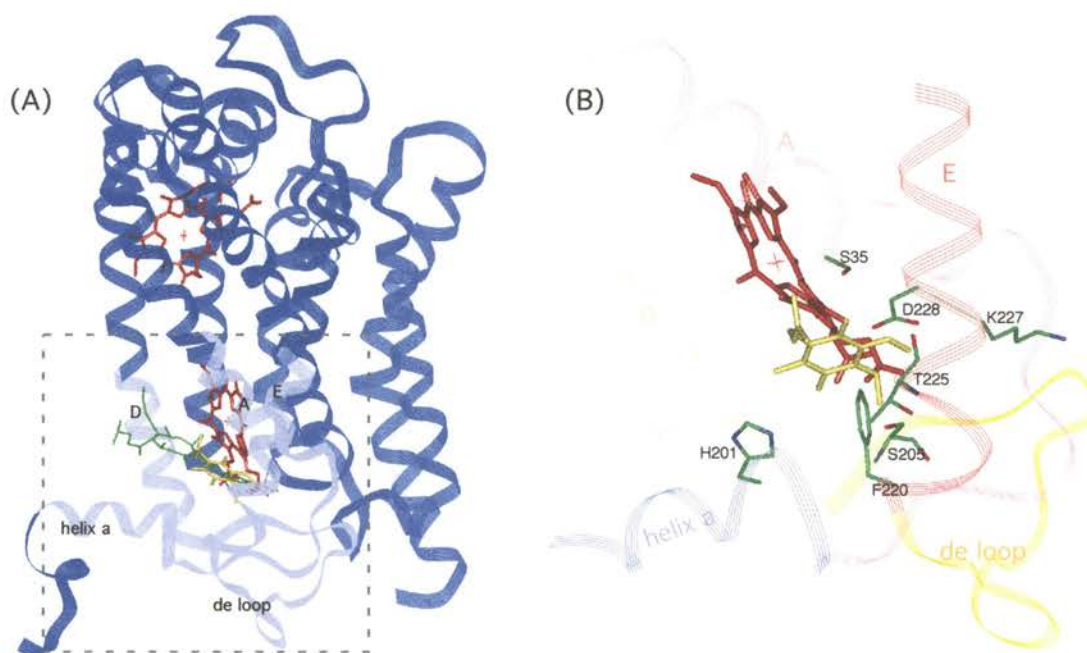


Figure 8. Q_i site of cytochrome *b* subunit. (A) Q_i site is formed by amphipathic helix a, de-loop, helices D and E. Antimycin (green), quinone (yellow) and heme (red) are displayed in stick. (B) The view is zoomed to make details visible.

transmembrane position of the complex (Figure 8). Since the reactions occurring at the Q_i site include the reduction of quinone by heme b_H and uptake of protons from matrix space, the putative proton donors in Q_i pocket are conserved amino acid residues D228 and H201, which are located in close proximity to quinone carbonyl groups of benzoquinone ring. Other less conserved amino acids such as S205, K227 and S35 may also interact with quinone through hydrogen bonding based on their spatial relationship to quinone and mutagenesis studies, although the specific hydrogen bonding information is uncertain at this stage of resolution.

Structural analysis of Q_o site:

All the Q_o site inhibitors occupy different subsites in the Q_o pocket in cytochrome *b*. The Q_o pocket is located toward the surface of intermembrane space and is surrounded by the C-terminal part of helix C, the N-terminal part of helix F and the ef loop. The pocket is sealed from the intermembrane space by the helix cd1. Unlike the Q_i site, this site is not in direct contact with heme b_L ; it is surrounded by aromatic residues that could mediate electron transfer. Binding of Q_o site inhibitors does not generate a negative electron density in the difference maps, indicating that ubiquinone may not be tightly bound in the Q_o pocket in the native crystal. The failure to detect the ubiquinone density in the Q_o pocket may be due to the low affinity of the Q_o site for oxidized quinone.

Although different types of Q_o site inhibitors bind to different domains of a relatively large pocket, their binding sites overlap. This can explain the mutually exclusive occupancy for these inhibitors seen in biochemical studies (36). The binding site of hydroxyquinone types of inhibitors, such as UHDBT, is close to ISP and referred as P1 site. The binding site of MOA type of inhibitors, such as MOA-stilbene and myxothiazol, is close to the heme b_L and referred as P2 site. Stigmatellin overlaps both binding sites (Figure 9A). This finding is in perfect agreement with the aforementioned spectroscopic changes caused by binding of these inhibitors, as well as with the mutagenesis studies (10) on the inhibitor resistant mutants. However the lack of quinol

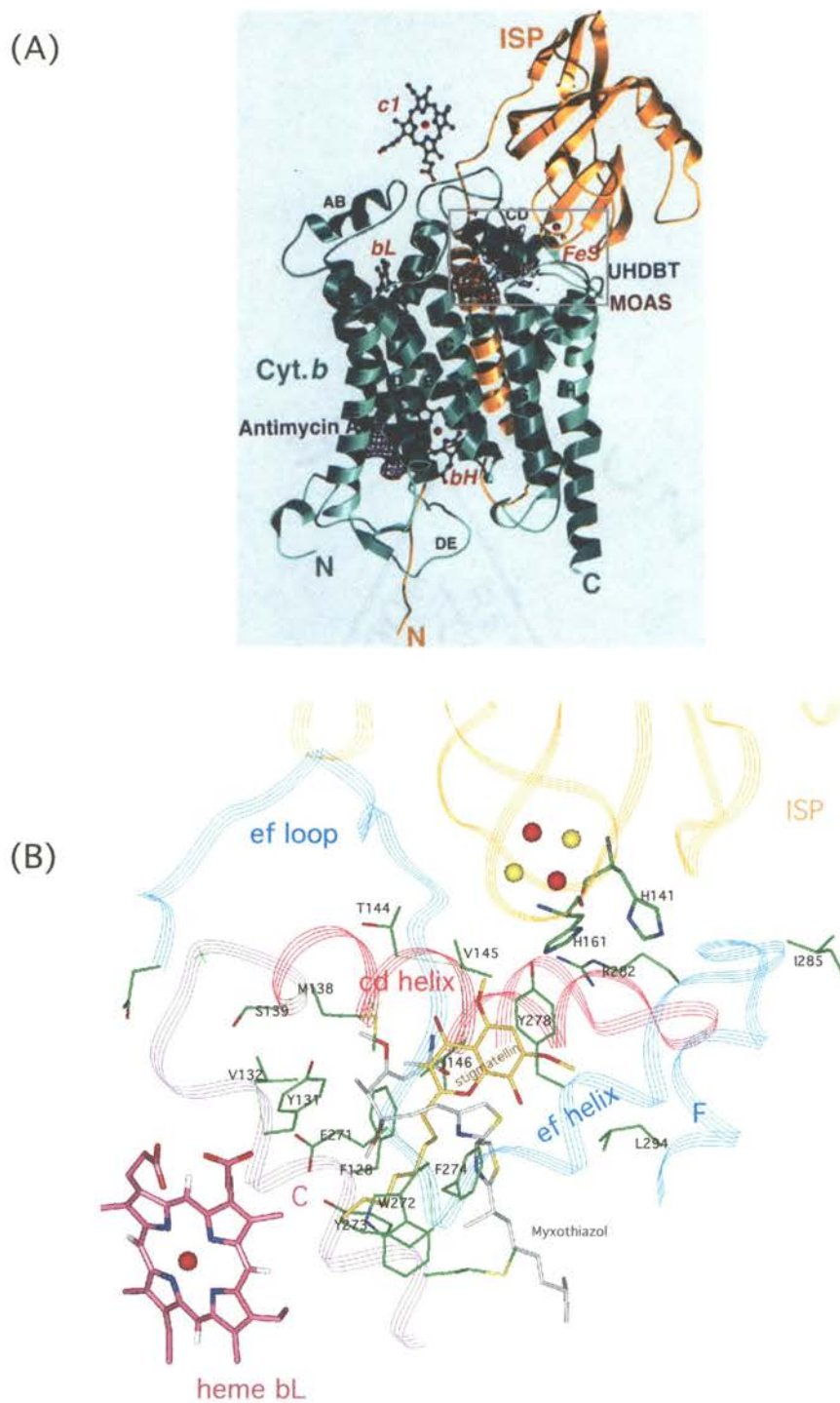


Figure 9. Q_o site of cytochrome *b* subunit. (A) Cytochrome *b*, ISP, hemes and difference densities for MOA stilbene, UHDBT and antimycin A. Q_o site is formed by helices C, F, amphipathic helices cd and ef, and ef loop. (B) The view is zoomed to make details visible.

density in the Q_o pocket posed difficulty in proposing the putative interactions between the substrate ubiquinol and the residues in the pocket. On the other hand, the inhibitor binding studies do provide valuable but indirect information about the electron transfer mechanism at this site. Since the most commonly used inhibitors in mutagenesis studies are stigmatellin and myxothiazol, we set out to investigate the subdomains in Q_o pocket surrounding these inhibitors.

The stigmatellin-binding site:

The stigmatellin-binding domain is part of the larger cavity of the Q_o pocket. The ring of stigmatellin occupies the end of the pocket distal to heme b_L . On the side near the ISP, the cavity opens onto the concave exterior surface, which forms the docking surface for ISP head domain. The inhibitor binds at a distance of ~ 12 Å from the nearest atom of heme b_L . Among the point mutations that lead to stigmatellin resistance, residues M124, F128, I146 and L294 contribute to the surface of the binding pocket for the inhibitor. Modifications are expected to change van der Waals interactions. There are residues such as G136, T147, N255, E271, W272, and V291, which do not impinge on the site, yet are involved in “stigmatellin-resistance”; they may play a more structural role.

Myxothiazol binding site:

Myxothiazol binds in the same cavity as stigmatellin but is displaced approximately 6 Å toward heme b_L and the center of the membrane. Although the edge-to-edge distance between myxothiazol and heme b_L is ~ 6 Å, helix C separate the inhibitor binding pocket from the heme face and from His-183, the ligand to the Fe of heme b_L . There is no contact between MOA-type inhibitors and heme b_L . Residues, at which mutation introduces resistance to both myxothiazol and stigmatellin, include M124, F128, L294, G136, N255, and W272 (10). The first three reside on the common surface for both inhibitors; the others may also have a structural role. Sites, at which mutations modify myxothiazol binding but are not resistant to stigmatellin, have also

been reported (A125, Y131, V132, M138, G142, and F274). They contribute to the surface of the Q_o -site in the proximal end to heme b_L .

There are a group of polar residues; E271, Y273, Y131, and S139, impinging on the surface that forms the end of the Q_o pocket near heme b_L . All mutations reported at these sites have led to lower electron transfer. E271 mutation even leads to stigmatellin resistance. However, there is no direct interaction between the polar side chains and inhibitors, the polar nature may suggest a possible role in proton processing (37).

IIIB-3. Conformational changes induced by binding of inhibitors

Q_i site inhibitor antimycin A binding induces no detectable conformational changes in the bc_1 structure except for subtle local changes near the binding site in order to accommodate antimycin. On the other hand, binding of Q_o site inhibitors has considerable influence on the heights and positions of peaks corresponding to the [2Fe-2S] cluster of ISP subunit in the anomalous difference maps. Details about these changes and the functional indication will be addressed in section IIID-3. Meanwhile, stigmatellin binding also induces noticeable changes in the surrounding area; these involve mainly cd1 and cd2 helix and the ef loop. The main effect is an enlargement of the volume of the site. This expansion involves a substantial displacement of the highly conserved -PEWY- loop in one direction, and of the cd1 helix in the opposite direction, to widen the volume by $\sim 2 \text{ \AA}$. At the opening from the Q_o -site to the ISP interface, Y278 rotates away from the entrance of the pocket and become closer to R281. As a result of this expanded opening of Q_o pocket, interaction between bound stigmatellin and the ligand of ISP [2Fe-2S] cluster H161 is made possible. Although the current level of resolution can not define clearly hydrogen bonding in this area, the close spatial relationship between them (3 \AA edge to edge) have convinced most of the researchers in the field that hydrogen bonding exists between stigmatellin and H161. Structural changes in co-crystals with myxothiazol are also apparent. They indicate a substantial expansion of the binding pocket to accommodate the inhibitor. The movement of the cd1

helix is less pronounced than that seen with stigmatellin. The small changes that are seen at the interface close the aperture between the Q_o -site and the aqueous phase. This closure involves a rotation of I146 within the pocket. Although no density in the Q_o pocket can be clearly assigned to quinone, it seems probable that similar conformational changes will accompany the binding of quinone or quinol at these sites.

IIIC. Cytochrome c_1 subunit:

Cytochrome c_1 is the electron exit point from the bc_1 complex and conducts electrons from a hydrophobic environment to a hydrophilic soluble protein cytochrome c . It is attached to the membrane by a transmembrane helix located at the C-terminal end of the protein. The hydrophilic extramembrane domain including the heme is in the intermembrane space region. Heme is covalently attached to the conserved CxyCH motif in all c -type cytochromes, and the fifth and sixth ligands for heme c_1 are His41 and Met160 (38). One of the heme propionate side chains forms a salt bridge with Arg120 (27). Cytochrome c_1 is an all- α helix-type protein that resembles other members of the type I cytochrome c family, although they bear little sequence homology. Often related proteins that have diverged to the point where little sequence identity remain still have similar folding pattern. The three functional helices, α_1 , α_2 , and α_3 , which form the heme c binding crevice in cytochrome c , also exist in cytochrome c_1 with similar orientation relative to each other and to heme c_1 (figure 10). These three helices, the heme binding fingerprint CxyCH, the residues around M160 ligand, and the conserved heme embracing tripeptide -PDL- can be superimposed onto cytochrome c within rms deviation of 1.0 Å. Like cytochrome c , the pyrrole C corner of heme is also exposed to the solvent at the “front face”, where electron transfer is thought to take place. The exposed C corner is surrounded by three regions of the protein, consisting of residues 36-41 (containing His ligand and cysteines), 104-106 (helix α_1 ”), and 158-163 (containing ligand M160). The difference between c_1 and c are the result of insertion and deletions in the loops, which appear to be connected to the specific functions of cytochrome c_1 , including the binding

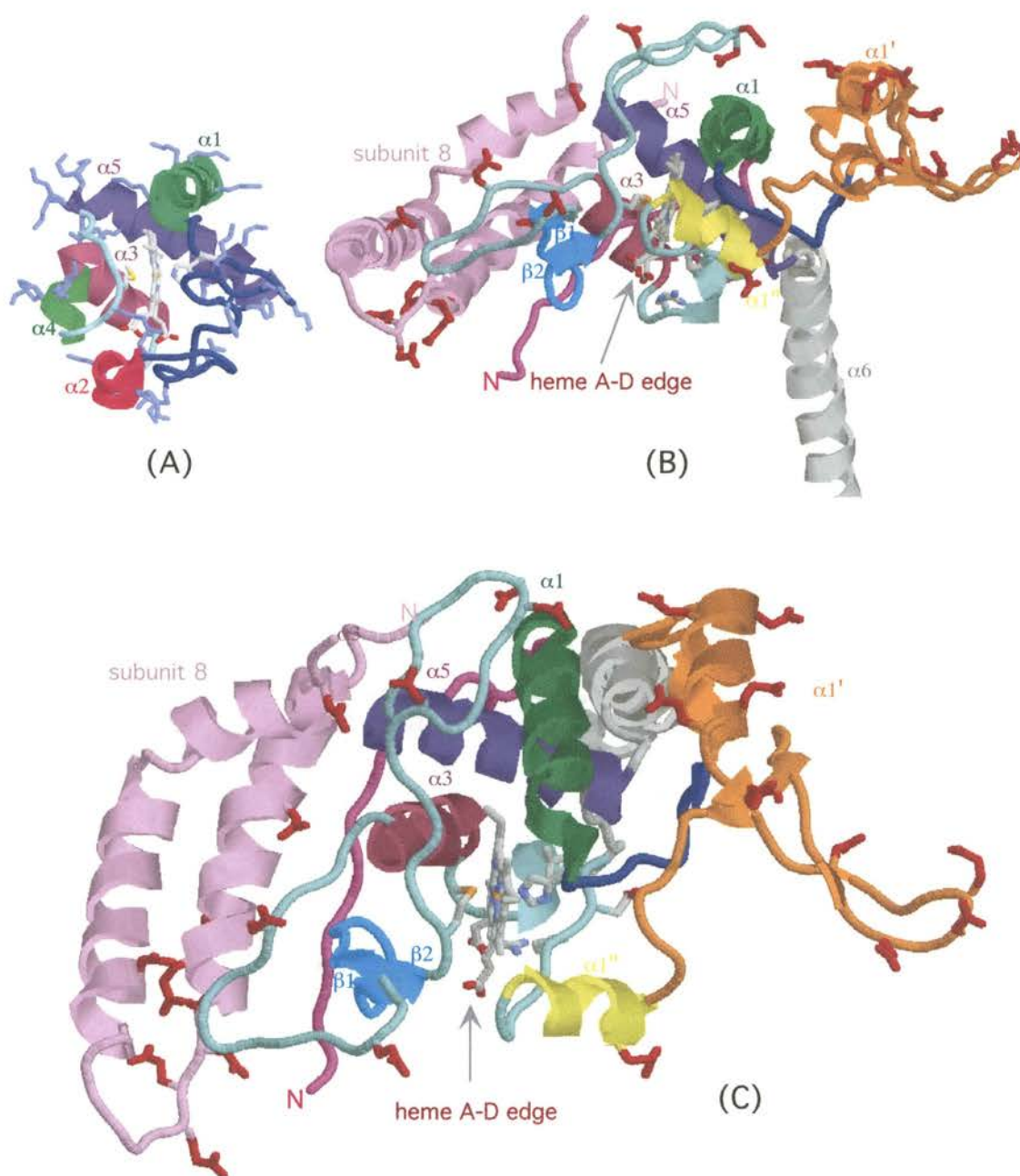


Figure 10. Comparison of structures of cytochrome c and c_1 . (A) The ribbon diagram of mitochondrial cytochrome c with corner C pyrrole of the heme group facing the Viewer, and the heme propionates directed downwards. All the basic residues are highlighted in blue. (B) Structure of cytochrome c_1 and subunit 8, viewed parallel to the membrane. Acidic residues exposed to the intermembrane space are shown in red. Heme ligands, H41 and M160, and conserved heme embracing tripeptide -PDL- are displayed in stick. Helices labelled $\alpha 1, \alpha 3$ and $\alpha 5$ correspond to similarly labelled and colored helices in cytochrome c . (C) Structure of c_1 and subunit 8 viewed from the intermembrane space down the membrane. Heme A-D edge is exposed to the solvent, where electron transfer between ISP and c_1 is thought to occur.

of ISP, subunit 8 and cytochrome *c*. The N-terminal extension of 24 residues interacts with subunit 8, the acid hinge protein implicated in cytochrome *c* binding (39).

Interestingly, the *Paracoccus* cytochrome c_1 has a long acidic insertion in this region, which appears to function as mitochondrial hinge protein in this species (40).

Cytochrome c_1 also has a long branched insertion of 58 residues (50-107) between the heme binding fingerprint and the heme-bracing tripeptide PDL. One branch, residues 48-67, is mainly a bended helix with acidic residues around 70 pointing toward the intermembrane space side. The second branch of this insert, residues 65-87, makes a loop that interacts with cytochrome c_1 $\alpha 1$ ' helix in the other monomer. The third insertion of 18 residues is found between M160 and helix 5 (161-178) including acidic residues 167-170 pointing away from the membrane. Chemical modification and cross-linking studies on cytochrome c_1 had indicated that the acidic residues around 70 and 167 may be involved in cytochrome *c* binding (41). The orientation of the side chains of these amino acids is in good agreement with the prediction. However, the two regions are spatially separated. They are protruding into the intermembrane space region. The loop connecting M160 and $\alpha 5$ is close to N-terminal of hinge protein subunit 8, another cytochrome *c* binding protein. Therefore, those two acidic regions may function together to recruit basic cytochrome *c* from the solvent.

In contrast to cytochrome *c*, the heme A-D edge, where propionate side chains are located, is exposed to the solvent. Iwata et al. (27) pointed out the possible hydrogen bonding between His161 of ISP and one of the propionates of heme c_1 , which is present in the $P6_322$ form of crystal but not in tetragonal bovine crystal.

IIID. Iron-sulfur protein (ISP):

The Rieske iron sulfur subunit is also anchored to the membrane by a transmembrane helix near the N-terminus. The majority of the protein including the [2Fe-2S] cluster is located in the intermembrane space region. The extramembrane water soluble domain of ISP containing residues 68-196 (ISF or ISP head domain) was

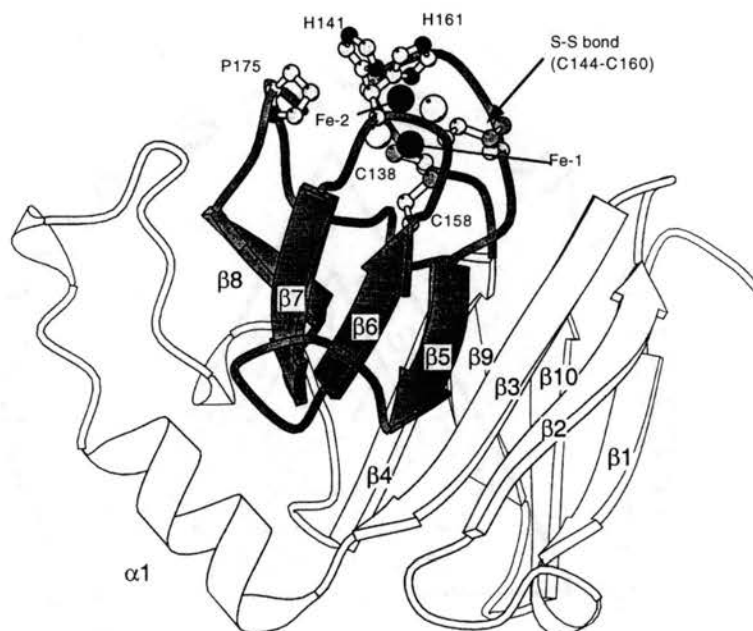


Figure 11. Ribbon diagram of the ISP head domain (ISF).

crystallized independent of the bc_1 core complex and the structure was refined at 1.5 Å (Figure 11). The overall structure is compact and rigid; it contains three layers of antiparallel beta sheets comprising a total of 10 β -strands (42). The overall shape is a flat spherical molecule with metal containing site located at the tip; the NεH groups of the coordinating histidines are accessible and exposed to the solvent within a hydrophobic surface formed by three loops. [2Fe-2S] cluster is hosted between the loop β 4- β 5 and loop β 6- β 7. Each loop contributes one cysteine and one histidine as ligands for [2Fe-2S] cluster. A disulfide bridge between conserved Cys144 and Cys160 (one on each loop) brings the two loops together and stabilizes this region. A third loop covers the cluster from the other side. It contains the totally conserved sequence GPAP. Mutation in this region decreases ISP stability, with no or little ISP being incorporated into the bc_1 complex (43).

IIID-1. The redox potential of ISP is pH dependent:

The redox potential of [2Fe-2S] cluster in ISP subunit is unusually positive (280-320mV), it is much higher than bacterial dioxygenases (E_m values ranging from -155-0mV) even though the type of the cluster and the EPR signals are the same in both cases. There are multiple factors that contribute to the high redox potential of the quinol oxidizing cluster (44): (i) The presence of multiple hydrogen bonds to the bridging and terminal sulfur atoms; (ii) The solvent exposure of the two histidine ligands for Fe (2). Perturbation of the hydrogen bonding network surrounding the cluster was proven to cause the decrease of ISP redox potential. In dioxygenases, the histidine ligands are not exposed to solvent and the NεH groups do not undergo redox-dependent deprotonation up to pH10 (45).

The pH dependency of ISP redox potential ($-\Delta E_m/\Delta pH > 60\text{mV}$) is observed in intact bc_1 complex as well as in the isolated protein ISF (46). This phenomenon can not be explained by a single deprotonation step. Two groups with redox dependent pKa values are involved. From the analysis of the direct electrochemistry of the ISF, the pKa

values are 7.6 and 9.2 on the oxidized protein and >11 on the reduced protein. Analysis of the pH dependence of the visible CD spectra of the oxidized ISF reveals that the protonatable groups are in the vicinity of the [2Fe-2S] cluster (47). Deprotonation leads to an electron-rich environment for [2Fe-2S] cluster, and thus redox potential decreases. This can explain why ISP redox potential decreases as the pH increases. The close spatial relationship between those groups and cluster can also explain why their pKa values are redox state dependent. The pKa values are lowered when the cluster is oxidized as a result of the electron withdrawing effect of the Fe^{III} from the oxidized cluster. Upon reduction, the withdrawing effect from the cluster is weakened; pKa increases to above 11, and one of the groups becomes protonated. The three-dimensional structure of reduced ISF reveals no obvious residues in the vicinity of the cluster which are likely to undergo redox-dependent deprotonation. The conserved Tyr165 is buried in the protein and hydrogen bonded to the S^γ of Cys139; this residue is structurally important but can not undergo deprotonation. FTIR spectroscopy studies excluded deprotonation of aspartate, glutamate or tyrosine (44). These results leads Links et al (46) to relate these two groups to histidine ligands of [2Fe-2S] cluster. Since H161 and H141 are exposed to the solvent in the three dimensional structure, and the histidine N^δ atoms in the imidazole ring serve as ligands for Fe-2 in the cluster, Link then proposed that NεH in the imidazole rings are the deprotonation groups. The imidazole ligands have different orientation with respect to the cluster (Figure 12), their interaction with the iron d orbitals will be different. From the symmetry of the cluster, the electron density to be donated to d orbitals of oxidized cluster will come from the π orbitals of the perpendicular imidazole (His161), but not from the π orbitals of the in-plane imidazole His141. This will decrease the electron density and therefore lower the pKa (pKa=7.6) values of His161 on the oxidised cluster. The effect will be smaller for His141(pKa=9.2). Upon reduction of the cluster, this difference disappears and the pKa of both groups increases to over 11. However, the pKa of NεH in free histidine is above

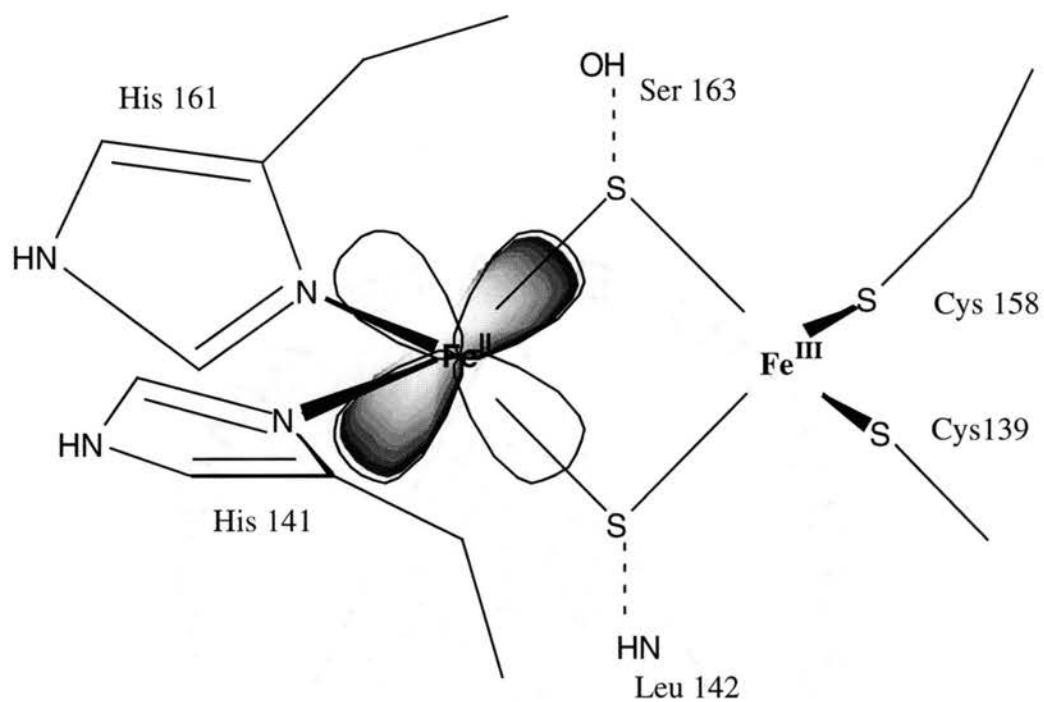


Figure 12. Structure of the "Rieske" [2Fe-2S] cluster.

14. The high pKa value in turn challenges this assignment. The structural analysis of reduced ISF provides no direct evidence to support Link's proposal since the Ne atoms are all in the protonated form. The deprotonated form only exists when the cluster is oxidized under neutral pH. Therefore it will be interesting to look for the electron density change around Ne in the oxidized crystal. So far, this form of crystal is not yet available. Furthermore, the conformational change induced by oxidation of the cluster, if there is any, will imply possible residues involved other than the histidine ligands.

IIID-2 ISP subunit in bovine tetragonal cytochrome bc_1 crystal:

In the crystal structure of native bc_1 complex, only the transmembrane helix region (1-62) is clearly defined; the head domain of ISP (ISF) is represented by weak, uninterpretable electron density indicating that this domain is highly mobile in the crystal. Despite the poor electron density, a strong iron peak corresponding to the cluster irons was obtained from the anomalous difference density maps (Figure 13). It lies near the P-side of the membrane at a position 27 Å to heme b_L and 31 Å to heme c_1 iron. However the peak height of [2Fe-2S] cluster is only half that of b_H heme, which is consistent with the movement hypothesis. It is worth mentioning that the distance between c_1 and ISP is too large to support the fast electron transfer rate observed between these two redox centers.

IIID-3. Conformational change in ISP induced by binding of Q_o inhibitors. There are three types of Q_o inhibitors; all of them bind exclusively to the Q_o pocket in cytochrome b subunit. However, binding of Q_o inhibitors has strong effect on the anomalous light scattering signal from the [2Fe-2S] cluster and this effect is correlated with the binding position of the inhibitors in the Q_o pocket (36). Among the three types of inhibitors, hydroxyquinone type of inhibitor UHDBT (type II) binds closest to ISP. UHDBT binding results in a significant increase of the anomalous signal of the [2Fe-2S] cluster (2.2 fold) and a strong positive density corresponding to the head domain ISP appears on the surface of Q_o pocket of cytochrome b , indicating that the head domain undergoes a

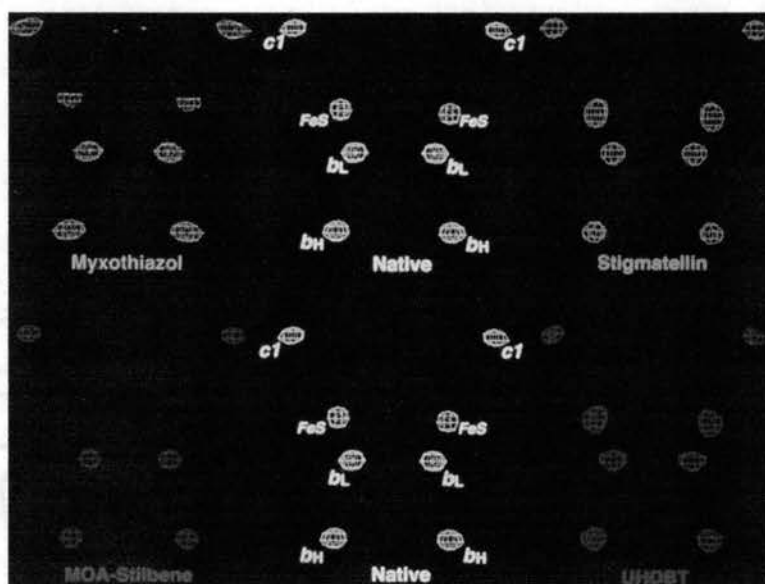


Figure 13. Effects of inhibitor binding on the anomalous, electron density peak of the [2Fe-2S] cluster. Iron peaks from anomalous diffraction experiments with and without bound inhibitors are shown, with MOA-type inhibitors on the left, the native in the middle, and stigmatellin, UHDBT on the right. The iron-peak height of b_H heme for each crystal is normalized to that for the native.

transition to a less mobile or completely immobilized state. Similar effect was observed for stigmatellin (type III), except that the anomalous signal increases even greater (2.5 fold). On the other hand, MOA-stilbene (type I) abolished the iron signal observed in the native crystals. The binding site of MOA-stilbene is deeper in the Q_o pocket and closest to heme b_L as compared with the other two types of inhibitors. The binding of another MOA-type inhibitor myxothiazol also results in a greater mobility of ISP head domain; the iron signal is lowered significantly after its binding (figure 13).

IIID-4. The docking interface between ISP head domain and cytochrome b in stigmatellin or UHDBT bound crystal.

In native bc_1 , the ISP head domain appears to be partitioned between a fixed and a loose state. Only molecules in the fixed state can be observed by crystallography. Binding of UHDBT and stigmatellin strongly increase the population of the fixed ISP state. A strong positive density corresponding to the head domain of ISP shows up above the surface of cytochrome b . The docking interface on cytochrome b is formed by helices of cd1 and cd2, the loop connecting ef helix and helix F, and the stretch 260-265 in ef loop which is located at the highest point from the membrane (Figure 9 and Figure 1 in chapter 5). These spans form a concave, exterior-facing and hydrophobic surface with the opening of the Q_o pocket at the bottom. The tip of ISP head domain where [2Fe-2S] cluster is located fits into this concave surface and may have contact with the occupant in the Q_o pocket, judging from the distance between [Fe-2S] cluster histidine ligands and the opening of the Q_o pocket.

EPR g_x signal of ISP and its role in monitoring docking between ISP and cytochrome b .

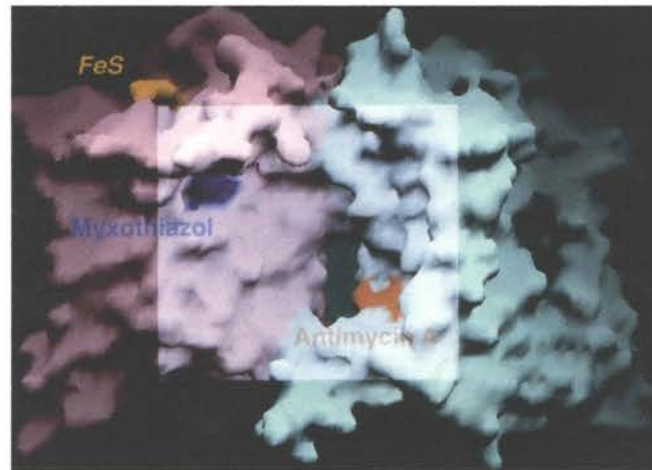
The [2Fe-2S] cluster contains two low spin irons. After reduction, the unpaired electron can be detected by electron paramagnetic resonance. The EPR spectrum shows three characteristic signals with resonances at $g= 2.02$, 1.9 , and 1.80 . The g_x signal at 1.8 is very sensitive to environmental changes. The isolated ISP retains g_y and g_z signals and g_x shifts to 1.765 (26). Inhibitor binding in Q_o pocket, particularly those located

close to the opening to the Q_o pocket such as UHDBT and stigmatellin induces upfield shift in g_x (1.78). Myxothiazol binding shifts g_x to 1.77. Many mutations along the opening of Q_o pocket or along the wall of Q_o pocket give modified g_x signals. The change in g_x signal is not profoundly related to the activity of bc_1 complex. Residue changes at M124, Y131, G136, E271 and F128 in cytochrome b subunit, which lead to loss of activity without loss of $g_x=1.8$ signal, cluster at the deeper end of the pocket, closer to the heme of cytochrome b_L , where myxothiazol binds. Changes at K287, L281, T144, G142, I268 which can be seen to project into the ISP interfacial surface, eliminate the g_x signal (37). In some cases, this is associated with complete loss of activity, but some of these strains show turnover at an uninhibited rate. In general, g_x signal is too sensitive to give a good correlation to the bc_1 activity. It reflects the microenvironment of [2Fe-2S] cluster, and this environment is related to cytochrome b docking interface for ISP and the occupant in Q_o pocket.

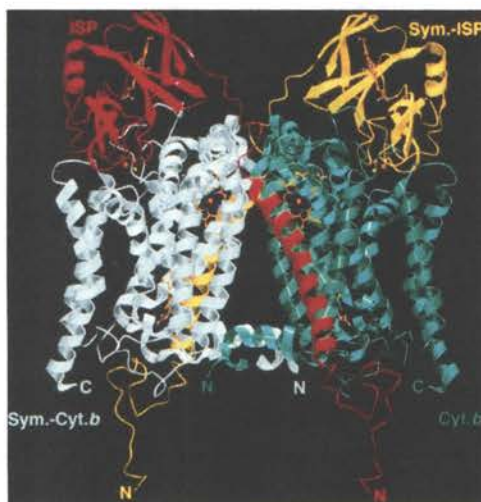
IV. Functional indication from structural analysis of cytochrome bc_1 complex

IVA. Cytochrome bc_1 complex exists as a functional dimer (26).

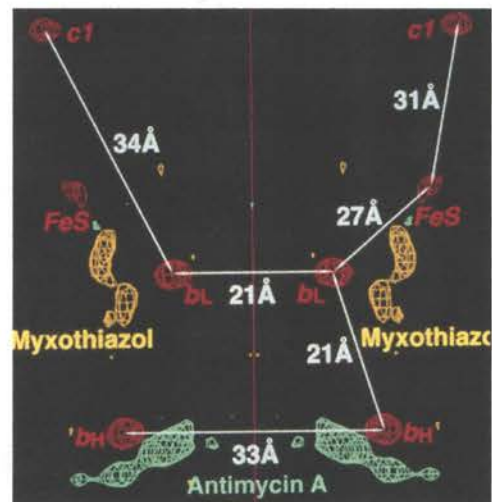
The dimeric association of cytochrome bc_1 complex has been reported extensively through out the literature (48-50). Crystallographic studies of the bc_1 complex not only show extensive physical dimeric association but also suggested that the dimer is the functional unit. The functional dimer hypothesis is supported by the following structural evidences (figure 14): (1) the dimeric cytochrome bc_1 forms two symmetry related cavities in the membrane spanning region. Each cavity connects Q_o site from one monomer to Q_i site of the other. Interestingly the two quinone binding sites from the same monomer do not connect each other. The membrane spanning cavity may help the transfer of quinone between Q_o and Q_i sites located on different monomers. As a result of that, quinone reduced at Q_i site of one monomer can be oxidized at the nearby Q_o site of



(A)



(B)



(C)

Figure 14. Cytochrome bc_1 complex exists as a dimer and function as a dimer. (A) Q binding cavity between *cyt.b* dimer. (B) Cross interaction between *cyt.b* and ISP. (C) Distance between iron centers of heme and [2Fe-2S] cluster.

the other monomer without leaving the bc_1 complex. This is consistent with the activity data showing that one mole of ubiquinone per mole of c_1 is sufficient for a maximal activity of electron transfer in the isolated succinate cytochrome c reductase (51). (2) the head domain of ISP of one monomer crosses over the two fold symmetry line and travels between the catalytic interface on cytochrome b and c_1 in the monomer. The N-terminal tail anchor is locked in a vice provided by both cytochrome b subunits and is also constrained by contacts with the transmembrane helices of cyt c_1 and subunit VII and X, and with subunit I in the matrix phase of the same monomer. (3) the iron to iron distance between two b_L hemes is only 21 Å, which is the same as the distance between b_L and b_H within a monomer. The distance between the edges of two heme b_L is even shorter than that between b_L and b_H . Therefore electron transfer between two heme b_L is possible, especially when the membrane is highly energized.

The specific role of membrane spanning cavities is still unclear. Access from the cavity to the lipid phase is far wider than the channel into either site. In bacteria system, which contains only 10 transmembrane helices in one monomer, the opening of the cavity to the lipid phase is much wider than what is seen in bovine complex. Such wide opening in the transmembrane region grants quinone/quinol in the Q pool greater accessibility to their desired binding sites. Purified bacterial enzyme always has higher Q content ($3Q/bc_1$) than bovine bc_1 ($0.5Q/bc_1$), therefore it may not be necessary to recycle only one quinone between Q_o and Q_i through the cavity. Instead, such a cavity may favor transfer between sites by some constraint on local diffusion from the cavity.

IVB. ISP head domain movement is required for bc_1 catalysis.

The poor electron density for ISP subunit in bovine tetragonal ($I4_122$) crystal indicates that the head domain of ISP is mobile. Judging from the height of the anomalous scattering signal from irons in the [2Fe-S] cluster, less than 50% ISP stayed in a “fixed” state at a position 31 Å to c_1 and 27 Å to heme b_L . The remaining population of ISP may distribute between the “fixed position” and somewhere near cytochrome c_1 with

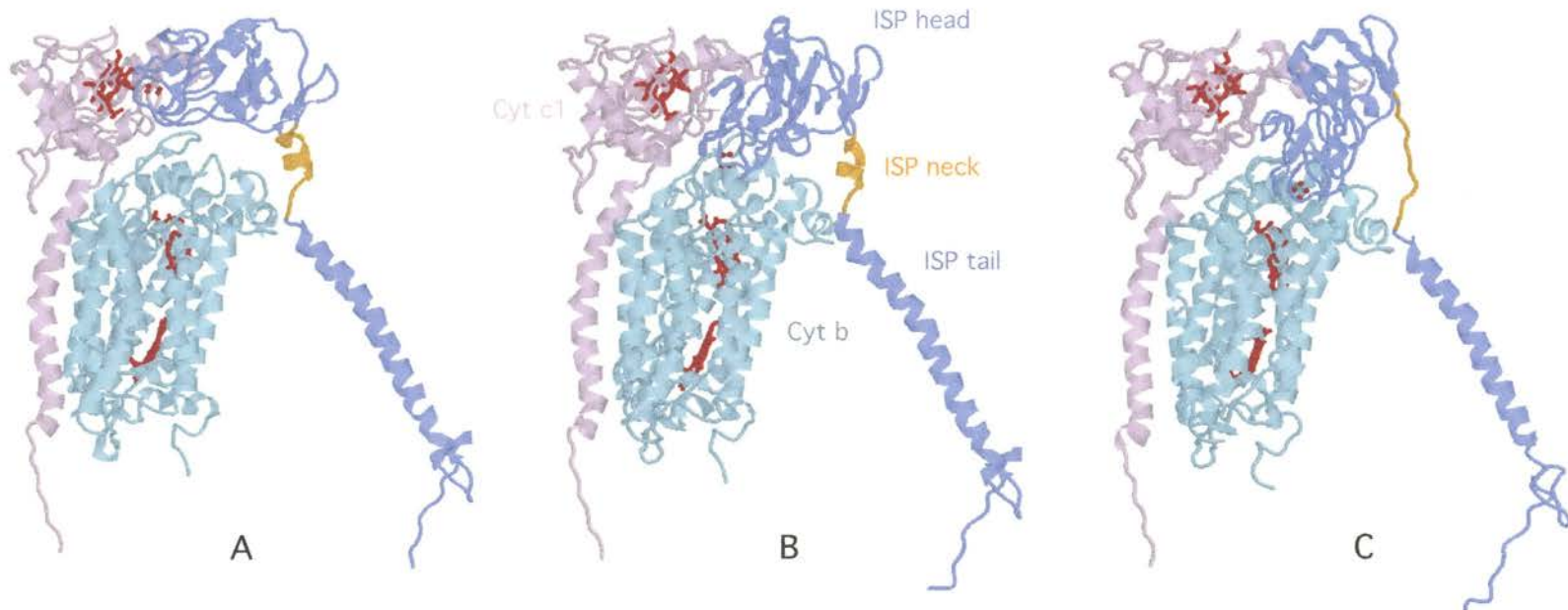


Figure 15. Different positions of ISP head domains in different crystal forms. (A) "c1 position" in bovine hexagonal (p6522) and orthorhombic chicken (p212121) crystals. (B) "Intermediate position" in bovine p65 crystal. (C) "b position" in native bovine tetragonal I4122, stigmatellin loaded bovine and chicken p212121 crystals. The ISP is shown in blue with its flexible neck region encompassing amino acid residues 63-73 in orange. Major conformational change is limited to the neck region between different positions of ISP.

no significant preference for any particular position. However, the [2Fe-2S] cluster was at a different position relative to the hemes in the different crystal forms (Figure 15). In native chicken $P2_12_12_1$ crystal form, ISP takes a position 21 Å to c_1 and 34 Å to heme b_L (c_1 position). Binding of stigmatellin in the chicken crystals shifts the [2Fe-2S] to a position close to heme b_L (b position). An intermediate position for ISP between c_1 -position and heme b_L -position was reported in bovine $P6_5$ crystal form. These results suggest the mobility of the head domain of ISP. However, the various position of ISP head domain in different native bc_1 crystal forms may result from: (1) crystal contacts involving the ISP head domain. In tetragonal crystal form, crystal contact is only limited to the matrix region, the electron density of ISP head domain is particularly poor; (2) different redox state of ISP and cytochrome c_1 . Bovine tetragonal bc_1 crystal was grown from totally oxidized enzyme, the redox state of other types of crystals have not yet been determined. According to their method of preparation, cytochrome c_1 subunit is partially reduced before applying to the hanging or sitting drop procedure. So far, none of these positions fits with the catalytic mechanism of the bc_1 complex because the [2Fe-2S] is too far from either its electron donor or acceptor for electron transfer through this center to occur at a kinetically competent rate. Therefore, the head domain of ISP may move during Q_o site catalysis has emerged as an attractive model to explain the fast electron transfer at Q_o site as well as the bifurcated electron transfer mechanism. ISP mobility is further supported by Q_o site inhibitors binding studies as has been discussed in section IID-3. Binding of UHDBT or stigmatellin enhances iron signal of ISP and arrests the movement of head domain, and thus positions it in the “fixed” state, the same position as the “ b -position” observed in chicken stigmatellin cocrystal. Upon MOAS binding, the iron signal disappeared and ISP is at a non-fixed position, referred as “loose state” in $I4_122$ crystal. Chapter 3 and 4 will provide functional evidence for the ISP head domain movement. The ongoing investigation focuses on the neck region of ISP (residues 63-72). Compared with the rigid ISP head and tail domains, the neck region seems to be the

most flexible part in ISP. Conformational change involving extension of the neck region is observed as ISP change from c_1 to b position in chicken $I2_12_12_1$ crystal form (figure 15). None of the amino acid residues constituting the flexible neck region of ISP plays an essential catalytic function per se, since all single substitutions in all positions tested yield almost wild type-like bc_1 complexes (52). Experiments are designed to decrease the flexibility and block the movement in order to test the hypothesis.

IVC. Two transient quinone binding sites may exist during quinol oxidation at the Q_o pocket.

Q_o site inhibitors were divided into three subgroups according to their structure motif. These inhibitors all bind exclusively in cytochrome b Q_o pocket and block electron transfer from QH_2 to cytochrome b and ISP. The fact that molecules with great difference in their molecular structure block the same reaction seems surprising at first sight, but this phenomenon was also found at the Q_b site of the photosynthetic reaction centers of thylakoid membranes of chloroplast (53) and chromatophores of *Rhodobacter* (54). Therefore the structural diversity in the inhibitors seems to be a general feature of ubiquinone binding pockets where quinone is either oxidized or reduced. Nevertheless, every inhibitor is specific to its particular reaction center and characteristic in its ligand-binding interaction. Those interactions may somehow freeze cytochrome b at a specific conformation mimicking different stages of quinol oxidation. Unlike MOA type of inhibitors, UHDBT and stigmatellin are located at the opening of Q_o pocket and directly contact ISP near the [2Fe-2S] cluster. Binding of these inhibitors increases the population of ISP in the fixed state. A close contact between ISP and inhibitors was expected from the large potential increase of the [2Fe-2S] cluster upon inhibitor binding (19). MOA-stilbene binds deeper in the Q_o pocket. There is no direct contact between ISP and inhibitor. The redox potential of ISP is not affected by the inhibitor. However ISP is released from the fixed state to the loose state after MOA-stilbene binding. The EPR spectrum of ISP in bovine MOA-stilbene treated bc_1 complex is similar to that of the

isolated free form ISP with $g_x=1.77$ (55). We speculated that a small conformational change in cytochrome *b* or ISP in response to MOA-stilbene binding may lead to such a transition. This hypothesis is supported by the non-competitive inhibition pattern of a weak MOA type inhibitor oudemansin A (56). Hydroquinone behaved non-competitively in kinetic assay and was not able to displace weakly binding oudemansin A from its binding site on cytochrome *b*, indicating a conformational change of the Q_o pocket being induced by binding of inhibitor. Therefore, the binding site of quinol is not identical with that for the MOA inhibitors. The primary quinol binding site could be where UHDBT or stigmatellin binds, the close contact between [2Fe-2S] cluster with the opening of the Q_o pocket will guarantee fast electron transfer from quinol to ISP. The binding site for MOA inhibitors may be involved in the transient binding of semiquinone during quinol oxidation. Binding of semiquinone at this site is accompanied by the enhanced random distribution of ISP. The detailed molecular mechanism of the transition of the ISP extramembrane domain from a fixed to a loose state in response to binding of ligands in the Q_o site must await the completion of crystallographic refinement of the atomic model at higher resolution and the analysis of crystallographic data on quinone binding at the Q_o site.

V. Other catalytic function of bc_1 complex

VA. Generation of superoxide anion at Q_o site.

Production of superoxide anion is thought to be a significant contribution to cellular damage. It is observed in isolated mitochondria in state 4 when high membrane potential across mitochondrial inner membrane is achieved, accounting for ~ 2% of O_2 uptake under physiological conditions. Several segments in the respiratory chain have been identified as the generators for O_2^- , including reduced flavin mononucleotide of NADH dehydrogenase in complex I, reduced FAD of succinate dehydrogenase in

complex II and two redox components ubiquinone and reduced b_L in the cytochrome bc_1 complex (57). Production of $O_2^{\cdot-}$ in bc_1 complex is directly related to the bifurcated electron transfer mechanism at Q_o site. High membrane potential and addition of antimycin are known to stimulate $O_2^{\cdot-}$ production, both of which would lead to the reduction of heme b_L and inhibition of oxidation of semiquinone at Q_o site. This reaction accounts for antimycin insensitive and oxygen dependent cytochrome c reduction catalyzed by bc_1 complex. Cytochrome c is reduced by the first electron removed from ubiquinol at Q_o site via ISP and cytochrome c_1 , the second electron of ubiquinol in the antimycin treated bc_1 leaks out of its normal electron transfer pathway at reduced heme b_L or semiquinone at Q_o site and reacts with O_2 to produce $O_2^{\cdot-}$. It seems likely that the Q_o site has evolved to minimize superoxide production. $O_2^{\cdot-}$ is produced in a hydrophobic environment since it is not easily accessible to superoxide dismutase (57). On the other hand, a hydrophobic molecule MCLA can easily reach Q_o site, form complex with $O_2^{\cdot-}$ and facilitate removal of $O_2^{\cdot-}$ from the generation site, which in turn increase the overall turn over and cytochrome c reduction. The crystallographic study of bc_1 complex has provided us with some valuable information toward the understanding the molecular mechanism for the generation of $O_2^{\cdot-}$. From the analysis of the architecture of Q_o site in section IIIB-2, we can conclude that the hydrophobic environment in $O_2^{\cdot-}$ generating site is provided by amino acid residues surrounding the Q_o site, especially those near the MOA-stilbene binding site which has been postulated to be the ubiquinone binding site (36). Binding of stigmatellin and MOA-stilbene both induce subtle changes in cytochrome b . The Q_o pocket opens up to ISP in order to accommodate stigmatellin. The aperture between the Q_o site and the aqueous phase is closed as a result of MOAS binding. This closure insulates the quinone binding pocket and the semiquinone occupant from ISP as well as the aqueous phase. $O_2^{\cdot-}$ production is prevented under normal physiological conditions. However when the membrane potential is high, the release of the second proton from QH^{\cdot} is prevented by the proton gradient across the

membrane and the binding of QH[•] is disfavored at both P1 and P2 sites. Therefore the closure on the quinone pocket will not be observed under this condition and semiquinone becomes accessible to oxygen molecule. When antimycin is added to the *bc*₁ complex, reoxidation of *b*_H by quinone at Q_i site is inhibited, heme *b*_L stays in the reduced state (Fe^{II}), which in turn prevents electron transfer from semiquinone to heme *b*_L. An indirect yet indispensable effect of having a reduced heme *b*_L (Fe^{II}) near the Q_o site is that it will increase the effective pK_a of QH[•] and prevent its deprotonation. The increased local concentration of QH[•] in the Q_o pocket induced by antimycin binding at Q_i site will ultimately increase O₂^{•-} production. Taken together they could probably account for O₂^{•-} production through ubisemiquinone. So far, there is no experimental evidence to differentiate the O₂^{•-} generation sites between ubisemiquinone and reduced heme *b*_L, even though O₂^{•-} production is sensitive to Q_o site inhibitors UHDBT and MOAS. The difficulty lies in the fast equilibrium between these two species. Crystallographic study indicates that heme *b*_L is buried inside of the protein in an even more concealed environment than semiquinone. No significant conformational change was observed after inhibitors binding, therefore direct interaction between O₂ and reduced heme *b*_L seems unlikely after antimycin binding. However, all the experiments tested so far have focused on the forward reduction of cytochrome *b*_L by quinol through Q_o site. Cytochrome *b* can be reduced through either the Q_o site (forward reaction) or the Q_i site (reverse reaction). It is of interest to investigate the superoxide anion production at reduced heme *b*_L produced through the reverse reaction pathway in the presence of Q_o site inhibitor UHDBT or MOAS. Site-directed mutagenesis studies on the “trap door” (residues Y278, I146) in cytochrome *b* Q_o pocket will also provide some valuable information about this hypothesis discussed here.

VB. The Role of the supernumerary subunits in the cytochrome *bc*₁ complex.

The *bc*₁ complexes from eukaryotic respiratory chain may vary in size and number of subunits between different organisms, but they all are much larger and more

complex than the complexes in the bacterial system. The simplest form of bc_1 complex containing only three redox active subunits is found in purple photosynthetic bacteria *Rhodobacter capsulatus*. Nevertheless, the general mechanism by which electron transfer is coupled to proton translocation across the membrane is the same in prokaryotes as in eukaryotes. The subunits that do not contain redox prosthetic group and are not directly involved in the catalytic function are referred to as “supernumerary” subunits. *Rhodobacter sphaeroides* contains only one supernumerary subunit, subunit IV, which is the smallest subunit in the complex with molecular weight of 15 Kda. The function of this subunit is believed to be involved in photosynthetic adaptation and stabilization of the whole complex (58). Subunit IV deletion strain of *Rhodobacter sphaeroides* requires more than 48 hours for photosynthetic adaptation from semiaerobic growth condition, while wild type strain needs less than 24 hours under the same condition. Although the enzyme activity of bc_1 complex containing only three subunits embedded in the chromatophore membrane of subunit IV deletion strain is very similar to that of the wild type strain, it is more labile toward detergent treatment. Approximately 75% bc_1 activity is lost after detergent extraction, indicating that this subunit is critical for maintaining the overall enzyme stability and assembly. The molecular mechanism for such function is still under investigation. Although the three-dimensional structure of mitochondria bc_1 complex is available, it is still difficult to relate structure to function for subunit IV because subunit IV bears no sequence similarity with any subunits present in the mitochondria complex.

Among the eight supernumerary subunits of mitochondrial bc_1 complex, core I and core II subunits show remarkable sequence similarity with the general mitochondria matrix processing peptidase (MPP). MPP, a heterodimer of α and β subunits localized in the mitochondrial matrix, cleaves the signal sequence of nucleus-encoded proteins after being imported into mitochondrion (59). The β subunit contains proteolytic activity whereas the α subunit does not, although it is thought to be involved in binding of

precursors before processing. Earlier, it was reported that bc_1 complex from potato, wheat and spinach possesses MPP activity (60). However, MPP activity can only be detected in bovine heart mitochondrial bc_1 complex under slightly unfolded condition through Triton X-100 treatment (61). The putative MPP catalytic site consisting of the conserved residue lysine 286 and arginine 287 of core II and the zinc binding motif of the core I was indicated by the three-dimensional structure. The structure also indicates that subunit 9 blocks the entrance to the active site and intertwines with core I and core II subunits, therefore no MPP activity was observed in the mature complex. Detergent treatment helps the removal of this inhibitory polypeptide and restores MPP activity to core I and core II subunits. Subunit 9 of mitochondria bc_1 is the presequence of ISP, which explains very well why subunit 9 ends up in the active site of MPP because pre-ISP is a natural substrate of core I and core II.

Subunit 8, also called hinge protein, was required for proper complex formation between cytochrome *c* and cytochrome c_1 . The high acidic residue content (24 out of 78 total) makes it an attractive candidate for the binding of basic cytochrome *c*. Subunit 8 is in close contact with the N-terminal extension, loop $\alpha 3$ - $\beta 1$ of cytochrome c_1 and predominantly exposed to the solvent. It is composed of two long helices connected by two disulfide bonds. No electron density is observed for the N-terminal 14 residues, which contain eight consecutive glutamic acids, suggesting that this segment is highly mobile and may form a part of cytochrome *c* docking site, together with helix $\alpha 1$ ' and loop $\beta 2$ - $\alpha 5$ of cytochrome c_1 . Since positive charges are scattered along the surface of inner membrane space region and pointing into the solvent on the same edge of heme c_1 , it is very difficult to assign specific regions that serve as docking interface or as recruiter for cytochrome *c*, without the co-crystallization of bc_1 and cytochrome *c*.

The functional role of other supernumerary subunits is uncertain at the present time. The structure indicated that they seem to have stabilizing interactions with other subunits and/or between monomers, but do not impinge on the catalytic interface.

Subunit VII, however, has an interesting N-terminal finger that reaches over to the channel in cytochrome *b*, connecting the Q_i -site to the aqueous phase. This subunit was previously identified as Q-binding protein by photoaffinity labeling with azidoquinone (62) even though its transmembrane helix is spaciouly separated from the both quinone binding sites. The transmembrane helix of subunit VII forms a bundle with helices F, G, H of cytochrome *b* subunit. Three lipid molecules have been identified within this bundle in yeast bc_1 crystal (Hunte C. personal communication).

VI. References:

- a) Jones, C. W. (1982) Introduction. In *Aspects of Microbiology 5, Bacterial Respiration and Photosynthesis* (Cole, J. A. and Knowles, D. J. eds.), Thomas Nelson and Sons Led, pp. 1-6.
- b) Voet, D. and Voet, J. G. (1995) Electron Transport and Oxidative Phosphorylation. In *Biochemistry* (Voet, D. and Voet, J.G. eds.), John Wiley & Sons, Inc. pp. 563-596.
3. Trumpower B. L. and Gennis , R. B. (1994) Energy transduction by cytochrome complexes in mitochondrial and bacterial respiration: the enzymology of coupling electron transfer reactions to transmembrane proton translocation. *Annu. Rev. Biochem.* **63**, 675-716.
4. Rich, P. R. (1984) Electron and proton transfers through quinones and cytochrome *bc* complexes. *Biochim. Biophys. Acta*, **768**, 53-79.
5. Ramasarma, T. (1985) Natural Occurrence and Distribution of Coenzyme Q. In *Coenzyme Q: Biochemistry, Bioenergetics and Clinical Application of Ubiquinone* (Lenaz, G. ed.), Jone Wiley & Sons, Inc. pp. 131-145.
6. Imhoff, J. F. (1992) Taxonomy, Phylogeny, and General Ecology of Anoxygenic Phototrophic Bacteria. In *Biotechnology Handbooks 6: Photosynthetic Prokaryotes* (Mann, N. H. and Carr, N. G. eds.), Plenum Press, New York, pp. 53-85.
7. Yu, C. A., Zhang, L., Kachurin, A. M., Shenoy, S. K., Deng, K. P., Yu, L., Xia, D., Kim, H. and Deisenhofer, J. (1999) The Crystal Structure of Mitochondrial Cytochrome *bc*₁ Complex. In *Frontier in Cellular Bioenergetics* (Papa, S., Guerrieri, F., and Tager, eds.), Kluwer Academic/Plenum Publishers, New York, pp. 263-289.
8. Yun C. H., Beci, R., Crofts, A. R., Kaplan, S. and Gennis R. B. (1990) Cloning and DNA sequencing of the *fbc* operon encoding the cytochrome *bc*₁ complex from *Rhodobacter sphaeroides*. *Eur. J. Biochem.* **194**, 399-411.

9. Gray, K. A., and Daldal, F. (1995) in *Anoxygenic Photosynthetic Bacteria* (Blankenship, R. E., Madigan, M. T., and Bauer, C. eds.), Kluwer, Academic Publishers, Dordrecht, The Netherlands, pp 747-774.
10. Brasseur, G., Saribas, A. S. and Daldal, F. (1996) A compilation of mutations located in the cytochrome *b* subunit of the bacterial and mitochondrial *bc₁* complex. *Biochim, Biophys. Acta.* **1275**, 61-69.
11. Wilstrom, M. K. F. and Berden, J. A. (1972) Oxidoreduction of cytochrome *b* in the presence of antimycin. *Biochim. Biophys. Acta*, **283**, 403-420.
12. Mitchell, P. (1975) The protonmotive Q cycle: a general formulation. *FEBS Lett.* **59**, 137-139.
13. Trumpower B. L. (1981) Function of the iron-sulfur protein of the cytochrome b-c₁ segment in electron-transfer and energy-conserving reactions of the mitochondrial respiratory chain. *Biochim. Biophys. Acta*, **639**, 129-155.
14. Erecinska, M., Wilson, D. F. and Miyata, Y. (1976) Mitochondrial cytochrome b-c complex: its oxidation-reduction components and their stoichiometry. *Arch. Biochem. Biophys.* **177**, 133-143.
15. von Jagow, G. and Link, T. (1988) Use of specific inhibitors on the mitochondrial *bc₁* complex. *Methods in Enzymology* **126**, 253-271
16. Yu, C.A., Nagoaka, L., Yu, L. and King, T. E. (1978) Evidence for the existence of a ubiquinone protein and its radical in the cytochromes *b* and *c₁* region in the mitochondrial electron transport chain. *Biophys. Res. Commun.* **82**, 1070-1073.
17. Slater, E. C. (1973) The mechanism of action of the respiratory inhibitor, antimycin. *Biochim, Biophys. Acta.* **301**, 129-154.
18. de Vires, S., Albracht, S.P.J., Berden, J. A. and Slater, E. C. (1981) *J. Biol. Chem.* **256**, 11996-11998.
19. Junemann, S., Heathcote, P., and Rich, P. R. (1998) On the mechanism of quinol oxidation in the *bc₁* complex. *J. Biol. Chem.* **273**, 21603-21607.

20. Crofts, A. R. and Wang, Z. (1989) How rapid are the internal reactions of the ubiquinol:cytochrome c_2 oxidoreductase? *Photosynth. Res.* **22**, 69-87.
21. Brand, M. D., Reynafarje, B. and Lehninger, A. L. (1976) Re-evaluation of the H⁺/site ratio of mitochondrial electron transport with the oxygen pulse technique. *J. Biol. Chem.* **251**, 5670-5675.
22. Brandt, U. (1996) Bifurcated ubihydroquinone oxidation in the cytochrome bc_1 complex by proton-gated charge transfer. *FEBS lett.* **387**, 1-6.
23. Yun, C.H., Van Doren, S. R., Crofts, A. R. and Gennis, R. B. (1991) The use of gene fusions to examine the membrane topology of the L-subunit of the photosynthetic reaction center and of the cytochrome b subunit of the bc_1 complex from *Rhodobacter sphaeroides*. *J. Biol. Chem.* **266**, 10967-10973.
24. Colson, A. M. (1993) Random mutant generation and its utility in uncovering structural and functional features of cytochrome b in *Saccharomyces cerevisiae*. *J. Bioenerg. Biomembr.* **3**:211-220.
25. Ohnishi, T. H., Schägger, H., Meinhardt, S. W., Loblutto, R., Link T. A. and Von Jagow, G. (1989) Spatial organization of redox active centers in the bovine heart ubiquinol-cytochrome c oxidoreductase. *J. Biol. Chem.* **264** 735-744.
26. Xia, D., Yu, C. A., Kim, H., Xia, J-Z., Kachurin, A., Zhang, L., Yu, L. and Deisenhofer, J. (1997) Crystal structure of the cytochrome bc_1 complex from bovine heart mitochondria. *Science* **277**, 60-66.
27. Iwata, S., Lee, J. W., Okada, K., Lee, J. K., Iwata, M., Rasmussen, B., Link, T. A., Ramaswamy, S. and Jap, B. K. (1998) Complete structure of the 11-subunit bovine mitochondrial cytochrome bc_1 complex. *Science* **281** 64-71.
28. Zhang Z. L., Huang, L., Shulmeister, V. M., Chi, Y-I., Kim, K. K., Hung L-W., Crofts, A. R., Berry, E. A. and Kim, S. H. (1998) Electron transfer by domain movement in cytochrome bc_1 . *Nature* **392** 677-684.

29. di Rago, J. P. and Colson, A. M. (1988) Molecular basis for resistance to antimycin and diuron, Q-cycle inhibitors acting at the Qi site in the mitochondrial ubiquinol-cytochrome *c* reductase in *Saccharomyces cerevisiae*. *J. Biol. Chem.* **263**, 12564-12570.
30. Crofts, A. R., Robinson, K., Andrews, S., Van Doren, and Berry, E. A. (1987) In *Cytochrome systems: Molecular Biology and Bioenergetics* (Papa, S., Chance, B., Ernster, L. eds.), Plenum, New York, pp 617-624.
31. Widger, W. R., Cramer, W. A., Herrmann, R. G. and Trebst, A. (1984) Sequence homology and structural similarity between cytochrome *b* of mitochondrial complex III and the chloroplast *b₆-f* complex: position of the cytochrome *b* hemes in the membrane. *Proc. Natl. Acad. Sci. U S A* **81**, 674-678.
32. Tian, H, unpublished data.
33. Saribas, A. S., Ding, H., Dutton, P. L. and Daldal, F. (1997) Substitutions at position 146 of cytochrome *b* affect drastically the properties of heme *b_L* and the Q_o site of *Rhodobacter capsulatus* cytochrome *bc₁* complex. *Biochim. Biophys. Acta.* **1319**, 99-108.
34. van den Berg, W. H., Prince, R. C., Bashford, C. L., Takamiya, K. I., Bonner, W. D. Jr and Dutton, P. L. (1979) Electron and proton transport in the ubiquinone cytochrome *b-c₂* oxidoreductase of *Rhodospseudomonas sphaeroides*. Patterns of binding and inhibition by antimycin. *J. Biol. Chem.* **254**, 8594-8604.
35. Link, T. A., Haase, U., Brandt, U. and von Jagow, G. (1993) What information do inhibitors provide about the structure of the hydroquinone oxidation site of ubihydroquinone: cytochrome *c* oxidoreductase? *J. Bioenerg. Biomembr.* **3**:221-232.
36. Kim, H., Xia, D., Yu, C-A., Xia, J-Z., Kachurin, A. M., Zhang, L., Yu, L. and Deisenhofer, J. (1998) Inhibitor binding changes domain mobility in the iron-sulfur protein of the mitochondrial bc1 complex from bovine heart. *Proc, Natl. Acad. Sci. USA* **95** 8026-8033.

37. Crofts, A.R., Barquera, B., Gennis, R.B., Kuras, R., Guergova-Kuras, M. and Berry, E.A. (1999) Mechanistic aspects of the Qo-site of the bc₁-complex as revealed by mutagenesis studies, and the crystallographic structure. In *The Phototrophic Prokaryotes* (Peschek, G. A., Loeffelhardt, W., Schmetterer, G. eds.), Plenum Publishing Corporation, New York, In press.
38. Gray, K. A, Davidson, E. and Daldal, F. (1992) Mutagenesis of methionine-183 drastically affects the physicochemical properties of cytochrome c₁ of the bc₁ complex of *Rhodobacter capsulatus*. *Biochemistry* **31**, 11864-11873.
39. Kim, C. H. and King, T. E. (1981) The indispensibility of a mitochondrial 15K protein for the formation of the cytochrome c₁-cytochrome c complex. *Biochem. Biophys Res Commun* **101**, 607-614.
40. Ludwig, B, Suda, K. and Cerletti, N. (1983) Cytochrome c₁ from *Paracoccus denitrificans*. *Eur. J. Biochem.* **137**, 597-602.
41. Broger, C., Salardi, S. and Azzi, A. (1983) Interaction between isolated cytochrome c₁ and cytochrome c. *Eur. J. Biochem.* **131**, 349-352.
42. Iwata, S., Saynovits, M., Link, T. A. and Michel, H. (1996) Structure of a water soluble fragment of the 'Rieske' iron-sulfur protein of the bovine heart mitochondrial cytochrome bc₁ complex determined by MAD phasing at 1.5 Å resolution. *Structure* **4**, 567-579.
43. Graham, L. A., Brandt, U., Sargent, J. S. and Trumpower, B. L. (1993) Mutational analysis of assembly and function of the iron-sulfur protein of the cytochrome bc₁ complex in *Saccharomyces cerevisiae*. *J. Bioenerg. Biomembr.* **25**, 245-257.
44. Link, T. A. and Iwata, S. (1996) Functional implications of the structure of the 'Rieske' iron-sulfur protein of bovine heart mitochondrial cytochrome bc₁ complex. *Biochim, Biophys. Acta.* **1275**, 54-60.
45. Link, T. A., Hatzfeld, O. M., Unalkat, P., Shergill, J. K., Cammack, R. and Mason, J. R. (1996) Comparison of the "Rieske" [2Fe-2S] center in the bc₁ complex and in

- bacterial dioxygenases by circular dichroism spectroscopy and cyclic voltammetry. *Biochemistry* **35**, 7546-7552.
46. Link, T. A., Hagen, W. R., Pierik, A. J., Assmann, C. and von Jagow, G. (1992) Determination of the redox properties of the Rieske [2Fe-2S] cluster of bovine heart *bc₁* complex by direct electrochemistry of a water-soluble fragment. *Eur. J. Biochem.* **208**, 685-691.
47. Link, T. A. (1994) *Biochim. Biophys. Acta.* **1185**, 81-84.
48. Nieboer, P. and Berden, J. A. (1992) Triple inhibitor titrations support the functionality of the dimeric character of mitochondrial ubiquinol-cytochrome *c* oxidoreductase. *Biochim. Biophys. Acta.* **1101**, 90-96.
49. Musatov, A. and Robinson, N. C. (1994) Detergent-solubilized monomeric and dimeric cytochrome *bc₁* isolated from bovine heart. *Biochemistry* **33**, 13005-13012.
50. Capaldi, R. A. (1982) Arrangement of proteins in the mitochondrial inner membrane. *Biochim. Biophys. Acta.* **694**, 291-306.
51. Yu, C.A. and Yu, L. (1981) Ubiquinone-binding proteins. *Biochim. Biophys. Acta.* **639**, 99-128.
52. Daldal, F, personal communication.
53. Saitoh, I., Miyoshi, H., Shimizu, R. and Iwamura, H. (1992) Comparison of structure of quinone redox site in the mitochondrial cytochrome-*bc₁* complex and photosystem II (QB site). *Eur. J. Biochem.* **209**, 73-79
54. Sinning, I., Michel, H., Mathis, P. and Rutherford, A.W. (1989) Characterization of four herbicide-resistant mutants of *Rhodospseudomonas viridis* by genetic analysis, electron paramagnetic resonance, and optical spectroscopy. *Biochemistry* **28**, 5544-5553.
55. Kachurin, A and Yu C-A. unpublished results.

56. Brandt, U. Schägger, H and von Jagow, G. (1988) Characterisation of binding of the methoxyacrylate inhibitors to mitochondrial cytochrome *c* reductase. *Eur. J. Biochem.* **173** 499-506.
57. Zhang, L, Yu, L. and Yu, C-A. (1998) Generation of superoxide anion by succinate-cytochrome *c* reductase from bovine heart mitochondria. *J. Biol. Chem.* **273** 33972-33976.
58. Chen, Y. R. Usui, S., Yu, C. A. and Yu, L. (1994) Role of subunit IV in the cytochrome b-c1 complex from *Rhodobacter sphaeroides*. *Biochemistry* **33**, 10207-10214.
59. Ou, W., Ito, A., Okazaki, H., and Omura, T. (1989) Purification and characterization of a processing protease from rat liver mitochondria. *EMBO J.* **8** 2605-2612.
60. Glaser, E., Eriksson, A. C., and Sjoling, S. (1994) Bifunctional role of the *bc*₁ complex in plants. Mitochondrial *bc*₁ complex catalyses both electron transport and protein processing. *FEBS Lett.* **346** 83-87.
61. Deng, K. P., Zhang, L., Kachurin, A. M., Yu, L. Xia, D., Kim, H., Deisenhofer, J. and Yu, C. A. (1998) Activation of a matrix processing peptidase from the crystalline cytochrome *bc*₁ complex of bovine heart mitochondria. *J. Biol. Chem.* **273** 20752-20757.
62. Usui, S., Yu, L. and Yu, C. A. (1990) The small molecular mass ubiquinone-binding protein (QPc-9.5 kDa) in mitochondrial ubiquinol-cytochrome *c* reductase: isolation, ubiquinone-binding domain, and immunoinhibition. *Biochemistry* **29**, 4618-4626.

CHAPTER II

The Involvement of Serine 175 and Alanine 185 of Cytochrome *b* of *Rhodobacter sphaeroides* Cytochrome *bc*₁ complex in Interaction with Iron-Sulfur Protein.

Hua Tian, Linda Yu, Michael W. Mather, Chang-An Yu

The Journal of Biological Chemistry, 272, 23722-23728 (1997)

ABSTRACT

An approach involving cysteine replacement of potentially noncritical amino acid residues, followed by chemical modification studies, was used to investigate structure-function of the "cd helix" of cytochrome *b* from *Rhodobacter sphaeroides*. Three amino acid residues, Ser-155, Ser-175, and Ala-185, which span this region of cytochrome *b*, were selected for this study. The S155C substitution yields cells unable to support photosynthetic growth, indicating that Ser-155 is a critical amino acid residue. Further mutational studies of Ser-155 indicate that the size of the amino acid side chain at this position is critical for photosynthetic growth of *R. sphaeroides*. On the other hand, the S175C and A185C substitutions yield cells with photosynthetic growth rates and enzyme kinetics of the bc_1 complexes very similar to those of the unmutated complex, indicating that Ser-175 and Ala-185 are noncritical residues. Thus, engineered cysteines at these two positions of cytochrome *b* are suitable for membrane topology and domain/subunit interaction studies. Cys-175 does not react with a sulfhydryl-modifying reagent, N-ethylmaleimide (NEM), either in sealed, inside-out chromatophores or in detergent-disrupted chromatophores, indicating that position 175 of cytochrome *b* is inaccessible from both sides of the membrane and is probably buried within the protein complex. Cys-185 reacts with NEM only after detergent disruption of the sealed, inside-out chromatophores, indicating that this position of cytochrome *b* is accessible on the outer (periplasmic) surface of the membrane. These results place the cd helix of cytochrome *b* on the periplasmic side of the chromatophore membrane. When purified A185C-substituted bc_1 complex was treated with NEM, about 87% of the activity was abolished due to NEM modification of Cys-185. The signature of the Rieske iron-sulfur center is broadened upon NEM modification of A185C, with the g_x signal shifting from $g = 1.80$ to $g = 1.75$, suggesting that Ala-185 of cytochrome *b* interacts with the iron-sulfur protein. When purified S175C-substituted bc_1 complex is treated with NEM, no change in the activity is observed, since

Cys-175 is inaccessible to NEM. However, when the iron-sulfur protein is removed from the S175C-substituted bc_1 complex, Cys-175 becomes accessible to NEM, indicating that Ser-175 of cytochrome b is shielded by the iron-sulfur protein in the bc_1 complex.

INTRODUCTION

The cytochrome bc_1 complex from the photosynthetic bacterium *Rhodobacter sphaeroides* has been purified and characterized in several laboratories (1-6). This complex catalyzes electron transfer from ubiquinol to cytochrome c_2 in the photosynthetic cyclic electron transfer system and concomitantly translocates protons across the membrane to generate a membrane potential and pH gradient for ATP synthesis. The purified complex contains four protein subunits and five redox-active centers. Subunit I houses cytochromes b (b_{565} and b_{562}), subunit II houses cytochrome c_1 , and subunit III houses the iron-sulfur cluster. Subunits I and IV have been identified as the Q1-binding proteins in the complex by photoaffinity labeling using an azido-Q derivative (7).

The *R. sphaeroides* cytochrome bc_1 complex is functionally analogous to the mitochondrial ubiquinol-cytochrome c reductase, and the three largest subunits are homologous to their mammalian counterparts. Biophysical, biochemical, and genetic (8, 9) studies of this bacterial complex have contributed greatly to our present knowledge of its electron and proton transfer mechanisms. It is generally believed that electron and proton transfer in this complex follows the Q-cycle mechanism (10-12), which hypothesizes two Q-binding sites, a ubiquinol oxidation site (Q_o) and a ubiquinone reduction site (Q_i site). The two Q-binding sites are thought to be on opposite sides of the membrane, with quinol oxidation occurring on the periplasmic side and quinone reduction occurring on the cytoplasmic side.

The cytochrome *b* polypeptide is major structural element of both Q-binding sites. Two Q-binding regions were identified in the cytochrome *b* subunit of bovine heart mitochondrial cytochrome *bc*₁ complex (13) by isolating and sequencing azido-Q-linked peptides from azido-Q-labeled cytochrome *b*. These two regions correspond to amino acid residues 158-171 and 369-379 of the *R. sphaeroides* cytochrome *b* sequence (14). According to the 8-helix structural model of cytochrome *b* (15, 16), the first Q-labeled peptide is located in the cd helix, an amphipathic helix in the amino-terminal portion of the connecting loop between transmembrane helices C and D. The second labeled peptide is in the transmembrane helix G. Mutational studies of the cd helix region of cytochrome *b* have been extensive; substitutions for Gly-158, Ile-162, and Thr-163 have been reported to confer resistance to Q_o center inhibitors (17, 18). These results are consistent with participation of the first labeled peptide in the formation of the Q_o site. The participation of the second labeled peptide in a Q-binding site has not been well established, since no mutation studies have been reported.

To further understand the Q_o site in the cytochrome *bc*₁ complex, we have replaced a number of relatively conserved amino acid residues in the cd helix region of the *R. sphaeroides* cytochrome *b*. Herein, we report generation and characterization of *R. sphaeroides* mutants carrying the S155C, S175C, or A185C amino acid substitution in cytochrome *b*, the topology of the cd helix region of cytochrome *b* in the chromatophore membrane, and involvement of S175 and A185 of cytochrome *b* in the interaction with the iron-sulfur protein of the cytochrome *bc*₁ complex. The involvement of Cys-167 of cytochrome *c*₁ in interaction with the iron-sulfur protein in the *bc*₁ complex was also observed.

EXPERIMENTAL PROCEDURES

Materials—Dodecylmaltoside (DM) was purchased from Anatrace. ³H-Labeled N-ethylmaleimide (NEM) was from Du Pont. Dithiothreitol (DTT) was from Sigma. All other chemicals were of the highest purity commercially available. pSELNB3503, which was used as the template for mutagenesis, and pRKDNB3505 and pRKDNB35KmBP, which were used for the transfer and expression of wild type and engineered *fbc* genes, were constructed in our laboratory (19). Restriction endonucleases and DNA-modifying enzymes were purchased from Promega, Life Technologies, Inc., New England Biolabs, U.S. Biochemical Corp, Perkin-Elmer, and Pharmacia Biotech Inc. *Escherichia coli* S17-1 (20) and *R. sphaeroides* BC17 (14) were generously provided by Dr. R. B. Gennis of the University of Illinois.

Growth of Bacteria—*E. coli* was grown at 37 °C on LB medium. Extra-rich media, e.g. TYP, were used in procedures for the rescue of single-stranded DNA or the purification of low copy number plasmids (21). *R. sphaeroides* cells were grown at 30 °C on an enriched Siström's medium (22) essentially as described (19). Antibiotics were added at the following concentrations: ampicillin, 100-125 mg/liter; tetracycline, 10-15 mg/liter for *E. coli* and 0.75-1.0 mg/liter for *R. sphaeroides*; kanamycin sulfate, 30-50 mg/liter for *E. coli* and 20-25 mg/liter for *R. sphaeroides*; trimethoprim, 85-100 mg/liter for *E. coli* and 25-30 mg/liter for *R. sphaeroides*.

Construction of Mutation(s) and Expression of Mutated Complexes in R. sphaeroides—Mutants were constructed by site-directed mutagenesis using the Altered Sites system from Promega Corp. (23), and oligonucleotides were synthesized at the OSU Recombinant DNA/Protein Core Facility. The oligonucleotides used were GTGGGGCCAGATGGCCTTCTGGGGCGCCACCGT, CGTGGGGCCAGATGTACTTCTGGGGCGCCACCGT, GTGGGCCAGATGACCTTCTGGGGCGCCACCGT, CCGTGGGGCCAGAAATGCGGTTCTGGGGCGCCACCGT, CCGTGGGGCCAGATG-

GACTTCTGGGGCGCCACCGT, GTGGGGCCAGATGGGCTTCTGGGGCGCCACCGT, GTGGGGCCAGATGCTCTTCTGGGGCGCCACCGT, and GGGGCCAGATGTGCTTCTGGGGCGCCAC for Ser-155 to Ala, Tyr, Thr, Arg, Asp, Gly, Leu, and Cys, respectively, and GGCATCGGCCATTGCATCCAGACCTGGCTGCT for the Ser-175 to Cys, and GCTGCTCGGCGGCCCGTGCGTGGACAATGCCA for Ala-185 to Cys mutations. The previously constructed plasmid pSELNB3503 (19), in which a *PinAI* site was introduced by a silent mutation at position 579 in the *fbcB* gene, a *BstEII* site outside of the *fbcFBC* operon coding region was eliminated, and a *XbaI* site was introduced between the *fbcB* and *fbcC* genes, was used as template DNA for mutagenesis.

Following mutagenesis, a 200-base pair *BstEII-PinAI* fragment from pSELNB3503 containing the altered codon was ligated into the *BstEII-PinAI* sites of pRKDNB35KmBP (19). The use of pRKDNB35KmBP to receive the mutated *BstEII-PinAI* fragments eliminates the possibility of retaining or recloning the wild type fragment when attempting to subclone the mutated fragments into the expression vector. Loss of kanamycin resistance was then used to screen for recombinant plasmids. pRKDNB3503 derivatives were conjugated into *R. sphaeroides* BC17 from *E. coli* S17-1 using a plate-mating procedure (19).

Other Recombinant DNA Techniques—General molecular genetic manipulations were performed essentially as described by Sambrook et al. (24). Nucleotide sequencing was performed with an Applied Biosystems model 373 automatic DNA sequencer. Sequencing of mutated DNA templates was conducted by amplification of a DNA segment including the entire *BstEII* to *PinAI* sequence using the polymerase chain reaction followed by conversion to the single-stranded form by treatment with T7 gene 6 exonuclease as described (25). The presence of engineered mutations and the absence of other changes in the template region was reconfirmed once for each mutant clone, following transfer to and expression in *R. sphaeroides* BC17, by purifying the expression plasmid from an aliquot of a photosynthetic culture and determining the nucleotide sequence as described (26).

Enzyme Preparations and Activity Assay—The sealed, inside-out chromatophores used for topology studies were prepared essentially according to the method described by Hunter et al. (27). Chromatophores used for isolation of the cytochrome bc_1 complex were prepared from frozen cell pastes of photosynthetically grown *R. sphaeroides* BC17 complement and mutant strains as described previously (28). The cytochrome bc_1 complexes were purified from chromatophores by the method of Mather et al. (19). Ubiquinol-cytochrome c reductase activity was measured at 23 °C in a 1-ml assay mixture containing 100 mM sodium/potassium phosphate buffer, pH 7.4, 0.3 mM EDTA, 50 μ M cytochrome c , and 25 μ M 2,3-dimethoxy-5-methyl-6-geranyl-1,4-benzoquinol (Q_2H_2). 30 μ M potassium cyanide was added to assays of chromatophores to inhibit oxidase activity. For determination of apparent K_m for Q_2H_2 , various concentrations of Q_2H_2 were used. Cytochrome bc_1 complex activity was determined by measuring the reduction of cytochrome c (the increase in absorbance at 550 nm) in a Shimadzu UV2101PC spectrophotometer, at 23 °C. Nonenzymatic oxidation of Q_2H_2 was determined under the same conditions in the absence of enzyme. A millimolar extinction coefficient of 18.5 was used to calculate the reduced cytochrome c concentration.

Preparation of the Rieske Iron-Sulfur Protein-depleted bc_1 Subcomplex—30 μ l of purified bc_1 complex (300 μ M cytochrome b) in 50 mM Tris-Cl, pH 7.4, was mixed with 100 μ l of a solution containing 80 mM Na_2CO_3 , 8 mM DTT and 0.6 M urea, pH 10.5. After incubation for 5 min at 0 °C, the sample was loaded onto a linear pH sucrose density gradient. The gradient was prepared from 5 ml each of 8% sucrose solution containing 80 mM Na_2CO_3 , 4 mM DTT, 0.6 M urea, and 0.01% DM, pH 10.5 and 16% sucrose solution containing 120 mM Tris-Cl, 0.2 mM DTT, and 0.01% DM, pH 6.5. After centrifugation for 9 h at 44,000 rpm (230,000 g) in a Beckman SW 50.1 rotor, the red fractions containing Rieske iron-sulfur protein-depleted bc_1 subcomplex were found in the lower third of the gradient. The Rieske iron-sulfur protein was mainly in the upper part of the gradient. The Rieske iron-sulfur protein-depleted bc_1 subcomplex was collected, and the buffer was

exchanged (to remove DTT) by repeated (3 times) dilution and concentration in a Centricon-30 device with a solution containing 50 mM Tris-Cl, pH 7.2, and 0.01% DM.

Reaction of NEM with the bc_1 Complexes—3 nmol of the cytochrome bc_1 complexes from complement, S175C, or A185C were incubated with [3 H]NEM at a 2:1 molar ratio to cytochrome b heme at 23 °C for 15 min. The radioactivity of NEM was 12,000 cpm/nmol. The NEM-treated samples were spotted onto a 3 M paper and developed with a mixture of chloroform and methanol (2:1, v/v) to remove unreacted NEM. To determine NEM distribution among bc_1 subunits, the denatured bc_1 complexes, which remained at the origin of the paper chromatogram, were eluted from the paper with 0.1 M Tris-Cl, pH 7.0, containing 1% SDS and 1% -mercaptoethanol and subjected to SDS-polyacrylamide gel electrophoresis (SDS-PAGE). The gels were cut into about 0.3-cm slices, and radioactivity was determined in a Packard Tri-Carb 1900CA liquid scintillation counter. To determine the amount of NEM incorporated into bc_1 complexes, the paper at the origin was cut into small pieces and subjected to liquid scintillation counting.

Isolation of [3 H]NEM-labeled Peptides from Cytochrome c_1 —The [3 H]NEM-labeled cytochrome c_1 band was excised from the SDS-PAGE gel, and the protein was eluted using an electroeluter from Bio-Rad. The electrophoretically eluted protein was concentrated with a Centricon-10 and precipitated with 50% cold acetone (20 °C). The precipitate was resuspended in 50 mM Tris-Cl buffer, pH 7.4, and digested with endoprotease Arg-C at 37 °C for 12 h. 100- μ l aliquots of the Arg-C-digested cytochrome c_1 protein were then separated by HPLC on a Synchro-pak RP-8 column (0.46 X 25 cm) using a gradient formed from 0.1% trifluoroacetic acid and 0.1% trifluoroacetic acid containing 90% acetonitrile, with a flow rate of 0.8 ml/min. Samples were collected in 0.8-ml fractions. The absorbance at 214 nm and the radioactivity of each fraction were measured. Peaks with high specific radioactivity were collected, dried, and subjected to peptide sequence analysis.

Other Biochemical Methods—Protein was determined by the Lowry method (29) with the inclusion of 1% SDS in samples and standards. For accurate measurement of the protein content of chromatophores, interfering pigments were removed by acetone/methanol extraction as described (30). Cytochrome *b* (31) and cytochrome c_1 (32) were determined according to published methods.

SDS-PAGE was performed according to Laemmli (33) using a Bio-Rad Mini-Protean dual slab vertical cell.

Low temperature EPR spectra were obtained with Bruker ER200D spectrometer equipped with an Air Products flow cryostat. Instrument setting details are provided in the legends of the relevant figures.

RESULTS AND DISCUSSION

Characterization of R. sphaeroides Mutants Expressing the S155C, S175C, and A185C Alterations in Cytochrome b—Previous studies of the cytochrome bc_1 complex from beef heart mitochondria have identified Q-binding peptides within cytochrome *b*, one of which corresponds to residues 158-171 of cytochrome *b* of *R. sphaeroides*. This peptide is located in an extra-membrane amphipathic cd helix in the eight-transmembrane helix model of cytochrome *b*. Certain mutations at Gly-158, Ile-162, and Thr-163 of cytochrome *b* confer resistance to Q_o center inhibitors, indicating that the cd helix may be involved in the Q_o site (17, 18). If this cd helix is indeed a part of the Q_o site, it would have to be located on the periplasmic side of the chromatophore membrane according to the Q-cycle mechanism. An approach involving cysteine substitution at noncritical amino acid residues, followed by chemical modification of engineered cysteines, was adopted for a study of the topology of the cd helix.

Three amino acid residues, Ser-155, Ser-175, and Ala-185, which are located before, within, and after the putative cd helix of cytochrome *b*, were chosen to be mutated to

Table I

Characterization of the S155C, S175C, and A185C cytochrome b mutations

Mutations	Photosynthetic growth	Enzymatic activity ^a	
		Chromatophores	Purified <i>bc</i> ₁
		μmol cytochrome <i>c</i> reduced/min/nmol cytochrome <i>b</i>	
Complement (no mutation)	++ ^b	1.9	2.2
S155C	— ^c	NA ^d	NA
S175C	++	1.7	2.0
A185C	++	1.8	2.3

a The K_m values of S175C and A185C are almost the same as that of the *bc*₁ from the complement strain, $K_m \sim 0.9 \mu\text{M Q}_2\text{H}_2$.

b ++, the photosynthetic growth phenotype is essentially the same as the "wild type."

c , no photosynthetic growth within 7 days.

d NA, not available.

cysteines. Table I summarizes the photosynthetic growth behavior of cells expressing the wild type cytochrome *b* (complement cells) and the S155C, S175C, and A185C cytochrome *b* replacement mutations, as well as the ubiquinol-cytochrome *c* reductase activities of chromatophores and purified bc_1 complexes derived from these recombinant strains. Replacing Ser-175 or Ala-185 with cysteine yields cells capable of photosynthetic growth at a rate similar to that of the complement cells. Since the electron transfer activities and the apparent K_m for Q_2H_2 of S175C- and A185C-substituted bc_1 complexes are essentially the same as those of the complex from the complement strain, both in chromatophore membranes and in the purified state, Ser-175 and Ala-185 of cytochrome *b* are apparently noncritical residues, and the engineered cysteines at these two positions can be used to study topology of the cd helix and its interaction with other subunits. On the other hand, the substitution of Ser-155 of cytochrome *b* with cysteine yields cells unable to grow photosynthetically in either rich or minimal medium, indicating that Ser-155 is a critical residue and that the engineered cysteine at this position is not suitable for topology and interaction studies.

The Effect of Size of the Amino Acid Side Chain at Position 155 of Cytochrome b on Photosynthetic Growth of R. sphaeroides—Since substitution of Ser-155 of cytochrome *b* with cysteine results in cells unable to support photosynthetic growth, the structural importance of Ser-155 was further examined by substituting glycine, alanine, threonine, tyrosine, leucine, aspartic acid, and arginine at this position. The cytochrome *b* S155G or S155A substitution results in cells having a photosynthetic growth rate comparable with that of the complement cells. The S155T substitution yields cells with a retarded photosynthetic growth rate (about half that of the complement strain). Substitutions of Ser-155 with tyrosine, leucine, aspartic acid, and arginine yield cells unable to support photosynthetic growth. These results indicate that the size of the amino acid side chain at position 155 of cytochrome *b* is critical for photosynthetic growth of *R. sphaeroides*. A similar size-activity

relationship was previously observed for Gly-158 of cytochrome *b* in *Rhodobacter capsulatus* (17).

To investigate whether the size limitation at position 155 of cytochrome *b* correlates with Q-binding, the enzymatic activity and apparent K_m for Q_2H_2 of the cytochrome bc_1 complexes in chromatophores of the photosynthesis-competent strains expressing the S155G, S155A, and S155T cytochrome *b* variants were measured and compared with those in chromatophores from complement cells. Although the ubiquinol-cytochrome *c* reductase activity differed significantly (S155G (100%), S155A (40%), S155T (10%)) the apparent K_m values for Q_2H_2 in all three mutated complexes were virtually the same as that of the complement bc_1 complex ($\sim 0.9 \mu\text{M}$), indicating that the structural requirement for a small amino acid residue at position 155 of cytochrome *b* may not be simply to accommodate a Q molecule at this position. This speculation is consistent with the crystallographic structural data from the bovine heart cytochrome bc_1 complex, which show that the corresponding amino acid residue does not contribute to the so-called Q_o cavity (34).

Since serine and alanine residues occupy virtually the same volume in proteins, the 2.5-fold reduction in activity observed when alanine replaces serine at position 155 of cytochrome *b* suggests that the hydroxyl moiety of this serine plays some role in maintaining the optimal protein structure and/or reactivity, perhaps by participating in an important hydrogen bond. In the case of the replacement of Ser-155 by glycine, which displayed full retention of activity, the hydroxyl group could be supplied by a cavity-filling water molecule, a situation thought to occur in several well studied proteins upon substitution of glycine for a serine (35-37).

Topology of the cd Helix of Cytochrome *b*—The topology of the cd helix of cytochrome *b* was studied by comparing the reaction of NEM with the cysteines of wild type and mutated bc_1 complexes contained within the membranes of sealed (inside-out) versus detergent-disrupted chromatophores. The intactness of sealed chromatophores preparations was confirmed by measuring the increase of the bc_1 complex activity upon the

addition of detergent; this increase averaged 6-fold after treatment with 0.2% potassium deoxycholate. Three parallel experiments were performed on each sealed chromatophore preparation (see Fig. 1) (1). The sealed chromatophores were treated with 1 mM NEM followed with 2 mM DTT to remove any unreacted NEM. The chromatophores were then treated with 0.2% deoxycholate to break the membrane. This reaction sequence will label -SH groups accessible on the outside of the chromatophore membrane (cytoplasmic surface) but not those exposed on the inside of the vesicles or buried within the membrane or protein interior (2). The sealed chromatophores were disrupted with 0.2% deoxycholate and then treated with 1 mM NEM. The excess NEM was removed by the addition of 2 mM DTT. This reaction sequence should label all of the externally accessible cysteines from either side of the chromatophore membrane (cytoplasmic and periplasmic surfaces) (3). The sealed chromatophores were broken with 0.2% deoxycholate and then treated with 2 mM DTT prior to reaction with 1 mM NEM. This control reaction sequence provides unlabeled membranes that have gone through the experimental procedure, but with sulfhydryl modification blocked by the addition of DTT before NEM.

When sealed chromatophores prepared from complement, S175C, and A185C-expressing cells were treated with NEM, no change in cytochrome *bc*₁ complex activity was observed. When deoxycholate-disrupted chromatophores were treated with NEM, about 85% of the cytochrome *bc*₁ complex activity in the cytochrome *b* A185C substitution was abolished, while no change in activity was observed with complement or the cytochrome *b* S175C substitution. Since no change in the cytochrome *bc*₁ activity was observed after NEM treatment of either sealed or broken chromatophores from complement cells, the endogenous cysteine residues contained in the cytochrome *bc*₁ complex are probably inaccessible to NEM treatment (see below). This result greatly simplifies our assessment of the location of the engineered cysteines in the chromatophore membrane. Ala-185 of cytochrome *b* is located on the inside surface of the chromatophore membrane (periplasmic side) because NEM did not react with the cysteine residue engineered at cytochrome *b*

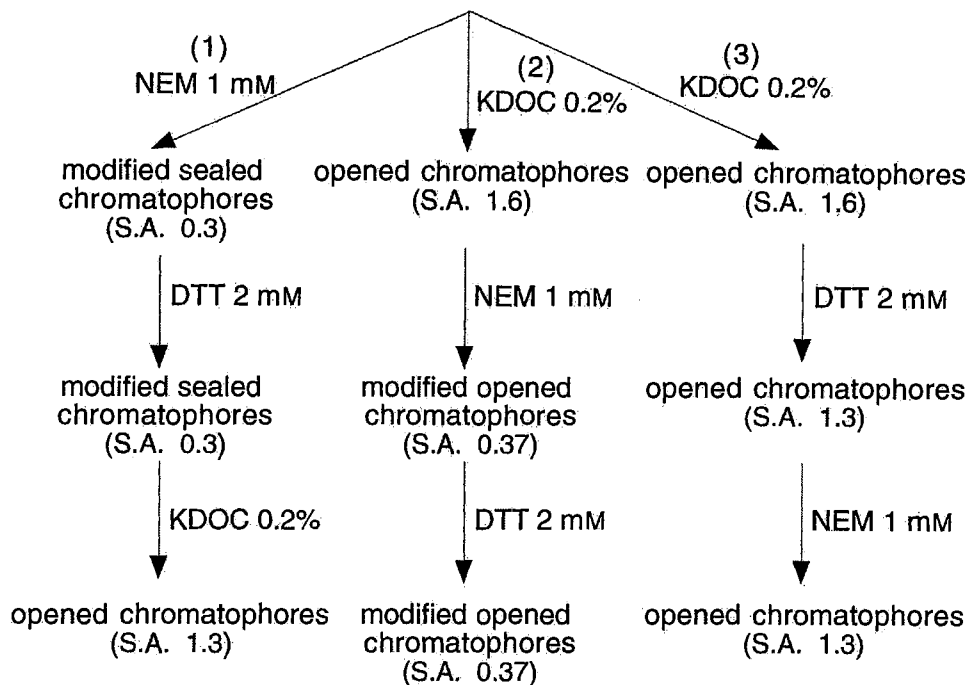


Figure 1. Reaction scheme for treatment of sealed and detergent-disrupted (opened) chromatophores with NEM for topological mapping. Sealed (inside-out) chromatophores were prepared as described under "Experimental Procedures." Three parallel experiments, as diagrammed in the figure, were performed on sealed chromatophore preparations obtained from complement, S175C, and A185C cells (see discussion under "Results and Discussion"). The specific activities (S.A.) observed with a representative preparation of chromatophores from cytochrome *b* A185C-expressing cells are provided as an illustrative example of the results obtained. A185C specific activity was 0.3 μmol of cytochrome *c* reduced/min/nmol of cytochrome *b*. KDOC, potassium deoxycholate.

position Ala-185 in the sealed inside-out chromatophore preparation, but it did react with this engineered cysteine in disrupted chromatophores. Since Ala-185 is contained in the cd loop connecting the C and D transmembrane helices of cytochrome *b*, the cd loop must also be on the periplasmic side of the chromatophore membrane. The placement of the cd loop on the periplasmic side of the chromatophore membrane is consistent with the current cytochrome *bc*₁ crystal structure from bovine heart, which describes the cytochrome *b* protein as a membrane-spanning polypeptide having eight transmembrane helices (named A-H) and several transversal helices on both sides of the membrane, including a cd helix comprising the amino-terminal portion of the cd loop located on the periplasmic side (34). The observation of no activity loss in both sealed and disrupted chromatophore preparations from the cytochrome *b* S175C mutant cells upon NEM treatment indicates that the Ser-175 position of the cd helix is inaccessible to the aqueous phase, either facing the interior of cytochrome *b* or covered by another subunit of the complex.

*Effect of NEM on Purified Cytochrome *bc*₁ Complexes from S175C and A185C Mutant Cells*—The cytochrome *bc*₁ complex contains nine cysteine residues: one in cytochrome *b*, four in cytochrome *c*₁, and four in the iron-sulfur protein. It has been established that two cysteines in the iron-sulfur protein are ligands to the [2Fe-2S] cluster (38), and two cysteines in cytochrome *c*₁ are covalently bonded to heme *c* (39). Thus, there are five free cysteines that are potential candidates for NEM modification. When the cytochrome *bc*₁ complex from complement strain was treated with NEM, no change in enzymatic activity was observed (Table II), indicating that cysteine residues contained in the cytochrome *bc*₁ complex are either inaccessible to NEM or the reaction product is functionally active. Radioactive NEM was used to distinguish these two possibilities. Since no radioactivity was found in any of the four subunits of the complement *bc*₁ complex treated with [³H]NEM (see Fig. 2), the lack of inhibition by NEM treatment must be due to the inaccessibility of the free cysteines rather than to formation of active cysteine-NEM products.

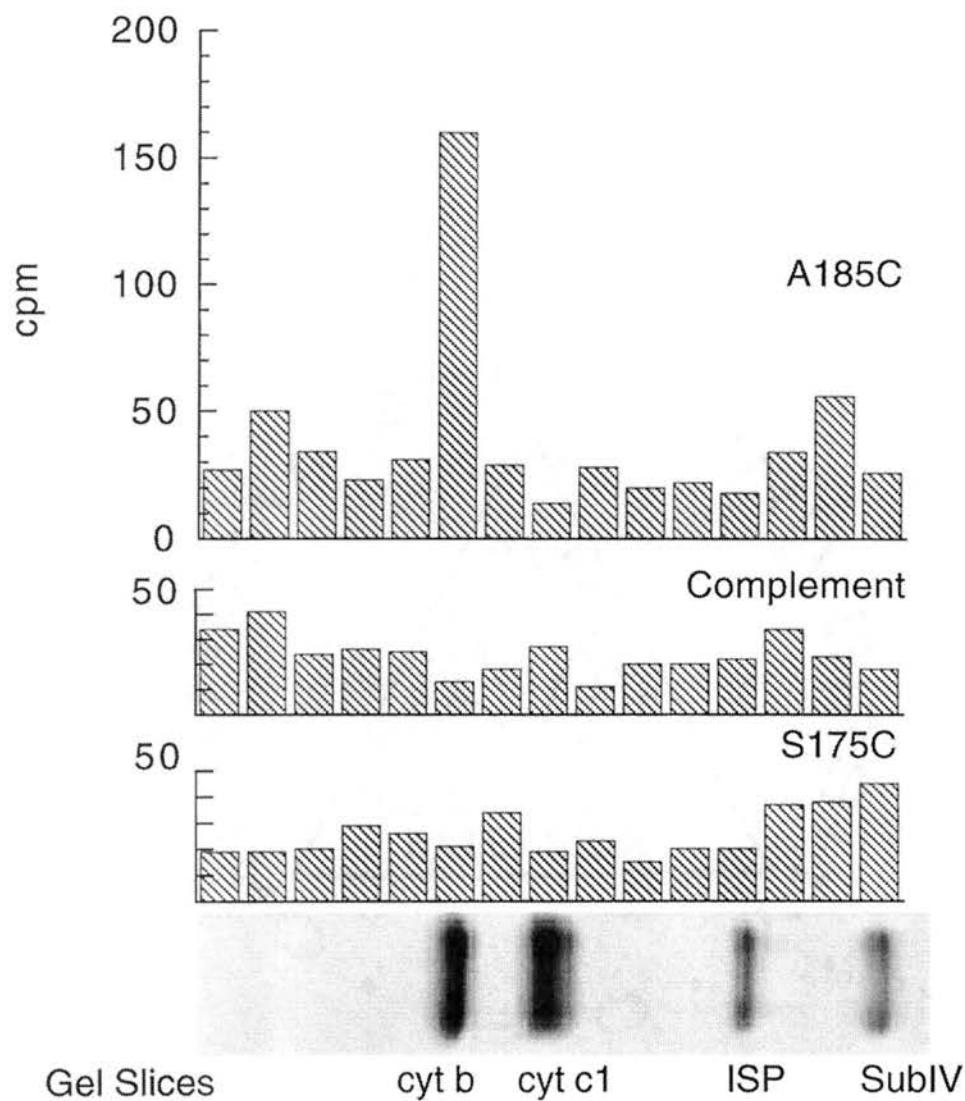


Figure 2. Radioactivity distribution among subunits of the cytochrome bc_1 complexes from complement, S175C, and A185C treated with $[^3\text{H}]\text{-NEM}$. Purified bc_1 complexes from complement, S175C, and A185C were incubated with $[^3\text{H}]\text{NEM}$ as described under "Experimental Procedures. ISP, iron-sulfur protein.

Table II.

The effect of NEM on the cytochrome bc₁ complexes from complement, S175C, and A185C cells

NEM (100 mM freshly prepared stock solution in H₂O) was added to the bc₁ complexes (10 nmol of cytochrome *b*/ml) at a 2-fold molar excess to cytochrome *b* heme. The treated samples were flushed briefly with nitrogen, sealed, and incubated at room temperature for 15 min before the cytochrome bc₁ complex activities were measured.

<i>bc</i> ₁ complex preparations	Activity (23°C)	
	No treatment	NEM treatment
	μmol cytochrome <i>c</i> reduced/min/nmol cytochrome <i>b</i>	
Complement	2.2	2.1
S175C	2.0	1.92
A185C	2.3	0.3

When the cytochrome bc_1 complex containing the cytochrome b S175C replacement was treated with NEM, no loss of activity was observed (see Table II), suggesting that Ser-175 of cytochrome b is shielded by other subunits or other parts of cytochrome b in the bc_1 complex. The inaccessibility of the engineered cysteine of cytochrome b to NEM treatment is further confirmed by the absence of radioactive labeling of the cytochrome b subunit of the cytochrome b S175C cytochrome bc_1 complex treated with [^3H]NEM (see Fig. 2). These results are consistent with the three-dimensional structure analysis of the bovine heart bc_1 complex, which shows that the amino acid residue corresponding to Ser-175 is not exposed on the surface of the molecule (34).

When the cytochrome b A185C-cytochrome bc_1 complex was treated with various concentrations of NEM, about 87% of the bc_1 activity was lost (Table II) when 2.0 mol of NEM/mol of cytochrome b heme was used, consistent with the results observed in chromatophores (see above). The loss of activity correlates with the incorporation of NEM into the cytochrome b subunit; when [^3H]NEM-treated cytochrome b A185C-cytochrome bc_1 complex, which had lost 87% of its activity, was subjected to SDS-PAGE, all of the radioactivity was located in the b subunit (Fig. 2). About 1 mol of NEM was incorporated into one mol of cytochrome b protein.

EPR Characteristics of Cytochrome b , Cytochrome c_1 , and Iron-Sulfur Cluster in NEM-treated, A185C Cytochrome bc_1 Complex—EPR spectra properties of cytochrome b , cytochrome c_1 , and the Rieske iron-sulfur cluster in the cytochrome b A185C-cytochrome bc_1 with and without NEM treatment, were examined in an attempt to identify which active centers of the complex are perturbed by the modification at position 185 and thus may interact with this region of cytochrome b .

Fig. 3 shows the EPR characteristics of cytochromes b in the cytochrome bc_1 complexes of complement and cytochrome b A185C with and without NEM treatment. The cytochrome b A185C-cytochrome bc_1 complex exhibits two EPR signals at $g = 3.5$ and $g = 3.76$, corresponding to b565 and b562, respectively. These two b signals are identical to

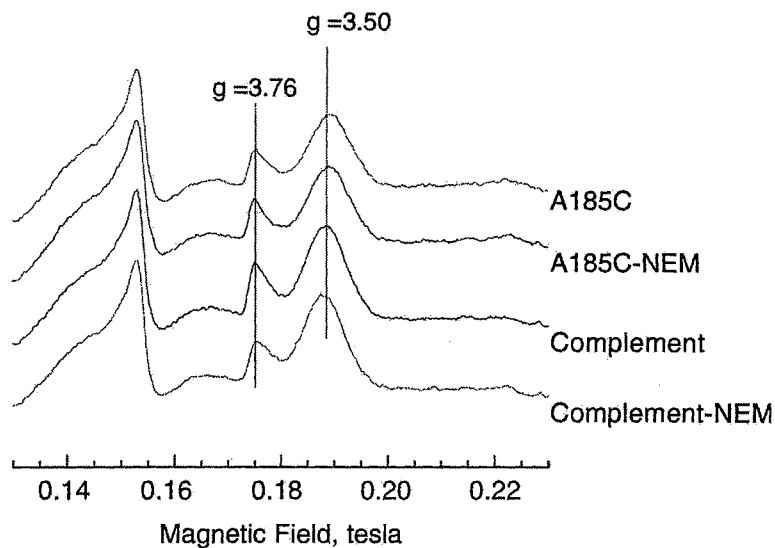


Figure 3. The EPR spectra of *b* cytochromes in purified *bc*₁ complexes of complement and mutant cytochrome *b*: A185C with and without NEM treatment.

Cytochrome *bc*₁ complexes were partially reduced by the addition of 1 mM sodium ascorbate. The samples were incubated at 0 °C for 20 min before freezing in liquid nitrogen. EPR spectra were recorded at 7 K with the following instrument settings: microwave frequency, 9.27 GHz; microwave power, 20 milliwatts; modulation amplitude, 20 G; time constant, 0.1 s; scan rate, 5 G/s.

those observed in cytochrome *b* of the complement bc_1 complex, indicating that the cytochrome *b* A185C substitution probably has little effect on the cytochrome *b* heme environments. When the cytochrome *b* A185C-cytochrome bc_1 complex was treated with NEM to inactivate the complex, the EPR characteristics of cytochrome *b* (Fig. 3) and cytochrome c_1 (data not shown) in the treated complex were the same as those in the untreated complex, suggesting that Ala-185 is not involved in interaction with the hemes of the cytochrome *b* molecule or with cytochrome c_1 .

Fig. 4 compares EPR characteristics of the Rieske iron-sulfur clusters in the cytochrome bc_1 complexes of complement and A185C, with and without NEM treatment. When complement and A185C-substituted bc_1 complexes were reduced by a small excess of ascorbate, the EPR signals of the Rieske iron-sulfur cluster in these two cytochrome bc_1 complexes were essentially the same, with resonances at $g_z = 2.02$, $g_y = 1.89$, and $g_x = 1.80$. However, when the A185C bc_1 was treated with NEM, the $g_x = 1.80$ signal broadened and shifted to 1.75, while no change in the iron-sulfur spectrum was observed in NEM-treated complement bc_1 complex. Upon complete reduction of the NEM-treated complement and A185C mutant bc_1 complexes with dithionite, the spectrum of the bc_1 complement complex is broadened, with g_x shifting to 1.75, as previously reported for the wild type bc_1 complex under fully reduced conditions (4, 5), whereas the dithionite-reduced spectrum of the NEM-treated A185C complex remains unchanged with $g_x = 1.75$. The NEM-treated A185C complex thus has a spectrum closely resembling the "reduced state" spectrum of the complement, regardless of the redox state of the ubiquinone pool.

The iron-sulfur subunit is thought to bind in the general vicinity of b565 on the positive side of the membrane to form part of the quinol-oxidizing center, because the iron-sulfur cluster is a primary electron acceptor from the quinol. The particular line shape observed for the [2Fe-2S] cluster is thought to be mediated by the oxidation state of the ubiquinone present in the Q_o site (4, 5, 40-42). When oxidized quinone is present, the g_x signal is sharper than that observed when quinol is present. The g_x of the bc_1 from *R*.

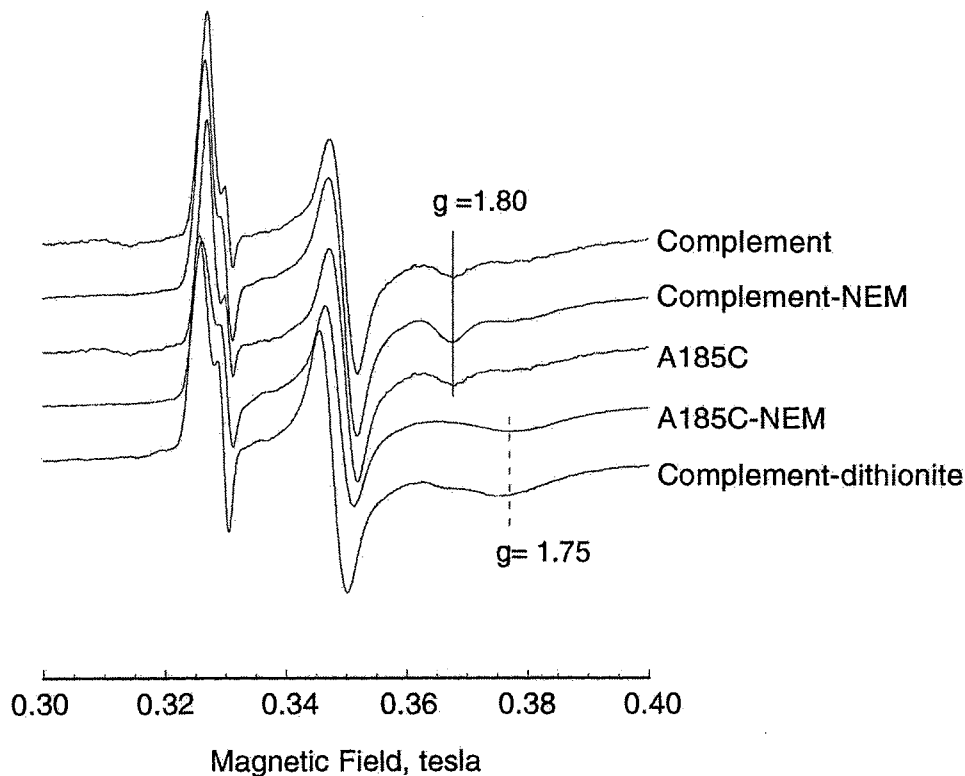


Figure 4. The EPR spectra of the Rieske [2Fe-2S] cluster in the cytochrome bc_1 complexes of complement and mutant cytochrome b : A185C with and without NEM treatment. Partially purified cytochrome bc_1 complexes obtained after the first ion-exchange column chromatography step during the purification process were treated with NEM. Excess modifying reagent was removed from the mixture by applying the treated sample to a second ion-exchange column and extensively washing with washing buffer. No free NEM was present in the purified bc_1 complex eluted from the second column. The ascorbate-reduced cytochrome bc_1 complexes were prepared as described in Fig. 3. The EPR spectra were recorded at 10 K. Instrument settings were the same as in Fig. 3.

sphaeroides is found at $g = 1.80$ when ubiquinone is present, but shifts to 1.75 and becomes much broader when ubiquinol is present. NEM modification of the engineered cysteine at position 185 of cytochrome *b* resulted in broadened [2Fe-2S] EPR signals with $g_x = 1.75$, independent of the redox potential. There was no detectable difference between the EPR spectrum of the NEM-treated A185C complex and the full reduction spectrum of the NEM-treated and -untreated complement bc_1 complex. The effect of NEM treatment on the iron-sulfur cluster spectrum suggests that the Ala-185 residue of cytochrome *b* interacts with the [2Fe-2S] cluster or is located in the close vicinity of the cluster. This idea is consistent with the current x-ray crystal structure of this part of the complex (34).

The effect of NEM treatment on the iron-sulfur cluster of the A185C bc_1 complex is also reminiscent of the change observed for the substitution of Leu for Phe-144 (F144L) in the cytochrome *b* from *R. capsulatus* (41). The F144L bc_1 complex in *R. capsulatus* chromatophores was reported to have a very low turnover rate with a broadened, redox state-insensitive, g_x value at 1.765. It was suggested that these properties of the F144L complex resulted from a reduced affinity for quinone and quinol exhibited by the Q_o center of the mutated complex. In a subsequent study of the effect of extraction of ubiquinone from chromatophore membranes on the iron-sulfur cluster, Ding et al. (42) found that the g_x signal of the "depleted state" at approximately $g = 1.765$ was broadened considerably beyond that seen in the presence of either ubiquinone or ubiquinol. Since the changes in the g_x signal of iron-sulfur clusters resulting from the NEM modification of Cys-185 of *R. sphaeroides* cytochrome *b* in the complex do not exhibit the extremely broad line shape reported for the quinone-depleted state, they are probably not due to a complete absence for quinone and quinol binding to the Q_o center.

[³H]NEM Modification of Rieske Iron-Sulfur Protein-depleted bc_1 Complex—Since we have shown that the Ala-185 residue of cytochrome *b* is near the iron-sulfur protein, the inaccessibility of the engineered cysteine at position 175 could be the result of close interaction between the iron-sulfur protein and the cd helix of cytochrome *b*. In that case,

removal of iron-sulfur protein from the bc_1 complex might expose Ser-175 and thus make it accessible to NEM. The bc_1 complex was dissociated into Rieske iron-sulfur protein and the iron-sulfur protein-depleted bc_1 subcomplex by incubation with Na_2CO_3 (pH 10.5) under reducing conditions (43). The addition of urea (0.6 M) to the solution helps the dissociation process. Since NEM is not stable at alkaline pH, modification of dissociated subcomplex cannot be carried out without neutralization. To prevent the reassociation of the iron-sulfur protein to the complex upon neutralization, the dissociated iron-sulfur protein was removed by pH sucrose density gradient centrifugation. This density gradient serves two purposes: to separate the iron-sulfur protein from the bc_1 subcomplex and to restore neutral pH to avoid further destruction of subcomplex. Under the centrifugation conditions used, the subcomplex and iron-sulfur protein fractions are well separated. A typical distribution of the two components obtained after centrifugation is shown in Fig. 5. The fractions at the top of the gradient contained iron-sulfur protein, whereas the fractions at the bottom contained the larger, faster sedimenting bc_1 subcomplex. The bc_1 subcomplex was modified with [^3H]NEM after removal of DTT by repeated dilution and concentration using Centricon-30. The incorporation of NEM into wild type bc_1 subcomplex was 1.1 NEM/ bc_1 , while 2.2 molecules of NEM were incorporated into subcomplex with the S175C replacement. Fig. 6 shows the ^3H radioactivity distribution among subunits of complement and S175C-substituted cytochrome bc_1 subcomplexes. When [^3H]NEM-treated complement cytochrome bc_1 subcomplex was subjected to SDS-PAGE, radioactivity was found in cytochrome c_1 subunit (see Fig. 6A), indicating that one of the cysteines in cytochrome c_1 is shielded by the iron-sulfur protein in the intact bc_1 complex and became accessible to NEM after its removal. When the cytochrome bc_1 subcomplex containing cytochrome b with the S175C mutation was treated with [^3H]NEM, both cytochrome b and cytochrome c_1 subunits became labeled (see Fig. 6B), indicating that Ser-175 of cytochrome b is also shielded by the iron-sulfur protein in the intact bc_1 complex.

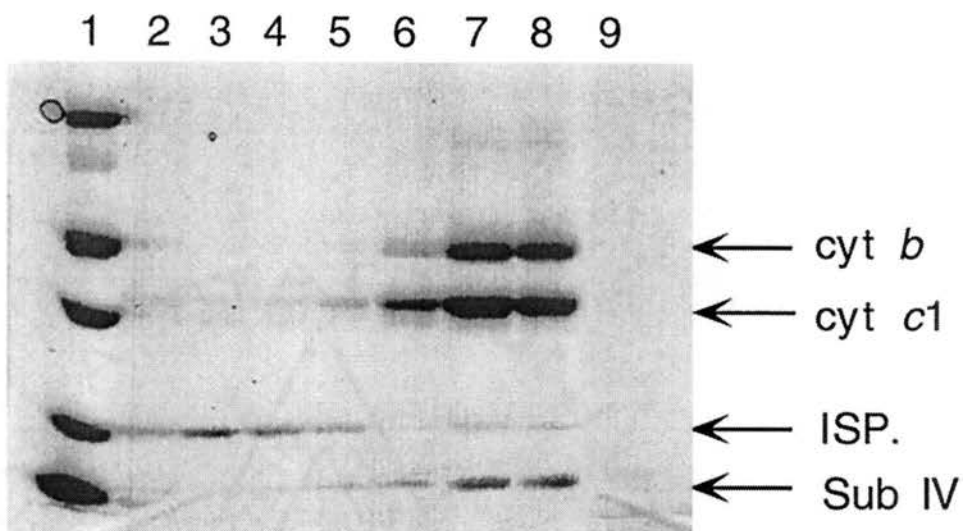


Figure 5. Gel pattern of pH sucrose gradient fractions of the alkaline-treated cytochrome *bc*₁ complex. Aliquots of selected fractions of the gradient were analyzed by SDS-PAGE. Lane 1, molecular weight standards; lanes 2-5, top four fractions from the gradient rich in iron-sulfur protein (ISP); lanes 6-8, red fractions from the middle of the gradient mainly consisting of cytochrome *b*, cytochrome *c*₁, and subunit IV (the pH of these middle fractions is neutral); lane 9, the bottom-most fraction, which contains no significant protein bands.

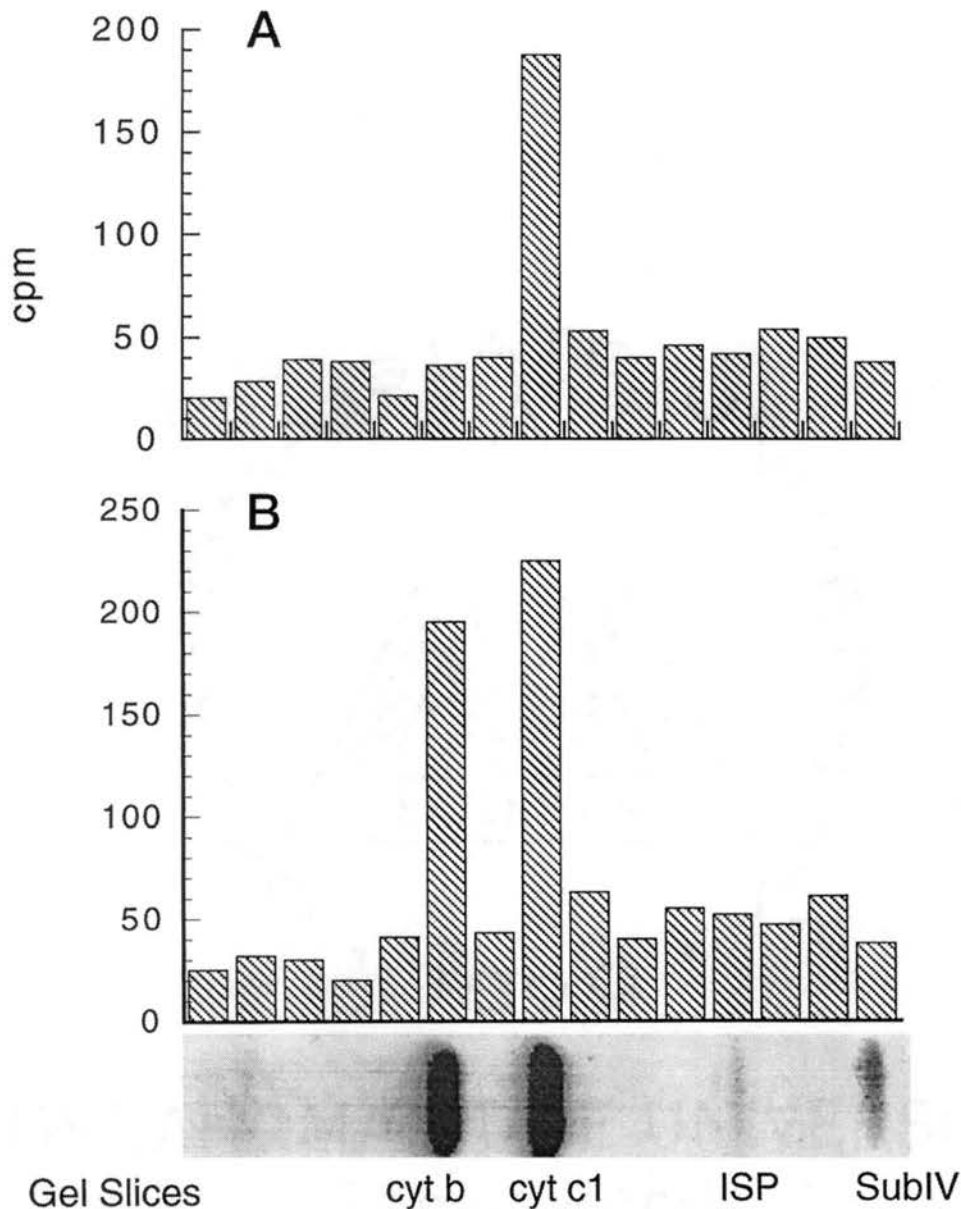


Figure 6. [³H]NEM distribution among subunits of the iron-sulfur protein (ISP)-depleted *bc*₁ subcomplexes. The iron-sulfur protein-depleted subcomplexes of complement (A) and S175C (b) cytochrome *bc*₁ were treated with [³H]NEM as described under "Experimental Procedures," and the samples were subjected to denaturing SDS-PAGE, along with control samples labeled with cold NEM. The gels containing radioisotope labeled samples were divided into 3-mm slices, and the radioactivity was counted. The positions of the subunits were determined by staining the control gels.

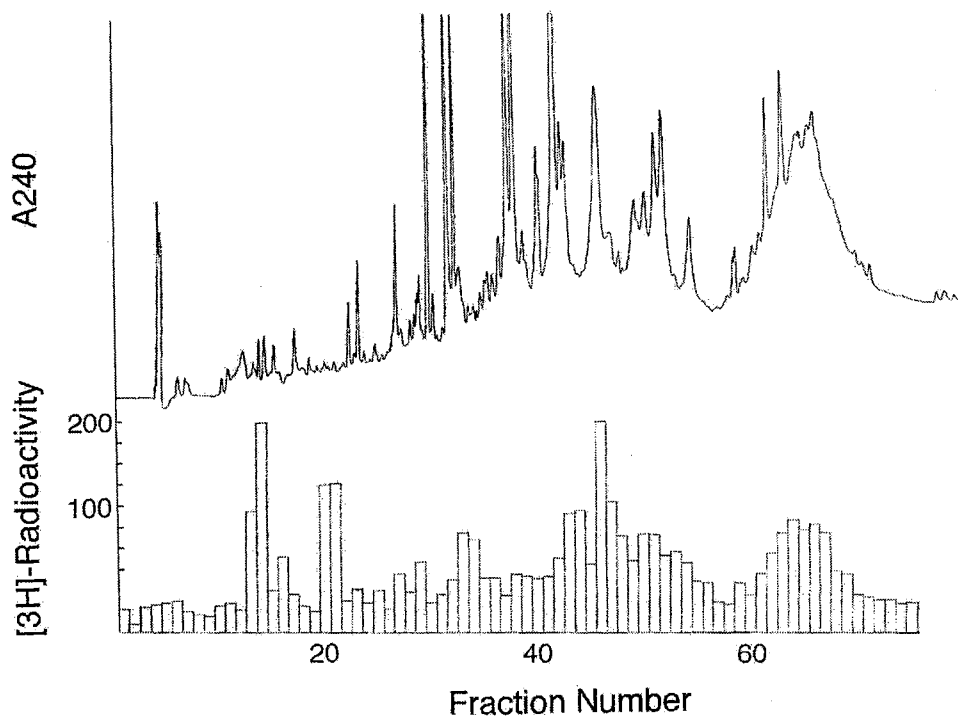


Figure 7. ^3H radioactivity distribution in an HPLC chromatogram of Arg-C-digested, ^3H NEM-labeled cytochrome c_1 protein. The ^3H NEM-labeled cytochrome c_1 (1mg/ml, 2×10^4 cpm/mg) was digested with Arg-C, and 100 μl aliquots of digested solution were subjected to HPLC separation as described under "Experimental Procedures". 100 μl aliquots of the separated HPLC fractions were with-drawn for radioactivity determination.

Isolation of a [³H]NEM-labeled Peptide from Cytochrome *c*₁—The fact that one of the cysteines from cytochrome *c*₁ became labeled in *bc*₁ subcomplex indicates that this cysteine may be located in the interface between cytochrome *c*₁ and the iron-sulfur protein. To identify which one of the cysteines reacts with NEM, [³H]NEM-labeled cytochrome *c*₁ was eluted from SDS-PAGE gels and digested with arginine-specific protease (Arg-C). Fig. 7 shows the radioactivity distribution among the Arg-C-digested peptides of cytochrome *c*₁ separated by HPLC. The majority of the radioactivity was found in fractions 14, 22, and 47. Since very few amino acids were detected in fractions 14 and 22, it is likely that they contained decomposed [³H]NEM. Some radioactivity was also found in fractions 60-70, due to the incomplete digestion of cytochrome *c*₁.

The partial N-terminal amino acid sequence of the labeled peptide in fraction 47 was determined to be AGFHGPMGT. From the primary sequence of cytochrome *c*₁, this can be seen to be the initial portion of the expected Arg-C proteolytic fragment encompassing residues 130-180. The only cysteine in this peptide is Cys-167, which is thought to be located in the soluble domain of cytochrome *c*₁. Our results suggest that the region containing Cys-167 forms part of the interface of cytochrome *c*₁ with the Rieske iron-sulfur protein. Elucidation of the exact docking surfaces of these two subunits, as well as of cytochrome *b* and the iron-sulfur protein, requires refinement of the crystal structure and/or other detailed protein characterizations.

REFERENCES

1. Gabellini, N., Bowyer, J. R., Hurt, E., Melandri, B. A., and Hauska, G. (1982) *Eur. J. Biochem.* **126**, 105-111.
2. Ljungdahl, P. O., Pennoyer, J. D., Robertson, D. E., and Trumpower, B. L. (1987) *Biochim. Biophys. Acta* **891**, 227-241.
3. Yu, L., Mei, Q-C., and Yu, C. A. (1984) *J. Biol. Chem.* **259**, 5752-5760.
4. McCurley, J. P., Miki, T., Yu, L., and Yu, C. A. (1990) *Biochim. Biophys. Acta* **1020**, 176-186.
5. Andrews, K. M., Crofts, A. R., and Gennis, R. B. (1990) *Biochemistry* **29**, 2645-2651.
6. Purvis, D. J., Theiler, R., and Niederman, R. A. (1990) *J. Biol. Chem.* **265**, 1208-1215.
7. Yu, L., and Yu, C. A. (1987) *Biochemistry* **26**, 3658-3663.
8. Trumpower, B. L., and Gennis, R. B. (1994) *Annu. Rev. Biochem.* **63**, 675-716.
9. Brasseur, G., Saribas, A. S., and Daldal, F. (1996) *Biochim. Biophys. Acta* **1275**, 61-69.
10. Mitchell, P. (1976) *J. Theor. Biol.* **62**, 327-367.
11. Trumpower, B. L. (1990) *J. Biol. Chem.* **265**, 11409-11412.
12. Brandt, U., and Trumpower, B. (1994) *Crit. Rev. Biochem. Mol. Biol.* **29**, 165-197.
13. He, D-Y., Yu, L., and Yu, C. A. (1994) *J. Biol. Chem.* **269**, 2292-2298 [Medline]
14. Yun, C. H., Beci, R., Crofts, A. R., Kaplan, S., and Gennis, R. B. (1990) *Eur. J. Biochem.* **194**, 399-411.
15. Crofts, A., Robinson, H., Andrew, K., Van Doren, S., and Berry, E. (1987) in *Cytochrome Systems: Molecular Biology and Bioenergetics* (Papa, S., Chance, B., and Ernster, L., eds), pp. 617-631, Plenum Publishing Corp., New York
16. di Rago, J. P., Coppee, J. Y., and Colson, A. M. (1989) *J. Biol. Chem.* **264**, 14543-14548
17. Atta-Asafo-Adjei, E., and Daldal, F. (1991) *Proc. Natl. Acad. Sci. U. S. A.* **88**, 492-496.
18. Ding, H., Daldal, F., and Dutton, P. L. (1995) *Biochemistry* **34**, 15997-16003.
19. Mather, M. W., Yu, L., and Yu, C. A. (1995) *J. Biol. Chem.* **270**, 28668-28675.

20. Simon, R., Prierer, U., and Puhler, A. (1983) *Bio/Technology* **1**, 784-791
21. Khosravi, M., Ryan, W., Websger, D. A., and Stark, B. C. (1990) *Plasmid* **23**, 138-143.
22. Sistrom, W. R. (1960) *J. Gen. Microbiol.* **22**, 778-785
23. Promega Corp. (1996) Altered Sites™ in Vitro Mutagenesis Systems, Technical Manual, Promega Corp., Madison, WI
24. Sambrook, J., Fritsch, E. F., and Maniatis, T. (1989) *Molecular Cloning: A Laboratory Manual, 2nd Ed.*, Cold Spring Harbor Laboratory, Cold Spring Harbor, NY
25. Du, Z., Hood, L., and Wilson, R. K. (1993) *Methods Enzymol.* **218**, 104-121.
26. Suwanto, A., and Kaplan, S. (1992) *J. Bacteriol.* **174**, 1124-1134.
27. Hunter, D. N., Pennoyer, J. D., Sturgis, J. N., Farrelly, D., and Niederman, R. A. (1988) *Biochemistry* **27**, 3459-3467
28. Yu, L., and Yu, C. A. (1991) *Biochemistry* **30**, 4934-4939.
29. Lowry, O. H., Rosebrough, N. J., Farr, A. L., and Randall, R. J. (1951) *J. Biol. Chem.* **193**, 265-275
30. Cohen-Bazzire, G., Sistrom, W. R., and Stanier, R. Y. (1957) *J. Cell. Comp. Physiol.* **49**, 25-68
31. Berden, J. A., and Slater, E. C. (1970) *Biochim. Biophys. Acta* **216**, 237-249.
32. Yu, L., Dong, J-H., and Yu, C. A. (1986) *Biochim. Biophys. Acta* **852**, 203-211.
33. Laemmli, U. K. (1970) *Nature* **227**, 680-685.
34. Xia, D., Kim, H., Deisenhofer, J., Yu, C. A., Xia, J-Z., Kachurin, A. M., Zhang, L., and Yu, L. (1997) *Science* **277**, 60-66.
35. Lewendon, A., Murray, I. A., Shaw, W. V., Gibbs, M. R., and Leslie, A. G. (1990) *Biochemistry* **29**, 2075-2080.
36. Paddock, M. L., Feher, G., and Okamura, M. Y. (1995) *Biochemistry* **34**, 15742-15750.
37. Cannon, W. R., Briggs, J. M., Shen, J., McCammon, J. A., and Quioco, F. A. (1995) *Protein Sci.* **4**, 387-393.

38. Davidson, E., Ohnishi, T., Atta-Asafo-Adjei, E., and Daldal, F. (1992) *Biochemistry* **29**, 3342-3351
39. Gray, K. A., Davidson, E., and Daldal, F. (1992) *Biochemistry* **31**, 11864-11873.
40. Meinhardt, S. W., Yang, X., Trumpower, B. L., and Ohnishi, T. (1987) *J. Biol. Chem.* **262**, 8702-8706.
41. Roberson, D. E., Daldal, F., and Dutton, P. L. (1990) *Biochemistry* **29**, 11249-11260
42. Ding, H., Robertson, D. E., Daldal, F., and Dutton, P. L. (1992) *Biochemistry* **31**, 3144-3152.
43. Szczepaniak, A., Huang, D., Keenan, T. W., and Cramer, W. A. (1991) *EMBO J.* **10**, 2757-2764.

CHAPTER III

Flexibility of the Neck Region of the Rieske Iron-Sulfur Protein Is Functionally Important in the Cytochrome *bc*₁ Complex

Hua Tian, Linda Yu, Michael W. Mather, and Chang-An Yu

The Journal of Biological Chemistry, 273 27953-27959 (1998)

ABSTRACT

The crystal structure of the mitochondrial cytochrome bc_1 complex suggests that movement of the extramembrane (head) domain of the Rieske iron-sulfur protein (ISP) is involved in electron transfer. Such movement requires flexibility in the neck region of ISP. To test this hypothesis, *Rhodobacter sphaeroides* mutants expressing His-tagged cytochrome bc_1 complexes with altered ISP necks (residues 39-48) were generated and characterized. Mutants with increased rigidity of the neck, generated by a double-proline substitution at Ala-46 and Ala-48 (ALA-PLP) or by a triple-proline substitution of ADV at residues 42-44 (ADV-PPP), have retarded (50%) or no photosynthetic growth, respectively. However, the mutant with a shortened neck, generated by deleting ADV (Δ ADV), has a photosynthetic growth rate comparable to that of complement cells, indicating that the length of the ISP neck is less critical than its flexibility in support of photosynthetic growth. The Δ ADV and ALA-PLP mutant membranes have 10 and 30% of the cytochrome bc_1 complex activity found in the complement membrane, respectively, whereas the ADV-PPP mutant membrane contains no cytochrome bc_1 complex activity. The loss of cytochrome bc_1 complex activity in the Δ ADV membrane is attributed to improper docking of the head domain of ISP on cytochrome b, as indicated by a drastic change in the EPR characteristics of the Rieske iron-sulfur cluster. The loss of cytochrome bc_1 complex activity in the ALA-PLP and ADV-PPP mutant membranes results from the decreased mobility of the ISP head domain due to the increased rigidity of the ISP neck. The ALA-PLP mutant complex has a larger activation energy than the wild-type complex, suggesting that movement of the head domain decreases the activation energy barrier of the cytochrome bc_1 complex. Using the conditions developed for the isolation of the His-tagged complement cytochrome bc_1 complex, a two-subunit complex (cytochromes b and c_1) was obtained from the Δ ADV and ADV-PPP mutants, indicating that mutations at the neck region of ISP weaken the interactions among cytochrome b , ISP, and subunit IV.

INTRODUCTION

The cytochrome bc_1 complex (ubiquinol-cytochrome c reductase) is an essential segment of the energy-conserving electron transfer chains of mitochondria and many respiratory and photosynthetic bacteria (1). The complex catalyzes electron transfer from ubiquinol to cytochrome c and concomitantly translocates protons across the membrane to generate a membrane potential and pH gradient for ATP synthesis. The polypeptide composition of the cytochrome bc_1 complex from different sources varies from 3 to 11 subunits. The redox subunits (cytochrome b , cytochrome c_1 , and the Rieske iron-sulfur protein (ISP) are conserved in all the cytochrome bc_1 complexes. The proton-motive Q-cycle model (2) has been favored for electron transfer and proton translocation in the complex. The key feature of this model is the presence of two separate ubiquinone- or ubiquinol-binding sites: a ubiquinol oxidation site (Q_o), near the P side of the inner mitochondrial membrane, and a ubiquinone reduction site (Q_i), near the N side of the membrane. The recently solved three-dimensional structure of the mitochondrial cytochrome bc_1 complex not only answered a number of questions concerning the arrangement of the redox centers, transmembrane helices, and Q-like inhibitor-binding sites, but also suggested an unexpected dynamic feature of this complex (3-9).

Mobility of ISP in the bc_1 crystal was first suggested by observation of a particularly low electron density area, in the intermembrane space portion of the complex, where the extramembrane domains of ISP and cytochrome c_1 reside (4). The mobility of the extramembrane (head) domain of ISP was further substantiated by the anomalous light scattering signals of the [2Fe-2S] cluster observed in native and co-crystals with Q_o site inhibitors, such as stigmatellin, 5-n-undecyl-6-hydroxy-4,7-dioxobenzothiazole, and methoxyacetylate stilbene (5, 6, 8). In a native beef bc_1 crystal, a much weaker anomalous light scattering signal was observed for the [2Fe-2S] cluster compared with that for the heme iron, b_H or b_L , despite the presence of two irons in the cluster. Furthermore, the

anomalous scattering signal of the [2Fe-2S] cluster was strongly enhanced in a co-crystal with stigmatellin, indicating that ISP is in a fixed state in the presence of this inhibitor. On the other hand, the signal diminished in a co-crystal with methoxyacetylate stilbene, suggesting that ISP is in a released state (6). Stigmatellin and methoxyacetylate stilbene are bound to different locations in the Q_o pocket, the former being closer to histidine ligands of the [2Fe-2S] cluster and the latter being closer to heme b_L .

In the beef bc_1 crystal, the distances between heme b_L and the [2Fe-2S] cluster and between the [2Fe-2S] cluster and heme c_1 , are 27 and 31 Å, respectively. Although the distance of 27 Å between heme b_L and the [2Fe-2S] cluster accommodates well the observed fast electron transfer between these two redox centers, the 31-Å distance between the [2Fe-2S] cluster and heme c_1 is difficult to understand in view of the rapid electron transfer rate observed for these two redox centers (10, 11). Movement of the extramembrane domain of ISP, as described below, offers an explanation for this paradox. The [2Fe-2S] cluster is reduced by the first electron of ubiquinol at a position 27 Å from heme b_L and 31 Å from cytochrome c_1 . The reduced [2Fe-2S] cluster cannot donate an electron to cytochrome c_1 before the second electron of ubiquinol is transferred to heme b_L . It was speculated that either the change of the ubisemiquinone binding position before the reduction of heme b_L or the electron transfer from heme b_L to b_H causes a conformational change in cytochrome b that forces or allows reduced [2Fe-2S] to move close enough to heme c_1 for fast electron transfer (6, 8). This model would also explain why ubisemiquinone, a more powerful reductant than ubiquinol, reduces heme b_L , but not the [2Fe-2S] cluster, during ubiquinol oxidation.

The ISP structure of beef heart mitochondria has three domains: the membrane-spanning N-terminal domain consisting of residues 1-62 (tail), the soluble C-terminal extramembrane domain consisting of residues 73-196 (head), and the flexible linking domain comprising residues 63-72 (neck). ISP is associated with the complex via the membrane-spanning N-terminal domain (4, 7, 9). The [2Fe-2S] cluster is located in the

rigid head domain as shown in the high resolution structure of the water-soluble fragment of ISP (12, 13). The electron density in the neck region is low; the structure was deduced by connecting the C-terminal end of the transmembrane helix to the N terminus of the head domain. No ordered secondary structure was reported in the neck region (4, 7).

Although the position of the iron-sulfur cluster changed from a fixed state to a released state upon methoxyacetylate stilbene binding (6), the three-dimensional structures of the head and tail domains of ISP remain the same in these two states, suggesting that a bending of the neck is required for movement of the head domain (7). For the neck region to bend, some flexibility is imperative. The beef ISP neck has 10 amino acid residues with a sequence of SASADVLAMS. This region is highly conserved in all iron-sulfur proteins (Fig. 1). The well conserved alanine residues may provide the needed flexibility. In the crystal structure, the neck region is in close contact with the cd1 helix of cytochrome *b*, but is not involved in compact docking between subunits, thus leaving enough space for bending (Fig. 2). The neck region is exposed to solvent as indicated by its susceptibility to several proteases, including thermolysin and trypsin (13).

If movement of the head domain of ISP is required for bc_1 catalysis and the neck region of ISP confers the necessary mobility, changing the flexibility of the neck region of ISP should drastically affect the catalytic activity of the bc_1 complex. One way to prove this suggestion is to prepare recombinant mutant ISP, with increased rigidity in the neck, by site-directed mutagenesis followed by in vitro reconstitution of mutant ISP to an ISP-depleted bc_1 complex. Biochemical and biophysical characterizations of the reconstituted bc_1 complexes should reveal the essentialness of neck flexibility. Although the beef cDNA for ISP has been cloned and sequenced (14), the unavailability of reconstitutively active recombinant ISP and the difficulty in preparing fully reconstitutively active ISP-depleted bc_1 complex (15) have prevented us from taking this approach. The four-subunit cytochrome bc_1 complex from the photosynthetic bacterium *Rhodobacter sphaeroides* is functionally analogous to the mitochondrial bc_1 complex. Since the largest three subunits are

Bo	SHTDIKVPDFSDYRRPEVL	<u>DSTKSSKESSEARKGFSYLV</u>	TATTTVGVAYA	AKNV	VSQFVMNMSA	SADVL	LAMS
Rs	MSNAEDHAG	TRRD	FLYY	ATAGAGAVATGAA	VWPLINQMNP	SADVQ	ALA
Rc	MSHAEDNAG	TRRD	FLYH	ATAATGVVVTGAA	VWPLINQMNA	SADVK	AMA
Sc		KST YRTPNFDDVL	KENNDADKGRSYAYFMV	GAMGLLSSAGAKSTVET	FISSMTAT	ADV	LAMA
Pd	MSHADEHAGDHGATR	TRRD	FLYY	ATAGAGTVAAGAA	AWTLVNQMNP	SADVQ	ALA
Nc	GSSSSTFESPFEGESKA	AKVPDFGKYMSKAPP	STNML	FSY FMVGTMGAITAAG	AKSTIQEFLKNMSA	SADV	LAMA

↓

Figure 1. Sequence alignment of amino-terminal portions of Rieske iron-sulfur proteins from different species. The neck regions are shaded. **Boldface** residues are conserved in at least five of the sequences. The **underlined** sequence is the transmembrane helix anchor of bovine ISP. The **arrow** indicates the thermolysin cleavage site that Link *et al.* (13) used to generate the head domain for structure analysis of the bovine protein. The ISPs are from bovine heart (*Bo*), *R. sphaeroides* (*Rs*), *R. capsulatus* (*Rc*), *S. cerevisiae* (*Sc*), *Paracoccus denitrificans* (*Pd*), and *Neurospora crassa* (*Nc*).

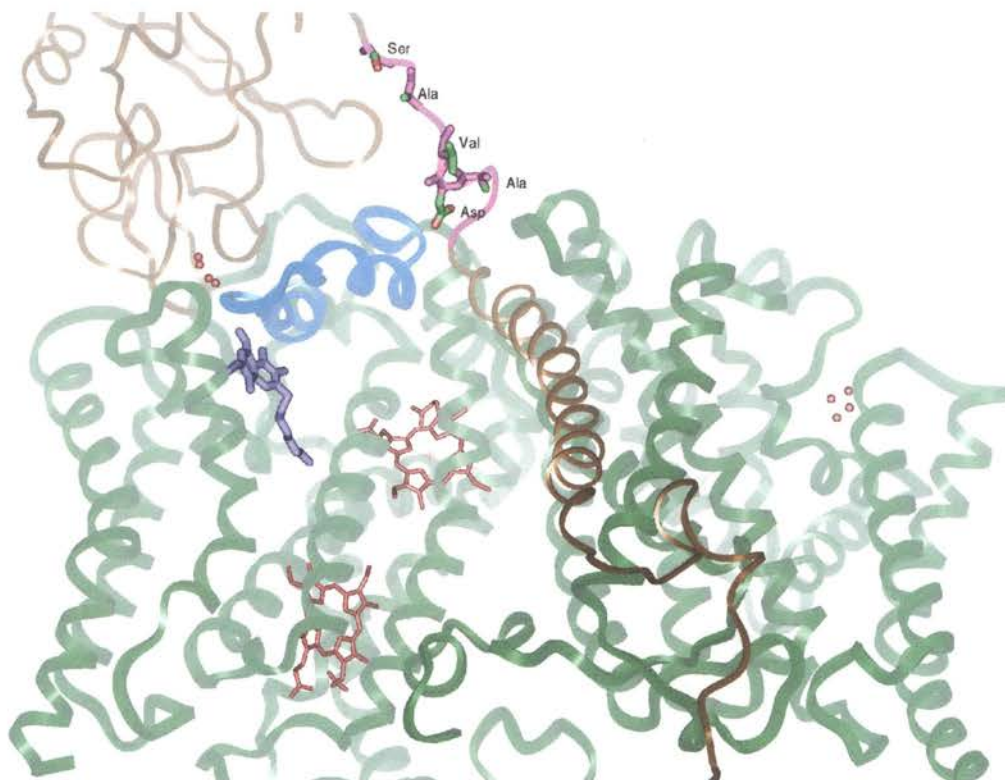


Figure 2. Local environment of the ISP neck region. ISP is brown ribbon, with the neck region highlighted in light purple. The side chains of conserved amino acid residues that were mutated are displayed as green sticks. Cytochrome *b* is a green ribbon, with the cd helices highlighted in blue. Stigmatelin (purple stick) is within the Q_o pocket.

homologous to their mitochondrial counterparts and are readily manipulated genetically, this organism is ideal for studying the neck region of ISP by site-directed mutagenesis.

Herein we report the generation and characterization of three *R. sphaeroides* mutants expressing His₆-tagged cytochrome *bc*₁ complexes with altered ISP neck regions. The length of the neck was shortened by deletion, and its rigidity was increased by proline substitution at various positions. The photosynthetic growth behavior, EPR characteristics of the Rieske [2Fe-2S] cluster, activation energy, and the cytochrome *bc*₁ complex activity in membranes and the purified state from the complement and mutant strains were examined and compared. The effect of the neck region of ISP on the interaction between cytochrome *b* and ISP or subunit IV was determined.

EXPERIMENTAL PROCEDURES

Materials-- Dodecyl maltoside (DM) and octyl glucoside were purchased from Anatrace. Stigmatellin was from Fluka. All other chemicals were of the highest purity commercially available. The Ni²⁺-NTA resin used for purification of the His₆-tagged cytochrome *bc*₁ complex was purchased from QIAGEN Inc. Restriction endonucleases and other DNA-modifying enzymes were purchased from Promega, Life Technologies, Inc., and New England Biolabs, Inc. pSELECT-1 plasmid, R408 helper phage, and BMH71-18 mutS and JM109 *Escherichia coli* strains used in mutagenesis were from Promega. pSELNB3503 and pRKD*fb*cFBCQ were constructed in our laboratory (16). *E. coli* S17 (17) and *R. sphaeroides* BC17 (18) were generously provided by Dr. R. B. Gennis (University of Illinois). 2,3-Dimethoxy-5-methyl-6-(10-bromodecyl)-1,4-benzoquinol (Q₀C₁₀BrH₂) was synthesized as described previously (19).

Growth of Bacteria—*E. coli* cells were grown at 37 °C on LB medium. Extra-rich medium (TYP) was used in procedures for the rescue of single-stranded DNA or the purification of low copy number plasmids (20). *R. sphaeroides* cells were grown at 30 °C

on enriched Sistrom's medium either semi-aerobically or photoheterotrophically (photosynthetic growth) as reported (21). Antibiotics were added at the following concentrations: ampicillin, 100-125 mg/liter; tetracycline, 10-15 mg/liter for *E. coli* and 1 mg/liter for *R. sphaeroides*; kanamycin sulfate, 30-50 mg/liter for *E. coli* and 20 mg/liter for *R. sphaeroides*; and trimethoprim, 85-100 mg/liter for *E. coli* and 25 mg/liter for *R. sphaeroides*.

Construction of an R. sphaeroides Strain Expressing the His₆-tagged Cytochrome bc₁ Complex—A 1.2-kb *Xba*I-*Hind*III fragment containing the *fb*cC and *fb*cQ genes from pRKD*fb*cFBCQ, containing *fb*cF, *fb*cB, *fb*cC, and *fb*cQ, was inserted into a modified pSELECT-1 vector in which the unique *Acc*65I site was eliminated. The resulting pSEL*fb*cCQ was used as template for site-directed mutagenesis to introduce an *Acc*65I recognition site right before the stop codon of the *fb*cC gene. The Altered Sites in Vitro Mutagenesis System from Promega (22) was used for all the site-directed mutagenesis constructions. Two complementary oligonucleotides with His₆ tag coding sequence and the *Acc*65I overhang attached at the 5'-ends (5'-GTACGGGC CAT CAC CAC CAC CAT CAC TAA-3' and 3'-CCCG GTA GTG GTG GTG GTA GTG ATTCATG-5') were synthesized, annealed together by heating up to 70 °C and cooling slowly to room temperature, and ligated into the *Acc*65I site of pSEL*fb*cCQ to generate pSEL*fb*cCHQ. The 6-histidine insertion was confirmed by DNA sequencing. A 1.2-kb *Xba*I-*Hind*III fragment containing *fb*cCHQ from pSEL*fb*cCHQ was subcloned into an expression vector (pRKD418) containing the *fb*cFBCQ genes to generate pRKD*fb*cFBCHQ, which was then mobilized into *R. sphaeroides* BC17 by parental conjugation.

Generation of R. sphaeroides Strains Expressing the bc₁ Complexes with Altered ISP-- Mutations were constructed by site-directed mutagenesis using the Altered Sites system. Oligonucleotides were synthesized at the Oklahoma State University Recombinant DNA/Protein Core Facility. The oligonucleotides used are GCTGATCAACCAAATGAATCCGTCGCAGGCCCTCGCCTCCATCTTCGTCG for

the Δ ADV mutant, CAAATGAATCCGTCGCCGCCGCCGCAGGCCCTCGCCTCC for the ADV-PPP mutant, and TCGGCCGACGTGCAGCCGCTCCCGTCCATCTTCGTC for the ALA-PLP mutant. The presence of engineered mutations was confirmed twice by DNA sequencing before and after photosynthetic or semi-aerobic growth of the cells.

Enzyme Preparations and Activity Assay—Chromatophore membranes were prepared from BC17 cells harboring complement (sequence is the same as the wild type) or mutant pRKD $_{bc}$ FmBCHQ as described previously (23) and stored at very high concentration in the presence of 20% glycerol at 80 °C. To purify the His₆-tagged cytochrome bc_1 complex, the chromatophore suspensions were thawed and adjusted to a cytochrome b concentration of 25 μ M with 50 mM Tris-Cl (pH 8.0 at 4 °C) containing 20% glycerol, 1 mM MgSO₄, and 1 mM phenylmethylsulfonyl fluoride. DM solution (10%, w/v) was added to the chromatophore suspension to 0.56 mg/nmol of cytochrome b , and the mixture was stirred at 4 °C for 30 min and then centrifuged at 27,000 X g for 30 min. The hard precipitates at the bottom of the centrifuge tubes were discarded, and the loose pellets and supernatants were collected. NaCl solution (4 M) was added to a final concentration of 0.1 M, and the suspension was stirred for 1 h at 4 °C. This mixture was centrifuged at 200,000 X g for 120 min. The supernatants were collected and stirred with Ni²⁺-NTA resin (100 nmol of cytochrome b /ml of resin) for 20 min at 4 °C. The mixture was packed into a column, and the effluent was reapplied to the column to maximize the binding of protein to the resin. The column, absorbed with bc_1 complexes, was then subjected to a sequence of washings with TN buffer (50 mM Tris-Cl (pH 8.0 at 4 °C) and 200 mM NaCl) containing 0.01% DM, TN buffer containing 5 mM histidine and 0.01% DM, and TN buffer containing 5 mM histidine and 0.5% octyl glucoside. The pure cytochrome bc_1 complex was eluted with TN buffer containing 200 mM histidine and 0.5% octyl glucoside and concentrated using a Centriprep-30 concentrator to a final concentration of 300 μ M cytochrome b or higher. The purified complex was stored at 80 °C in the presence of 20% glycerol.

Ubiquinol-cytochrome *c* reductase activity was assayed at room temperature in a Shimadzu UV2101PC spectrophotometer (24). The purified cytochrome *bc*₁ complex was diluted with TN buffer containing 0.01% DM to a final concentration of cytochrome *b* of 5 μM. 3 μl of diluted *bc*₁ complex was added to an assay mixture (1 ml) containing 25 mM sodium/potassium phosphate buffer (pH 7.4), 0.3 mM EDTA, 125 μM cytochrome *c*, and 25 μM Q₀C₁₀BrH₂. Activity was determined by measuring the reduction of cytochrome *c* (by following the increase in absorbance at 550 nm) using a millimolar extinction coefficient of 18.5 cm⁻¹. Nonenzymatic oxidation of Q₀C₁₀BrH₂, determined under the same conditions in the absence of enzyme, was subtracted. 30 μM potassium cyanide was added to the assay mixture to inhibit the oxidase activity when the *bc*₁ activity in chromatophores was determined.

Determination of the Activation Energy of the Cytochrome bc₁ Complex—The activation energy of the *bc*₁ complex was determined in both chromatophore membrane and purified preparations. This is essentially assaying steady-state enzyme activity at various temperatures. The temperatures of the assay mixture were controlled (±0.1 °C) by a Shimadzu TCC controller installed on a Shimadzu UV2101PC spectrophotometer. Activity was measured from 9 to 30 °C at 3 °C intervals. The activation energy was calculated from an Arrhenius plot.

Other Biochemical and Biophysical Techniques—Protein concentration was measured by the method of Lowry et al. (25). Cytochrome *b* (26) and cytochrome *c*₁ (27) were determined according to published methods. SDS-polyacrylamide gel electrophoresis was performed according to Laemmli (28) using a Bio-Rad Mini-Protean dual-slab vertical cell. Western blotting was performed using rabbit polyclonal antibodies against cytochrome *c*₁, ISP, and subunit IV of the *R. sphaeroides* *bc*₁ complex. The polypeptides separated on the SDS-polyacrylamide gel were transferred to polyvinylidene difluoride membrane for immunoblotting. Goat anti-rabbit IgG conjugated to alkaline phosphatase or protein A conjugated to horseradish peroxidase was used as the second antibody.

EPR spectra were recorded with a Bruker ER 200D apparatus equipped with a liquid N₂ Dewar at 77 K. Instrument settings are detailed in the figure legends.

RESULTS AND DISCUSSION

Characterization of the His₆-tagged Cytochrome *bc*₁ Complex—The cytochrome *bc*₁ complex, which was overexpressed in *R. sphaeroides* BC17 cells by a low copy number expression vector (pRKD418) containing the *fb*cFBCQ genes, was routinely purified from chromatophore preparations by DM solubilization followed by DEAE-Bio-Gel A and DEAE-Sepharose CL-6B column chromatography. Although this purification scheme produces an enzyme complex of high purity and activity, it is time-consuming and gives low yields. This procedure requires extensive washing of the DEAE-Bio-Gel A column (usually 20 column volumes) to remove contaminating proteins, chlorophyll, and other pigments from the absorbed *bc*₁ complex. This step takes at least 8 h.

To speed up the preparation of the *bc*₁ complex from complement and mutant cells, a His₆ tag was genetically engineered into the C terminus of the cytochrome *c*₁ subunit to allow the use of Ni²⁺-NTA affinity agarose in a one-step purification. This construction was achieved by ligating annealed His₆-tag coding oligonucleotides, with the *Acc65I* overhang attached at the 5'-ends, into the *Acc65I* site created right before the stop codon of the *fb*cC gene in pSEL*fb*cCQ plasmid to generate pSEL*fb*cCHQ. The fragment containing the *fb*cCQkm genes in pRKD*fb*cFBCQkm was replaced with the fragment containing the *fb*cCHQ genes from pSEL*fb*cCHQ to generate pRKD*fb*cFBCHQ. *R. sphaeroides* BC17 cells harboring pRKD*fb*cFBCHQ have photosynthetic and respiratory growth behaviors similar to those of untagged cells. This construction adds 9 amino acid residues (GTGHHHHHH) to the C terminus of cytochrome *c*₁ in the expressed *bc*₁ complex.

The spectral properties and *bc*₁ complex activity in the His₆-tagged chromatophores are similar to those in untagged chromatophores. The effectiveness of DM in the

solubilization of tagged and untagged cytochrome bc_1 complexes from their respective chromatophores is comparable; ~95% of the cytochrome b present in chromatophores was solubilized when 0.56 mg of DM/nmol of cytochrome b was used. About 50% of the cytochrome bc_1 complex in chromatophores was recovered from the Ni^{2+} -NTA column. The His₆-tagged bc_1 complex has purity, activity, and cytochrome content similar to those of the untagged enzyme complex. The yield of the purified His₆-tagged bc_1 complex was twice that of untagged bc_1 preparations. The total time for purification of the His-tagged complex was ~6 h as compared with 2 days for the conventional purification. The molecular mass of the His₆-tagged bc_1 complex, determined by sedimentation velocity or sedimentation equilibrium, is 220 kDa, indicating that the isolated complex is in a dimeric state. The EPR characteristics of the [2Fe-2S] cluster in the purified His₆-tagged bc_1 complex are the same as those in the untagged complex (data not shown).

Characterizations of the Cytochrome bc_1 Complexes Containing an Altered ISP

Neck—To establish that flexibility of the neck region of ISP is essential for the head domain movement required for bc_1 catalysis, mutants expressing bc_1 complexes with increased ISP neck rigidity were generated and characterized. The *R. sphaeroides* ISP neck is composed of residues 39-48 with the sequence NPSADVQALA; Ala-42, Asp-43, Val-44, Ala-46, and Ala-48 are the conserved amino acid residues. We focused our mutational studies on these 5 residues. The flexibility of the ISP neck is expected to decrease when proline residues are introduced because proline has a conformational constraint due to the cyclic nature of its pyrrolidine side chain. Since the ADV residues are located in what appears to be the most flexible part of the neck, deletion of these residues is expected to affect the movement or the positioning of the head of ISP.

Three *R. sphaeroides* mutant strains were generated: Δ ADV, in which the ADV residues (residues 42-44) are deleted; ALA-PLP, in which Ala-46 and Ala-48 are substituted with prolines; and ADV-PPP, in which Ala-42, Asp-43, and Val-44 are substituted with prolines. All mutations were constructed by site-directed mutagenesis

using a 3.5-kb *EcoRI-HindIII* *R. sphaeroides* DNA carrying the *fbCFBC* genes in pSELECT-1 plasmid (pSELNB3503) as template. A 2.5-kb *EcoRI-PinAI* fragment containing the kanamycin-resistant gene in pRKD*fbCFBC6HQ*km was replaced with a 1.7-kb *EcoRI-PinAI* fragment containing the mutated ISP gene from pSELNB3503 to generate pRKD*fbCFmBCHQ* plasmid, which was then mobilized into *R. sphaeroides* BC17 cells. Mutations in pRKD*fbCFmBCHQ* harbored in *E. coli* S17-1 (before conjugation) and photosynthetically or semi-aerobically dark-grown *R. sphaeroides* cells (after conjugation) were confirmed by DNA sequencing after the targeted DNA fragment was amplified by polymerase chain reaction.

The Δ ADV mutant cells grew photosynthetically at a rate similar to that of complement cells. The ALA-PLP mutant was also capable of photosynthetic growth, but at a maximal doubling rate of ~50% that of the complement strain. The ADV-PPP mutant was unable to grow photosynthetically (Table I, first column), but could grow under semi-aerobic conditions. These results indicate that the ISP neck flexibility is more critical than its length in supporting photosynthetic growth.

To investigate whether mutations at the neck region of ISP affect cytochrome *bc*₁ complex activity, ubiquinol-cytochrome *c* reductase activity in chromatophores from the Δ ADV and ALA-PLP strains and in the intracytoplasmic membrane (ICM) of the ADV-PPP strain was assayed and compared with that of the complement strain. To study subunit association of cytochrome *bc*₁ complexes in the membrane, Western blot analyses of chromatophores and ICM of mutants were performed and compared with those of the complement strain. Chromatophores from the Δ ADV and ALA-PLP mutant cells had 10 and 30% of the ubiquinol-cytochrome *c* reductase activity found in the complement chromatophores, respectively. As expected, ICMs of the ADV-PPP mutant had no ubiquinol-cytochrome *c* reductase activity because the cytochrome *bc*₁ complex is an obligatory enzyme complex for photosynthetic growth, and this mutant was unable to grow photosynthetically. These results indicate that shortening the length or decreasing the

Table I.
Characterization of ISP neck mutants.

Mutations	Growth		Enzymatic Activity ^a		Subunit Composition	
	Photosyn- thetic	Semi- aerobic	Chromatophore or ICM	Purified Complex	Chromatophore or ICM	Purified Complex
Complement	++ ^b	++	2.0	2.5	FBCQ ^d	FBCQ
ΔADV	++	++	0.2	0	FBCQ	BC
ALA-PLP	+	++	0.7	0.7	FBCQ	FBCQ
ADV-PPP	- ^c	++	0	0	FBCQ	BC

^a enzymatic activity is expressed as μmol cytochrome *c* reduced /min / nmol cytochrome *b*

^b ++, the growth phenotype is essentially the same as the "wild type".

^c -, no photosynthetic growth within 7 days.

^d FBCQ indicate gene products of the *fbcF* (ISP), *fbcB* (cytochrome *b*), *fbcC* (cytochrome *c*₁) and *fbcQ* (subunit IV), respectively.

flexibility of the ISP neck drastically decreases the cytochrome bc_1 complex activity in membranes. It should be noted that the cytochrome bc_1 complex activities in the photosynthetic chromatophore membrane and in semi-aerobic ICM from complement cells are the same.

When membranes from these three mutants and the complement cells were subjected to Western blot analysis with antibodies against *R. sphaeroides* cytochrome c_1 , ISP, and subunit IV, stoichiometric amounts of these three subunits were detected in all three mutant membranes (Fig. 3). Absorption spectral analysis also revealed that the ratio of cytochrome b to c_1/c_2 in all these mutant membranes was similar to that in the complement membrane. These results indicate that these mutations did not affect the assembly of ISP protein into the membrane. However, we observed an apparently elevated level of the bc_1 complex in the Δ ADV mutant membrane, as indicated by the elevated level of cytochrome b (19 nmol/mg of protein), relative to that found in membranes from complement cells (16 nmol/mg of protein). It should be noted that membranes from complement cells already possess three times the amount of cytochrome b found in wild-type *R. sphaeroides*, presumably due to a gene dosage effect. Therefore, the increased level of expression could be a regulatory response compensating the lowered electron transfer activity in the Δ ADV mutant. This explains why 10% bc_1 (specific) activity observed in the mutant complex is sufficient to support the photosynthetic growth.

Effect of Mutation on the Rieske Iron-Sulfur Cluster and on Assembly of ISP into the Cytochrome bc_1 Complex-- Since the bc_1 complex activity decreased by 90, 70, and 100% in the Δ ADV, ALA-PLP, and ADV-PPP mutant membranes, respectively, with no decrease in the amount of ISP, it is important to determine whether the activity loss resulted from improper assembly of ISP into the complex or from the fact that the ISP head domain is less mobile. We addressed this question by comparing EPR characteristics of the [2Fe-2S] cluster in complement and mutant membranes because EPR signals from the iron-sulfur protein, especially the g_x signature, are very sensitive to changes in its microenvironments.

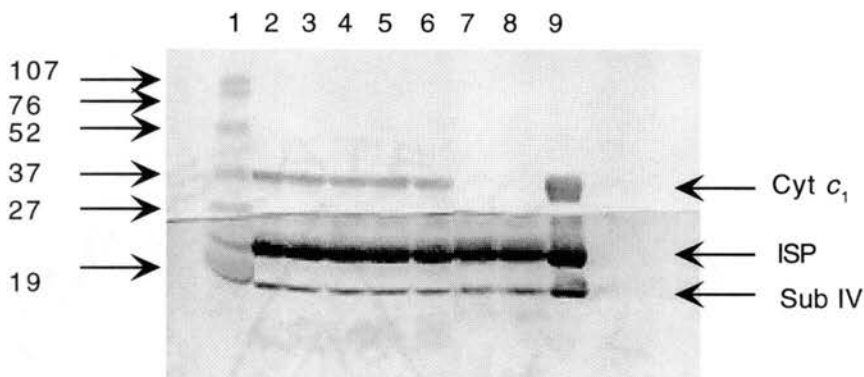


Figure 3. Western blot analysis of chromatophore membranes from mutant and wild-type complement strains. Membrane samples containing 75 pmol of cytochrome *b* were loaded into each well and subjected to SDS-polyacrylamide gel electrophoresis. The gel was transferred electrophoretically to a polyvinylidene difluoride membrane. Polyclonal antibodies raised against subunits of *R. sphaeroides* *bc*₁ complex (cytochrome *c*₁ (Cyt *c*₁), ISP, and subunit IV (Sub IV)) were used to detect these three subunits. The antibody's titer for cytochrome *c*₁ is much higher than those for subunit IV and ISP. To reduce the nonspecific background reaction, the membrane was cut into two pieces so that the upper part, containing proteins with a molecular mass >23 kDa, including cytochrome *c*₁, was developed with a horseradish peroxidase system. The bottom section, containing the low molecular mass proteins, was developed with an alkaline phosphatase system. *Lane 1*, prestained molecular mass standards; *lane 2*, photosynthetic growth wild-type complement chromatophores; *lane 3*, semi-aerobic wild-type complement ICM; *lane 4*, ΔADV mutant chromatophores; *lane 5*, ALA-PLP mutant chromatophores; *lane 6*, ADV-PPP mutant ICM; *lanes 7 and 8*, effluent from the Ni²⁺-NTA column, which is the unbound portion from the detergent extraction mixture for the ΔADV and ADV-PPP mutants; *lane 9*, purified His₆-tagged complement *bc*₁ complex.

Also, we compared the subunit stoichiometry in the purified His₆-tagged mutant complexes with that found in the complement complex.

When the [2Fe-2S] cluster was reduced by a small excess of ascorbate, the complement chromatophore or ICM had a spectrum that was essentially the same as that previously reported for the chromatophores from wild-type *R. sphaeroides*, with resonance at $g_x = 1.80$ and $g_y = 1.9$ (Fig. 4, *spectra A and D*). The $g_z = 2.02$ signal of the [2Fe-2S] cluster could not be resolved in membrane preparations because it was shielded by many other signals.

The [2Fe-2S] cluster in Δ ADV chromatophore membranes showed no detectable g_x signal (totally broadened) and a very small g_y signal (Fig. 4, *spectrum B*), indicating that the microenvironments of the iron-sulfur cluster have been drastically altered in this deletion mutant. In the bc_1 crystal structure, the iron-sulfur cluster sits at the tip of the head domain of ISP, and this tip of ISP fits into the concave hydrophobic surface of the Q_o pocket located in the cytochrome *b* subunit (4). Changing the microenvironments of the [2Fe-2S] cluster by mutation of residues in the docking interface of ISP and cytochrome *b*, such as Leu-132 (29) and Gly-133 (30) in ISP and Ile-292 (31) in cytochrome *b*, resulted in a loss of the g_x signal of the [2Fe-2S] cluster and a decrease in electron transfer activity. Since the neck region is spatially separated from the docking interface of ISP and cytochrome *b*, the change of microenvironments of the [2Fe-2S] cluster in the Δ ADV mutant complex, indicated by the g_x/g_y signal change, is probably due to the improper docking of the head domain of ISP on cytochrome *b* as a result of the shortened neck. Loss of cytochrome bc_1 complex activity (90%) in the Δ ADV membrane is therefore attributed to improper assembly of ISP into the complex. It should be noted that the drastic decrease in the amplitude of the g_y signal in the Δ ADV mutant chromatophores is not due to a destabilizing effect on the oxidized [2Fe-2S] cluster as reported for the T134R, T134H, or T134G mutation in ISP of *Rhodobacter capsulatus* (29) since the signal was not increased in EPR measurements of Δ ADV chromatophores prepared by including 20 mM ascorbate to keep

the [2Fe-2S] cluster in the reduced state. Such a decrease in the EPR signal is not caused by a labile [2Fe-2S] cluster as the result of ADV deletion because when the membrane was prepared by a gentler method, such as treating freshly grown cells with lysozyme and an appropriate amount of detergent to disrupt the membrane, no increase in EPR signals and the membrane bc_1 activity was observed. However, when the mutant membrane was incubated with 100 μ M stigmatellin, a small but distinctive $g_x = 1.78$ signal showed up, similar to that of the stigmatellin-treated complement membrane (data not shown). No bc_1 activity was detected in this inhibitor-treated Δ ADV membrane, which further confirmed the typical response of g_x signal to Q_0 site inhibitor. Therefore, the decrease in the EPR signal in the mutant membrane is not due to the destruction of the [2Fe-2S] cluster during the preparation of the membrane, but rather an intrinsic property of the mutant. Similar results were observed when cell pastes were used in EPR analysis (data not shown).

If ISP is indeed improperly assembled into the bc_1 complex in the Δ ADV mutant chromatophore, the mutant complex is expected to be less stable than the wild type. In other words, the binding affinity of ISP for other subunits in the Δ ADV mutant complex is probably weaker than that in the wild-type complex. To confirm this speculation, chromatophore membranes from the Δ ADV and complement cells were treated with dodecyl maltoside at 0.55 mg/nmol of cytochrome b . Although the amounts of cytochromes b and c_1 , ISP, and subunit IV solubilized from these two chromatophore membranes were the same, no bc_1 complex activity was detected in the detergent-solubilized membrane fraction from Δ ADV. When dodecyl maltoside-solubilized chromatophore membranes from Δ ADV and complement cells were individually applied to a Ni^{2+} -NTA column and analyzed for subunit composition in the histidine-eluted fractions, the His₆-tagged Δ ADV complex was found to contain only cytochromes b and c_1 (Fig. 5, lane 5). ISP and subunit IV were detected in the unbound fraction by Western blot analysis (Fig. 3, lane 7), whereas the complement complex contained cytochromes b and c_1 , ISP, and subunit IV (Fig. 5, lanes 2 and 3). Although the lack of ISP in the Δ ADV complex was expected, the lack of subunit

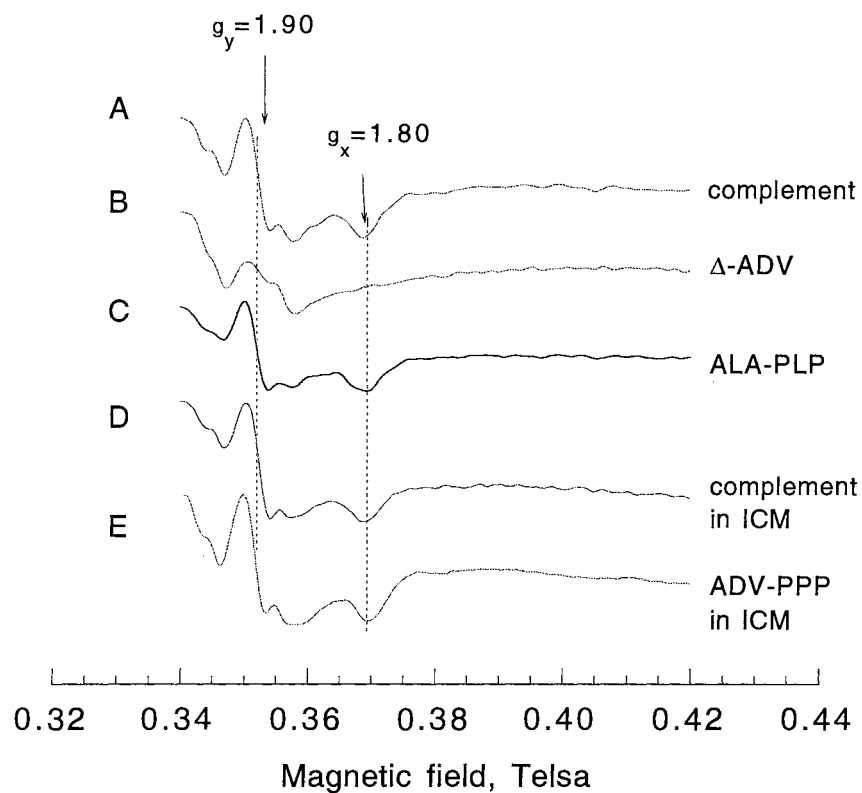


Figure. 4. EPR spectra of the [2Fe-2S] cluster of Rieske iron-sulfur protein in chromatophore membranes from the complement, Δ ADV, and ALA-PLP and in ICM from the complement and ADV-PPP. Chromatophore pastes were partially reduced by addition of 5 mM ascorbate. The samples were incubated on ice for ~20 min and frozen in liquid nitrogen. EPR spectra were recorded at 77 K with the following instrument settings: microwave frequency, 9.336 Hz; microwave power, 20 milliwatts; modulation amplitude, 20 G; modulation frequency, 100 kHz; time constant, 0.1 s; and scan rate, 20 G/s.

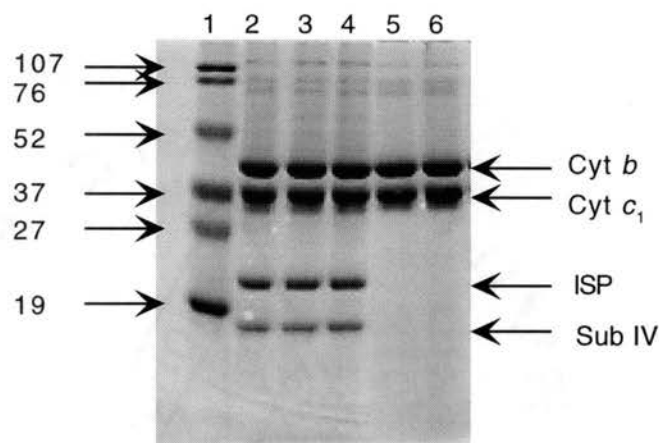


Figure 5. SDS-polyacrylamide gel electrophoresis of purified His₆-tagged *bc*₁ complexes. Aliquots of mutant and wild-type complement *bc*₁ complexes containing ~75 pmol of cytochrome *b* were loaded into each well. *Lane 1*, pre-stained molecular mass standards; *lane 2*, cytochrome *bc*₁ from the wild-type complement strain (photosynthetic growth); *lane 3*, cytochrome *bc*₁ from the wild-type complement strain (semi-aerobic growth); *lane 4*, cytochrome *bc*₁ from the ALA-PLP mutant (photosynthetic growth); *lane 5*, cytochrome *bc*₁ from the Δ ADV mutant (photosynthetic growth); *lane 6*, cytochrome *bc*₁ from the ADV-PPP mutant (semi-aerobic growth). *Cyt*, cytochrome; *Sub IV*, subunit IV.

IV in the complex was rather surprising. Perhaps residues Δ ADV of the ISP neck are involved in the packing of ISP and subunit IV with cytochrome *b* and *c* in the complex.

EPR characteristics of the Rieske [2Fe-2S] cluster in the ADV-PPP membrane (ICM) (Fig. 4, *spectrum E*) are the same as those of the [2Fe-2S] cluster in complement chromatophores, and binding of the Q_o site inhibitor stigmatellin induces an upfield shift in the g_x signal that is similar to that observed with complement chromatophores (data not shown). These results indicate that the environments of the iron-sulfur cluster are not changed by this mutation (ADV-PPP). Although the increased rigidity of the ISP neck did not affect the docking of the ISP head domain on the cytochrome *b* protein, the complex was unstable as evident from the dissociation of ISP and subunit IV from cytochromes *b* and c_1 when this mutant complex was purified from the DM-solubilized membrane (Fig. 5, *lane 6*). The complete lack of cytochrome bc_1 complex activity in the ADV-PPP membrane may be attributed to weak binding of ISP and subunit IV with cytochromes *b* and c_1 as well as to a lesser head domain mobility of ISP during bc_1 catalysis.

EPR characteristics of the Rieske [2Fe-2S] cluster in the ALA-PLP chromatophore membrane (Fig. 4, *spectrum C*) are the same as those of the [2Fe-2S] cluster in complement chromatophores, indicating similar iron-sulfur cluster environments, *i.e.* the head domain of ISP is properly docked on cytochrome *b* in this mutant chromatophore. When the complex in the ALA-PLP chromatophore membrane was solubilized with dodecyl maltoside and applied to a Ni^{2+} -NTA affinity gel, four subunits, corresponding to cytochromes *b* and c_1 , ISP, and subunit IV with unit stoichiometry were recovered in the histidine eluate (Fig. 5, *lane 4*), indicating that this mutation does not affect the binding affinity of ISP for other subunits of the complex. However, the cytochrome bc_1 complex activity in the chromatophore membrane and in the purified complex from the ALA-PLP mutant was 30% of that found in corresponding preparations from complement cells. These results, together with the fact that the ALA-PLP cytochrome bc_1 complex differs from the complement complex only in the increased rigidity of the ISP neck, suggest that the 70% loss of bc_1

activity in the ALA-PLP complex results from decreased mobility of the ISP head domain. Apparently, head domain movement of ISP is required for bc_1 complex activity.

Effect of Mutation on the Activation Energy of the Cytochrome bc_1 Complex—If the head domain movement of ISP is required for bc_1 activity, it is important to know whether this step contributes to the activation energy barrier of the bc_1 -catalyzed reaction. This question can be addressed by comparing the activation energies of the cytochrome bc_1 complexes, in chromatophores or in the purified state, of ALA-PLP mutant and complement cells. An increase in activation energy for the ALA-PLP complex would indicate that the head domain movement of ISP contributes to the activation energy barrier. This deduction is based on the fact that the only difference between the ALA-PLP mutant complex and the complement complex is the decreased ISP head mobility of the former. Fig. 6 shows Arrhenius plots of bc_1 complex activity in ALA-PLP mutant and complement chromatophores. Since the concentrations of electron donor (ubiquinol) and electron acceptor (cytochrome *c*) used in the bc_1 activity assay mixture were at the saturation level, diffusion limitation of cytochrome *c* was avoided, and no product inhibition was observed. An activation energy of 24.7 kJ/mol was obtained for the complement complex and 69 kJ/mol for the ALA-PLP mutant, indicating that a decrease in head domain movement in ISP increases the activation energy of the bc_1 complex. Similar results were obtained with purified bc_1 complexes. The activation energy obtained for the complement cytochrome bc_1 complex was the same as that obtained for the beef heart mitochondrial bc_1 complex under similar assay conditions (32, 33).

Although head domain movement of ISP is thought to lower the activation energy barrier of the bc_1 complex, based on the observation of an increased activation energy for the ALA-PLP complex, the complexity of the kinetics of the bc_1 complex prevents us from ruling out other steps as contributors to the activation energy barrier of this reaction. There are several distinct catalytic sites in the bc_1 complex: one for ubiquinol oxidation at the Q_o site, one for ubiquinone reduction at the Q_i site, one for reduction and reoxidation of ISP as

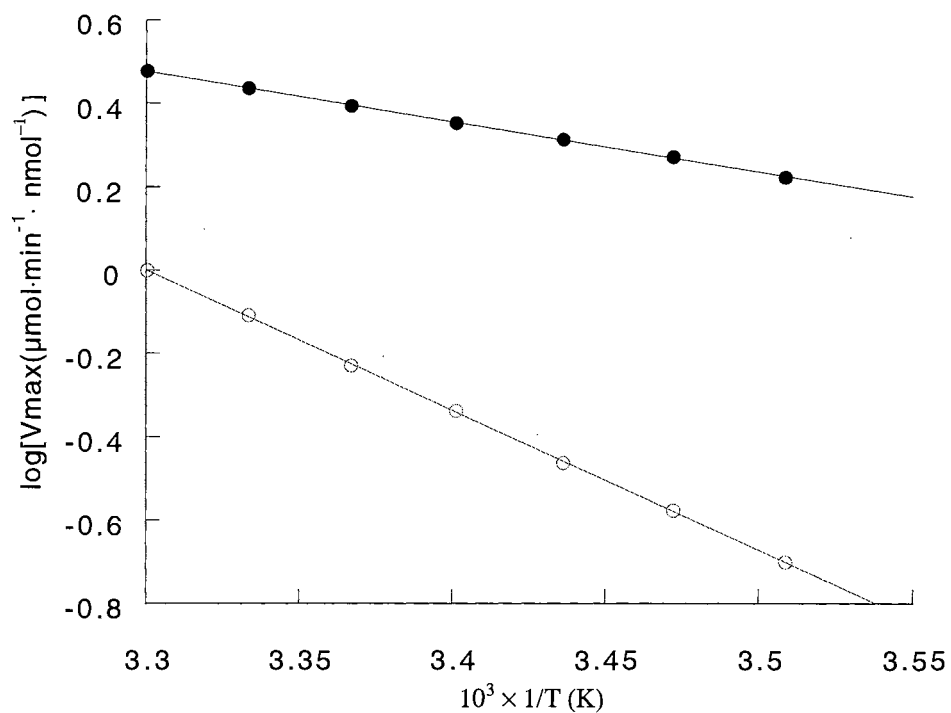


Figure. 6. Arrhenius plots of the cytochrome bc_1 complexes of the ALA-PLP mutant and complement chromatophore membranes. The conditions for activity assays were as follows: 50 mM sodium/potassium phosphate (pH 7.4), 120 μM cytochrome c , 25 μM $\text{Q}_0\text{C}_{10}\text{BrH}_2$, 300 μM EDTA, and 5 pmol of bc_1 complex at the indicated temperatures. ●, complement; ○, ALA-PLP mutant.

well as cytochrome c_1 , and one for reduction of cytochrome c . Any one of these steps may contribute to the activation energy barrier of the overall reaction.

Based on flash kinetic studies of the bc_1 complex in *R. sphaeroides* chromatophore membranes showing a large activation energy for cytochrome b_L or b_H reduction by ubiquinol-10 (~32 kJ/mol), Crofts and Wang (34) proposed that the activation energy barrier of the bc_1 complex activity was associated with the oxidation of QH_2 , either during QH_2 oxidation to an intermediate (Q^\cdot) or during further oxidation of the semiquinone by ISP at the Q_o site. The formation of a transient ubisemiquinone radical at the Q_o site (Em for $Q^\cdot/Q = -300-400$ mV) may be the largest activation energy barrier of this reaction (34). Failure to detect a Q_o site inhibitor-sensitive ubisemiquinone radical in beef cytochrome bc_1 complexes as well as in *R. sphaeroides* bc_1 complexes (34) under oxidant-induced reduction conditions (35) raises questions concerning this hypothesis.

Link (36) proposed a "proton-gated affinity change" mechanism for cytochrome bc_1 complex catalysis in which a stable semiquinone species is present at the Q_o site and the first step for Q oxidation is the deprotonation of ubiquinol. Brandt and Okun (37) have shown that deprotonation of ubiquinol ($\Delta G = 24$ kJ/mol at pH 7) accounts for most of the activation barrier by measuring the pH dependence of the activation energy during steady-state turnover of bovine and yeast cytochrome bc_1 complexes. They found that it decreased linearly from pH 5.5 to 9.0. This deprotonation hypothesis has been questioned recently by Trumpower and co-workers (38). They have demonstrated that the midpoint potential difference between the [2Fe-2S] cluster and the electron donor ubiquinol is the driving force for the electron transfer at center P. Mutational study of Ser-183 and Tyr-185 in the *S. cerevisiae* Rieske iron-sulfur protein indicated that elimination of the hydrogen bond from the hydroxyl group of Ser-183 to S-1 of the [2Fe-2S] cluster or of Tyr-185 to S- γ of Cys-159 lowers the midpoint potential of the [2Fe-2S] cluster, which in turn slows down the intracomplex electron transfer from ubiquinol to cytochrome c . Ubiquinol-cytochrome c reductase activity decreases as the potential of ISP declines from approximately +280 to

+100 mV, which confirms that oxidation of ubiquinol by ISP is the rate-limiting partial reaction in the bc_1 complex and that the rate of this reaction is extensively influenced by the midpoint potential of the [2Fe-2S] cluster. These investigators suggested that deprotonation of ubiquinol is not the rate-limiting step in the ubiquinol oxidation catalyzed by the cytochrome bc_1 complex.

The abbreviations used are: ISP, Rieske iron-sulfur protein; Q, ubiquinone; Q_0 , ubiquinol oxidation site; Q_1 , ubiquinone reduction site; b_L , low potential cytochrome b ; b_H , high potential cytochrome b ; DM, dodecyl maltoside; NTA, nitrilotriacetic acid; $Q_0C_{10}BrH_2$, 2,3-dimethoxy-5-methyl-6-(10-bromodecyl)-1,4-benzoquinol; kb, kilobase pair; ICM, intracytoplasmic membrane.

REFERENCES

1. Trumpower, B. L., and Gennis, R. B. (1994) *Annu. Rev. Biochem.* 63, 675-716.
2. Mitchell, P. (1976) *J. Theor. Biol.* 62, 327-367.
3. Yu, C.-A., Kachurin, M. A., Yu, L., Xia, D., Kim, H., and Deisenhofer, J. (1996) *Biochim. Biophys. Acta* 1275, 47-53.
4. Xia, D., Yu, C.-A., Kim, H., Xia, J. Z., Kachurin, A. M., Zhang, L., Yu, L., and Deisenhofer, J. (1997) *Science* 277, 60-66.
5. Kim, H., Xia, D., Deisenhofer, J., Yu, C.-A., Kachurin, A., Zhang, L., and Yu, L. (1997) *FASEB J.* 11, 1084a
6. Kim, H., Xia, D., Yu, C.-A., Kachurin, A., Zhang, L., Yu, L., and Deisenhofer, J. (1998) *Proc. Natl. Acad. Sci. U. S. A.* 95, 8026-8033.
7. Zhang, Z. L., Huang, L.-S., Shulmeister, V. M., Chi, Y.-I., Kim, K. K., Huang, L.-W., Crofts, A. R., Berry, E. A., and Kim, S.-H. (1998) *Nature* 392, 677-684.
8. Yu, C.-A., Xia, D., Kim, H., Deisenhofer, J., Zhang, L., Kachurin, A. M., and Yu, L. (1998) *Biochim. Biophys. Acta* 1365, 151-158.

9. Iwata, S., Lee, J. W., Okada, K., Lee, J. K., Iwata, M., Rasmussen, B., Link, T. A., Ramaswamy, S., and Jap, B. K. (1998) *Science* 281, 64-71.
10. Crofts, A. R., and Meinhardt, S. W. (1982) *Biochem. Soc. Trans.* 10, 201-203.
11. Tsai, A. L., Olson, J. S., and Palmer, G. (1987) *J. Biol. Chem.* 262, 8677-8684.
12. Iwata, S., Saynovits, M., Link, T. A., and Michel, H. (1996) *Structure* 4, 567-579.
13. Link, T. A., Saynovits, M., Assmann, C., Iwata, S., Ohnishi, T., and Von Jagow, G. (1996) *Eur. J. Biochem.* 237, 71-75.
14. Usui, S., Yu, L., and Yu, C.-A. (1990) *Biochem. Biophys. Res. Commun.* 167, 575-579.
15. Engel, W. D., Michalski, C., and Von Jagow, G. (1983) *Eur. J. Biochem.* 132, 395-402.
16. Mather, M. W., Yu, L., and Yu, C.-A. (1995) *J. Biol. Chem.* 270, 28668-28675.
17. Simon, R., Priefer, U., and Pühler, A. (1983) *Bio/Technology* 1, 784-791.
18. Yun, C. H., Beci, R., Crofts, A. S., Kaplan, S., and Gennis, R. B. (1990) *Eur. J. Biochem.* 194, 399-411.
19. Yu, C.-A., and Yu, L. (1982) *Biochemistry* 21, 4096-4101.
20. Khosravi, M., Ryan, W., Websger, D. A., and Stark, B. C. (1990) *Plasmid* 23, 138-143.
21. Daldal, F., Tokito, M., Davidson, E., and Faham, M. (1989) *EMBO J.* 8, 3951-3961.
22. Promega Corp. (1996) *Altered Sites in Vitro Mutagenesis Systems Technical Manual*, Promega Corp., Madison, WI.
23. Yu, C.-A., and Yu, L. (1991) *Biochemistry* 30, 4934-4939.
24. Tian, H., Yu, L., Mather, M. W., and Yu, C.-A. (1997) *J. Biol. Chem.* 272, 23722-23728.
25. Lowry, O. H., Rosebrough, N. J., Farr, A. L., and Randall, R. J. (1951) *J. Biol. Chem.* 193, 265-275.
26. Berden, J. A., and Slater, E. C. (1970) *Biochim. Biophys. Acta* 216, 237-249.
27. Yu, L., Dong, J. H., and Yu, C.-A. (1986) *Biochim. Biophys. Acta* 852, 203-211.
28. Laemmli, U. K. (1970) *Nature* 227, 680-685.
29. Liebl, U., Sled, V., Brasseur, G., Ohnishi, T., and Daldal, F. (1997) *Biochemistry* 36, 11675-11684.

30. Van Doren, S. R., Gennis, R. B., Barquera, B., and Crofts, A. R. (1993) *Biochemistry* 32, 8083-8091.
31. Crofts, A. R., Barquera, B., Bechmann, G., Guergova, M., Salcedo-Hernandes, R., Hacker, B., Hong, S., and Gennis, R. B. (1995) in *Photosynthesis: From Light to Biosphere* (Mathis, P., ed), Vol. II, pp. 493-500, Kluwer Academic Publishers, Dordrecht, The Netherlands.
32. Degli Esposti, M., and Lenaz, G. (1991) *Arch. Biochem. Biophys.* 289, 303-312.
33. Zhang, L., Yu, L., and Yu, C.-A. (1998) *Biophys. J.* 74, 198 (abstr.)
34. Crofts, A. R., and Wang, Z. (1989) *Photosynth. Res.* 22, 69-87.
35. de Vries, S., Albracht, S. P. J., Berden, J. A., and Slater, E. C. (1981) *J. Biol. Chem.* 256, 11996-11998.
36. Link, T. A. (1997) *FEBS Lett.* 412, 257-264.
37. Brandt, U., and Okun, J. U. (1997) *Biochemistry* 36, 11234-11240.
38. Denke, E., Merbitz-Zahradnik, T., Hatzfeld, O. M., Snyder, C. H., Link, T. A., and Trumpower, B. L. (1998) *J. Biol. Chem.* 273, 9085-9093.

CHAPTER IV**Evidence for the Head Domain Movement of the Rieske Iron-Sulfur Protein in Electron Transfer Reaction of the Cytochrome *bc*₁ Complex**

Hua Tian, Steve White, Linda Yu, and Chang-An Yu

The Journal of Biological Chemistry Vol. 274 pp.7146-7152 (1999)

ABSTRACT

The three-dimensional structure of the mitochondrial cytochrome bc_1 complex suggests that movement of the extramembrane domain (head) of the Rieske iron-sulfur protein (ISP) may play an important role in electron transfer. Such movement requires flexibility in the neck region of ISP, since the head and transmembrane domains of the protein are rather rigid. To test this hypothesis, *Rhodobacter sphaeroides* mutants expressing His-tagged cytochrome bc_1 complexes with cysteine substitution at various positions in the ISP neck (residues 39-48) were generated and characterized. The mutants with a single cysteine substitution at Ala⁴² or Val⁴⁴ and a double cysteine substitution at Val⁴⁴ and Ala⁴⁶ (VQA-CQC) or at Ala⁴² and Ala⁴⁶ (ADVQA-CDVQC) have photosynthetic growth rates comparable with that of complement cells. Chromatophore membrane and intracytoplasmic membrane (ICM) prepared from these mutants have cytochrome bc_1 complex activity similar to that in the complement membranes, indicating that flexibility of the neck region of ISP was not affected by these cysteine substitutions. Mutants with a double cysteine substitution at Ala⁴² and Val⁴⁴ (ADV-CDC) or at Pro⁴⁰ and Ala⁴² (PSA-CSC) have a retarded (50%) or no photosynthetic growth rate, respectively. The ADV-CDC or PSA-CSC mutant ICM contains 20 or 0% of the cytochrome bc_1 complex activity found in the complement ICM. However, activity can be restored by treatment with β -mercaptoethanol (β -ME). The restored activity is diminished upon removal of β -ME but is retained if the β -ME-treated membrane is treated with the sulfhydryl reagent *N*-ethylmaleimide or *p*-chloromercuribenzoic acid. These results indicate that the loss of bc_1 complex activity in the ADV-CDC or PSA-CSC mutant membranes is due to disulfide bond formation, which increases the rigidity of ISP neck and, in turn, decreases the mobility of the head domain. Using the conditions developed for the isolation of His-tagged complement cytochrome bc_1 complex, a two-subunit complex (cytochromes *b* and c_1) is obtained from all of the double cysteine-substituted mutants. This suggests that introduction

of two cysteines in the neck region of ISP weakens the interactions between cytochromes *b*, ISP, and subunit IV.

INTRODUCTION

The cytochrome bc_1 complex (ubiquinol-cytochrome *c* reductase) is an essential segment of the energy-conserving electron transfer chains of mitochondria and many respiratory and photosynthetic bacteria (1). This complex catalyzes electron transfer from ubiquinol to cytochrome *c* and concomitantly translocates protons across the membrane to generate a membrane potential and pH gradient for ATP synthesis. Although the cytochrome bc_1 complexes from different sources vary in their polypeptide compositions, they all contain four redox prosthetic groups: two *b*-type cytochromes (b_{566} or b_L and b_{562} or b_H), one *c*-type cytochrome (cytochrome c_1), and one high potential Rieske iron-sulfur cluster [2Fe-2S]. The proton-motive Q cycle model (2) has been favored for electron transfer and proton translocation in the complex. The key feature of this model is the presence of two separate ubiquinone- or ubiquinol-binding sites: a ubiquinol oxidation site near the P side of the inner mitochondrial membrane and a ubiquinone reduction site near the N side of the membrane.

Recently, the cytochrome bc_1 complex from beef heart mitochondria was crystallized and its three-dimensional structure solved at 2.9-Å resolution (3, 4). The structural information obtained not only answered a number of questions concerning the arrangement of the redox centers, transmembrane helices, and inhibitor binding sites but also suggested movement of an extramembrane domain within the iron-sulfur protein (ISP) during electron transfer (4). This suggestion arose from observation of an uneven electron density in the $I4_122$ crystal data of native bovine cytochrome bc_1 complex. A particularly low electron density area is observed in the intermembrane space portion of the complex, where the extramembrane domains of ISP and cytochrome c_1 reside (4). This movement hypothesis

was further supported by the finding that the position of the iron-sulfur cluster in the complex is affected by ubiquinol oxidation site inhibitor binding (5, 6, 8) and by the crystal form (7, 9).

The anomalous light scattering signal of the [2Fe-2S] cluster is enhanced in co-crystals with stigmatellin or UHDBT but is diminished in the co-crystal with (E)-methyl-3-methoxy-2-(4'-trans-stilbenyl) acrylate (5). Thus, binding of stigmatellin or UHDBT arrests the movement of the extramembrane domain of ISP, fixing the iron-sulfur cluster 27 Å from heme b_L and 31 Å from heme c_1 (referred to as the "fixed state" of ISP), the same position it occupies in the $I4_122$ crystal of native bovine cytochrome bc_1 complex. The position of the iron-sulfur cluster changes from the fixed state to somewhere closer to heme c_1 (referred to as the "released state" of ISP) upon (E)-methyl-3-methoxy-2-(4'-trans-stilbenyl) acrylate binding. The recent report of Iwata *et al.* (9), showing the iron-sulfur cluster at two different positions in two crystal forms, further supports the presence of a variable position of in the "released state" of the iron-sulfur cluster.

Movement of the head domain of ISP during electron transfer in cytochrome bc_1 complex can be explained as follows. The [2Fe-2S] cluster is reduced by the first electron of ubiquinol at a position 27 Å from heme b_L and 31 Å from heme c_1 (ISP in "fixed state"). Since a reduced [2Fe-2S] cluster cannot donate an electron to cytochrome c_1 before the second electron of ubiquinol is transferred to heme b_L , it was postulated that either the change of the ubiquinone binding position during reduction of b_L or the electron transfer from b_L to b_H causes a conformational change in cytochrome b , which forces or allows reduced [2Fe-2S] to move close enough to heme c_1 (ISP in "released state") for electron transfer (5, 7). This model would also explain why ubisemiquinone, a more powerful reductant than ubiquinol, reduces b_L , but not the [2Fe-2S] cluster, during ubiquinol oxidation.

ISP has three domains: the membrane-spanning N-terminal domain consisting of residues 1-62 (tail), the soluble C-terminal extramembrane domain consisting of residues

73-196 (head), and the flexible linking domain comprising residues 63-72 (neck). ISP is associated with the complex primarily via the membrane-spanning N-terminal domain (4, 7, 9). The [2Fe-2S] cluster is located at the tip of the head domain (12, 13). Since the three-dimensional structures of the head and tail domains are the same in the fixed and released states, movement of the head domain of ISP in the bc_1 complex requires flexibility in the neck region.

If movement of the head domain of ISP is required for bc_1 catalysis and the neck region of ISP confers the required mobility, decreasing the flexibility of the neck region of ISP should affect bc_1 complex activity. This hypothesis can be tested by site-directed mutagenesis followed by biochemical and biophysical characterization of mutant expressing cytochrome bc_1 complexes with altered ISP necks. However, site-directed mutagenesis in bovine heart mitochondria is not practical. *R. sphaeroides* is an ideal system to study the neck region of ISP by molecular genetics approach. The four-subunit complex is functionally analogous to the mitochondrial enzyme; the largest three subunits are homologous to their mitochondrial counterparts; and this system is readily manipulated genetically. In addition, the recent generation of *R. sphaeroides* expressing His₆-tagged cytochrome bc_1 complex greatly speeds up the preparation of the bc_1 complex from wild-type or mutant cells (14).

The *R. sphaeroides* ISP neck is composed of residues 39-48 (corresponding to residues 63-72 of bovine ISP) with a sequence of NPSADVQALA. Ala⁴², Asp⁴³, Val⁴⁴, Ala⁴⁶, and Ala⁴⁸ are the conserved amino acid residues. We have previously generated mutants with increased ISP neck rigidity by double or triple proline substitution of the conserved residues. The results demonstrated that flexibility in the ISP neck is important in bc_1 catalysis (14). The ALA-PLP and ADV-PPP mutant membranes have, respectively, 30 and 0% of the cytochrome bc_1 complex activity found in the complement membrane. The ALA-PLP mutant complex has a larger activation energy than the wild-type complex,

suggesting that movement of the head domain decreases the activation energy barrier of the bc_1 complex.

To better define the structure and function relationship of the neck region of ISP in the bc_1 complex, we recently generated mutants expressing His₆-tagged bc_1 complex with single or double cysteine substitution at various positions in the ISP neck. We predict that formation of a disulfide bond between a pair of genetically engineered cysteines in the neck will decrease its flexibility and thus decrease electron transfer activity. Measuring the bc_1 activity in these cysteine-substituted mutants should give insight into the dynamic state of the ISP neck. Herein we report procedures for generating *R. sphaeroides* mutants expressing His₆-tagged cytochrome bc_1 complexes with altered ISP necks by introducing single cysteines or a pair of cysteines at different positions. The photosynthetic growth behavior, the cytochrome bc_1 complex activity, and the EPR characteristics of the Rieske [2Fe-2S] cluster in membranes and the purified state from complement and mutant strains are examined and compared. The effect of sulfhydryl reagents on cytochrome bc_1 complexes from complement and mutant membranes is also examined.

EXPERIMENTAL PROCEDURES

Materials—2-Mercaptoethanol (β -ME), *N*-ethylmaleimide (NEM), and *p*-chloromercuribenzoic acid (PCMB) are from Sigma. All other chemicals are of the highest purity commercially available.

Generation of R. sphaeroides Strains Expressing the bc_1 Complexes with Altered ISP—Mutations were constructed by site-directed mutagenesis using the Altered Sites system from Promega. The oligonucleotide primers used for mutagenesis were as follows: ADV(42-44)-CDC, GCTGATCAACCAAATGAATCCGTCGTIGCGACTGCCCAGGCC TCGCCTCCATCTTCGTCG; A42C, CAAATGAATCCGTCGTIGCGACGTGCCAGGCC CTCGCCTCCATCT; V44C, ATGAATCCGTCGGCCTACTIGCCCAGGCCCTCGCCTCC

ATCT; VQA(44-46)-CQC, AACCAAATGAATCCGTCGGCCGACTIGCCAGTGCCTCG
 CCTCCATCTTCGTTCGATGTGA; PSA(40-42)-CSC, TGGCCGCTGATCAACCAAATG
 AATIGCTCGTIGCGACGTGCAGGCCCTCGCCTCCATCTT; ADVQA(42-46)-
 CDVQC, TCGIGCGACGTCCAGTGCCTCGCCTCCATCTT.

The method for construction of ISP mutants is essentially the same as previously reported by Tian *et al.* (14). The ADVQA(42-46)-CDVQC mutant was constructed by annealing the oligonucleotide primer with single-stranded pSELNB3503 carrying a A42C mutation in ISP. The presence of engineered mutations were confirmed by DNA sequencing before and after photosynthetic or semiaerobic growth of the cells. Expression plasmid pRKD*fbcF_m*BCHQ was purified from an aliquot of a photosynthetic or semiaerobic culture using the Qiagen plasmid Mini Prep kit. Since *R. sphaeroides* cells contain four types of endogenous plasmids, the isolated plasmids are not pure and concentrated enough for direct sequencing. Thus, a 1.2-kilobase pair DNA segment containing the mutation sequence was amplified from the isolated plasmids by polymerase chain reaction and purified by 1% agarose gel electrophoresis. The 1.2-kilobase pair polymerase chain reaction product was recovered from the gel by a gel extraction kit from Qiagen.

Growth of Bacteria — *Escherichia coli* was grown at 37 °C in an enriched medium (TYP) in order to shorten growth time and increase plasmid yield (15). For photosynthetic growth of the plasmid-bearing *R. sphaeroides* BC17 cells, an enriched Sistrom's medium containing 5 mM glutamate and 0.2% casamino acids was used. The pH of the medium was adjusted to 7.1 with a mixture of 6 N NaOH and 2 N KOH to increase the sodium and potassium ion content of the medium to a more optimal level (16). Photosynthetic growth condition of *R. sphaeroides* was essentially as described previously (14); cells harboring mutated *fbc* genes on the pRKD*fbc*FBCQ plasmid were grown photosynthetically for one or two serial passages to minimize any pressure for reversion. For semiaerobic growth of *R. sphaeroides*, an enriched Sistrom's medium supplemented with 20 amino acids and extra

rich vitamins was used. These semiaerobic cultures were grown in 0.5 liters of enriched medium in 2-liter Bellco flasks with vigorous shaking (220 rpm) for 26 h. The inoculation volumes used for both photosynthetic and semiaerobic cultures were always at least 5% of the total volume. Antibiotics were added to the following concentrations: ampicillin (125 mg/liter), tetracycline (10 mg/liter for *E. coli* and 1 mg/liter for *R. sphaeroides*), kanamycin sulfate (30 mg/liter for *E. coli* and 20 mg/liter for *R. sphaeroides*), trimethoprim (87.5 mg/liter for *E. coli*).

Enzyme Preparations and Activity Assays — Cells were harvested, washed, and passed twice through a French pressure cell at 846 p.s.i. as described previously (17). The chromatophore fraction was pelleted by ultracentrifugation of broken cells in a Beckman Ti 50.2 rotor at 48,000 rpm for 2 h at 4 °C. Membrane was washed with 50 mM Tris-Cl, pH 8.0, containing 1 mM MgSO₄ and stored at 80 °C in the presence of 20% glycerol. The His₆-tagged cytochrome *bc*₁ complexes were purified from chromatophores by the method of Tian *et al.* (14). His₆ tag is located at the C terminus of the cytochrome *c*₁ subunit.

Ubiquinol-cytochrome *c* reductase activity was measured at 23 °C in a 1-ml assay mixture containing 100 mM sodium/potassium phosphate buffer, pH 7.4, 0.3 mM EDTA, 100 μM cytochrome *c*, 25 μM, 2,3-dimethoxy-5-methyl-6(10-bromodecyl)-1,4-benzoquinol, and an appropriate amount of membrane or purified cytochrome *bc*₁ complex. Chromatophores or ICM were diluted with 50 mM Tris-Cl, pH 8.0, containing 20% glycerol and 1 mM MgSO₄ to a final concentration of cytochrome *b* of 5 μM. No detergent was added to the diluted mixture in order to preserve the *bc*₁ activity. 5 μl of diluted membrane was added to the assay mixture. Activity was determined by measuring the reduction of cytochrome *c* (the absorbance increase at 550 nm), using a millimolar extinction coefficient of 18.5 cm⁻¹ mM⁻¹. Nonenzymatic oxidation of 2,3-dimethoxy-5-methyl-6(10-bromodecyl)-1,4-benzoquinol, determined under the same conditions in the absence of enzyme, was subtracted. The purified *bc*₁ complex activity assay is essentially as described previously (14).

Treatment of Membranes with β -ME — β -ME was added to membrane preparations (40 μ M cytochrome *b*) to a final concentration of 100 μ M. After incubation on ice for 10 min, aliquots were removed from the mixture for assay. β -ME was removed from the treated membrane by washing with 50 mM Tris-Cl, pH 8.0, and 1 mM MgSO₄ and centrifuging at 80,000 rpm for 30 min with a Beckman TL ultracentrifuge. This process was repeated three times.

Reaction of Genetically Engineered Cysteine Residues in Membranes with NEM or PCMB — Freshly prepared NEM (100 mM in H₂O) was added to the β -ME-pretreated chromatophore or ICM (concentration is at 40 μ M cytochrome *b*) to a final concentration of 500 μ M. The mixture was flushed briefly with nitrogen, sealed, and incubated at room temperature for 15 min before measuring cytochrome *bc*₁ complex activity. The stock solution of PCMB was prepared by first dissolving PCMB powder in 0.5 N NaOH followed by neutralization. Modification of cysteine with PCMB was carried out as described for NEM. Excess NEM and PCMB was removed by repeated washing and centrifuging, and enzymatic activity was redetermined.

Molecular Modeling — Molecular modeling was carried out in a Indigo II Silicon Graphics Station. A peptide with NCSCQVQALA sequence, corresponding to the ISP neck sequence of the *R. sphaeroides* PSA-CSC mutant, was built using the Builder Module from Insight II software from Molecular Simulation, Inc. Whether this peptide has acceptable geometry for disulfide bond formation was examined by minimizing the structure as follows: (a) continued iterations using steepest descents minimization until the maximum derivation was less than 10 kcal/Å; (b) continued iterations using conjugate minimization until the maximum derivation was less than 1.0 kcal/Å; (c) continued iterations using va09a minimization until the maximum derivation was less than 0.01 kcal/Å; (d) creation of a disulfide bond; (e) minimization of the peptide using the Optimize command in Builder; and (f) visual examination of geometry and comparison with a control (no disulfide bond) using the print energy per residue command.

Other Biochemical and Biophysical Techniques—Protein concentration was determined by the method of Lowry *et al.* (18). Cytochrome *b* (19) and cytochrome *c*₁ (20) were determined according to published methods. SDS-polyacrylamide gel electrophoresis (SDS-PAGE) was performed according to Laemmli (21) using a Bio-Rad Mini-protean dual slab vertical cell. Western blotting was performed using rabbit polyclonal antibodies against cytochrome *b*, cytochrome *c*₁, ISP, and subunit IV of the *R. sphaeroides* *bc*₁ complex. The polypeptides separated in the SDS-PAGE gel were transferred to polyvinylidene difluoride membrane for immunoblotting. Goat anti-rabbit IgG conjugated to alkaline phosphatase or protein A conjugated to horseradish peroxidase was used as the second antibody.

EPR spectra were recorded with a Bruker ER 200D apparatus equipped with a liquid N₂ Dewar at 77 K. Instrument settings are detailed in the figure legends.

RESULTS AND DISCUSSION

Characterization of the Mutants Carrying Cysteine Substitutions in the Neck Region of the Iron-Sulfur Protein—Six *R. sphaeroides* mutants expressing His₆-tagged cytochrome *bc*₁ complexes with single or double cysteine substitutions at various positions in the ISP neck region were generated to test the hypothesis that neck flexibility allows ISP head domain movement required for *bc*₁ catalysis. The flexibility of the neck should decrease when a disulfide bond is formed between a pair of substituted cysteines.

Of the six mutants, two, A42C and V44C, are single substitutions, in which Ala-42 or Val-44 is replaced with cysteine. The other four are double cysteine substitutions, PSA-CSC, ADV-CDC, VQA-CQC, and ADVQA-CDVQC, in which Pro⁴⁰ and Ala⁴², Ala⁴² and Val⁴⁴, Val⁴⁴ and Ala⁴⁶, or Ala⁴² and Ala⁴⁶ are replaced with cysteines. A plate mating technique was used (22) to transfer the pRKD*fb*cF_mBC_{6H}Q plasmid from *E. coli* S17 to *R. sphaeroides* BC17. The mating took place in less than 16 h on the LB/SIS plates. *R. sphaeroides* BC17 cells harboring pRKD*fb*cF_mBC_{6H}Q plasmid were selected by spreading the conjugated cell mixture on enriched Siström's plate containing tetracycline and

kanamycin sulfate. It took 4 days for the A42C, V44C, ADVQA-CDVQC, and VQA-CQC mutant colonies to show up on the plate, the same time period as that required for complement colonies. However, it took about 7 days for the ADV-CDC and PSA-CSC mutant colonies to appear. This slower growth rate on the plates is an indication of zero or reduced bc_1 activity in the virtual absence of environmental selection pressure. A similar phenomenon was observed with several cytochrome *b* mutants that had no bc_1 activity.

When mid-log phase, aerobically grown complement and mutant cells were inoculated into enriched Sistrom medium and subjected to anaerobic photosynthetic growth conditions, the A42C, V44C, VQA-CQC, and ADVQA-CDVQC mutants grow at a rate comparable with that of complement cells, the ADV-CDC mutant has a retarded (50%) growth rate, and PSA-CSC does not grow photosynthetically (Table I). Chromatophores from the A42C, V44C, and ADVQA-CDVQC mutant cells have cytochrome bc_1 complex activity comparable with that of the complement chromatophores. The VQA-CQC and ADV-CDC mutant chromatophores have, respectively, 77 and 68% of the bc_1 complex activity found in complement chromatophores. ICM from the PSA-CSC mutant have no ubiquinol-cytochrome *c* reductase activity. This was expected, since bc_1 complex is required for photosynthetic growth and this mutant does not grow photosynthetically.

To determine whether the loss (or decrease) of the cytochrome bc_1 complex activity in the mutant membranes results from a lack of or improper assembly of ISP protein in the membrane, the amount of ISP and its EPR characteristics in mutant and complement membranes were compared. Western blot analysis with antibodies against *R. sphaeroides* cytochrome *b*, cytochrome c_1 , ISP, and subunit IV revealed that the amount of these four subunits in the six mutant membranes is the same as that in the complement membrane (Fig. 1, lanes 2-8). Absorption spectral analysis shows that the content of cytochrome *b* and c_1/c_2 in all of these mutant membranes is the same as that in complement membrane. These results indicate that the mutations did not affect the assembly of ISP protein into the membrane. The [2Fe-2S] cluster in all of these mutant membranes has an EPR spectrum

Table I
 Characterization of ISP neck cysteine(s) mutants

Strains	Position of cysteine(s) substitutions	Photosynthetic growth	Enzymatic activity ^a			Subunit composition	
			Chromatophore	ICM	Purified complex	Chromatophore or ICM	Purified complex
Complement	none	++ ^b	2.2	2.1	2.5	FBCQ ^c	FBCQ
A42C	Ala ⁴²	++	1.8	— ^d	2.8	FBCQ	FBCQ
V44C	Val ⁴⁴	++	1.9	—	2.6	FBCQ	FBCQ
ADVQA-CDVQC	Ala ⁴² , Ala ⁴⁶	++	1.9	2.0	0	FBCQ	BC
VQA-CQC	Val ⁴⁴ , Ala ⁴⁶	++	1.7	1.8	0	FBCQ	BC
PSA-CSC	Pro ⁴⁰ , Ala ⁴²	- ^e	0	0	0	FBCQ	BC
ADV-CDC	Ala ⁴² , Ala ⁴⁴	+	1.5	0.3	0	FBCQ	BC

a, The enzymatic activity is expressed as μmol cytochrome *c* reduced/min/nmol cytochrome *b*

b, ++, the growth rate is essentially the same as that of the complement cells.

c, FBCQ indicates gene products of the *fbcF* (ISP), *fbcB* (cytochrome *b*), *fbcC* (cytochrome *c*₁) and *fbcQ* (subunit IV), respectively.

d —, Sample is not available

e -, no photosynthetic growth within 4 days.

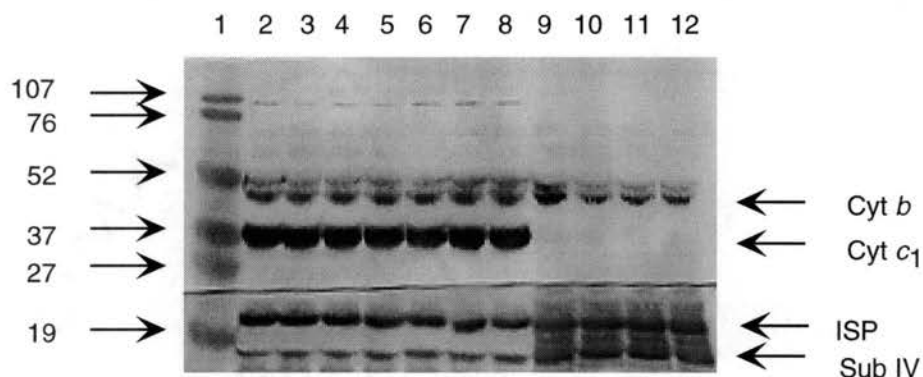


Figure 1. Western blot analysis of the cytochrome bc_1 complexes in mutant and chromatophore membranes. Membrane samples containing 75 pmol of cytochrome b were loaded into each well and subjected to SDS-PAGE. The proteins in the gel were transferred electrophoretically to a polyvinylidene difluoride membrane and reacted with antibodies against *R. sphaeroides* cytochrome b (Cyt b), cytochrome c_1 (Cyt c_1), ISP, and subunit IV (Sub IV). After transfer, membrane was cut into two pieces so that the upper part contained proteins with a molecular mass greater than 23 kDa, including cytochromes b and c_1 , and the bottom part contained the low molecular mass proteins, including ISP and subunit IV. Since antibodies against *R. sphaeroides* cytochrome bc_1 complex available in our laboratory have antibody titers for cytochromes b and c_1 much higher than those for ISP and subunit IV, the top section of the membrane was developed with a horseradish peroxidase system, whereas the bottom section was developed with an alkaline phosphatase system. Lane 1, prestained molecular mass standards; lane 2, the complement chromatophores; lanes 3-7, the A42C, V44C, VQA-CQC, ADV-CDC, and ADVQA-CDVQC chromatophores; lane 8, the PSA-CSC ICM; lanes 9-12, effluent from the Ni^{2+} -NTA column, which is the unbound portion from detergent (1% DM)-solubilized membrane fraction of the VQA-CQC, ADV-CDC, PSA-CSC, and ADVQA-CDVQC mutants.

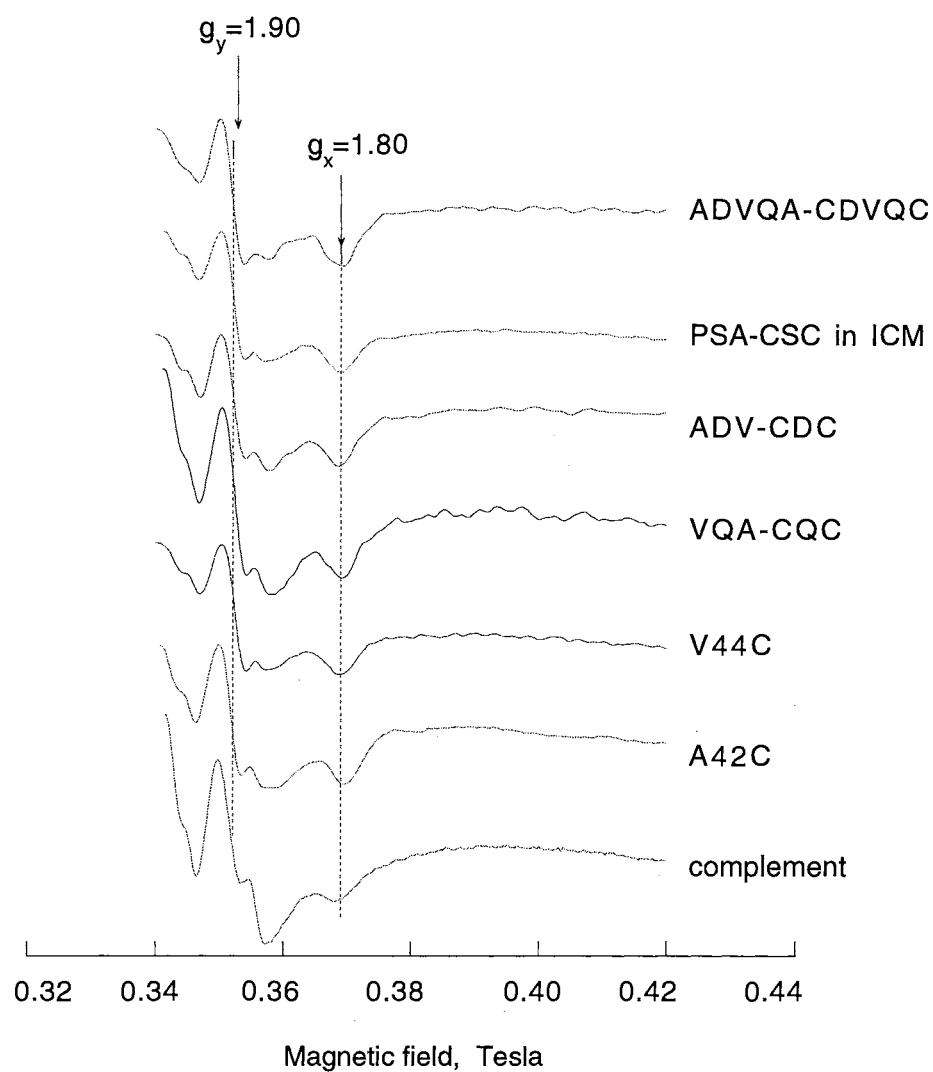


Figure 2. EPR spectra of the [2Fe-2S] cluster of the Rieske iron sulfur protein in mutant and complement membranes. Chromatophore membranes from the A42C, V44C, VQA-CQC, ADV-CDC, and ADVQA-CDVQC mutants and complement cells and ICM from the PSA-CSC mutant were incubated with a small amount of ascorbate on ice for about 10 min and frozen in liquid nitrogen. EPR spectra were recorded at 77 K with the following instrument settings: microwave frequency, 9.37 Hz; microwave power, 20 milliwatts; modulation

identical to that observed in complement chromatophores, with resonance at $g_x = 1.80$ and $g_y = 1.9$ (Fig. 2). Thus the mutations did not change the microenvironment of the iron-sulfur cluster.

Effect of Mutation on the Disulfide Bond Formation in the Neck Region of the Iron-Sulfur Protein—The bc_1 complex activity decreased by 23, 32, 14, and 100% in the VQA-CQC, ADV-CDC, ADVQA-CDVQC, and PSA-CSC mutant membranes, respectively, with no change in the amount of ISP incorporated into the membrane and the EPR characteristics of the [2Fe-2S] cluster. Did this activity loss result from increased neck region rigidity due to the formation of a disulfide bond? We addressed this question by comparing cytochrome bc_1 complex activity in mutant and complement membranes with and without β -ME treatment. Also, we used molecular modeling to examine the feasibility of disulfide bond formation in the PSA-CSC mutant.

When ICM from the PSA-CSC mutant, which has no bc_1 activity, was treated with β -ME, about 60% of the activity found in complement ICM was restored (Table II). It should be emphasized that the observed activity restoration is not due to nonenzymatic reduction of cytochrome c by β -ME, because less than 0.05 μ M β -ME is present in the assay mixture, and the restored activity is sensitive to antimycin. This restored cytochrome bc_1 complex activity is diminished when β -ME is removed by repeated centrifugation and suspension. However, the restored bc_1 activity is retained if the β -ME-treated membrane is reacted with sulfhydryl modifying reagents, such as NEM or PCMB, at 5-fold molar excess to β -ME, followed by repeated centrifugation and suspension (Table II). Activity restoration is not observed when the PSA-CSC mutant membrane is treated with NEM or PCMB without prior reduction with β -ME. These results indicate that the complete lack of the bc_1 activity in the PSA-CSC mutant membrane results from decreased mobility of the ISP head domain, due to a neck region made rigid by the formation of a disulfide bond between Cys⁴⁰ and Cys⁴². The addition of β -ME reduces this disulfide bond, restoring flexibility to the neck region. Modification of β -ME released SH- groups with NEM or PCMB has no effect

Table II

The effect of β -ME, NEM and PCMB on the cytochrome bc_1 complex in chromatophore and ICM membrane

Strains	Cytochrome bc_1 activity					
	Chromatophore			ICM		
	No treatment	β -ME	NEM/PCMB ^a	No treatment	β -ME	NEM/PCMB
Complement	2.2	2.2	2.2	2.1	2.0	2.0
A42C	1.8	1.8	1.8	— ^b	—	—
V44C	1.9	1.9	1.9	—	—	—
ADVQA-CDVQC	1.9	1.9	1.9	2.0	2.0	2.0
VQA-CQC	1.7	1.7	1.7	1.8	1.8	1.8
PSA-CSC	—	—	—	0	1.2	1.2
ADV-CDC	1.5	1.5	1.5	0	1.4	1.4

^a NEM or PCMB was added at 5-fold molar excess to β -ME pretreated membrane.

^b Sample is not available

on the flexibility of the neck region but blocks reformation of the disulfide bond, thus guaranteeing retention of the restored activity.

Formation of a disulfide bond between Cys⁴⁰ and Cys⁴² in the ISP neck of the PSA-CSC mutant is also supported by molecular modeling using the peptide sequence of NCSCQVQALA, corresponding to the neck sequence of the PSA-CSC mutant. In the bovine *bc*₁ structure (4), the distance between C- atoms of Ala64 and Ala66 (corresponding to residues 40 and 42 of *R. spheroides* ISP) is 5.2 Å, and the side chains of the two residues point in the same direction relative to the backbone of this stretch. Molecular modeling, based upon this structural information, indicates that a disulfide bond can be formed. This would result in an 11-membered ring structure. A distance of 5.2 Å for disulfide bond formation is slightly longer than the 4.1 Å observed for the two C- atoms of the disulfide bond, between Cys¹⁶⁰ and Cys¹⁴⁴ of ISP, in bovine *bc*₁ crystals (4).

The possibility that the lack of *bc*₁ activity in the PSA-CSC mutant ICM is due to the formation of an intermonomer disulfide bond between one of the two cysteines at positions 40 or 42 and a cysteine in the other monomer is ruled out because *bc*₁ complex activity in the A42C mutant chromatophore or ICM is the same as that in complement membranes and is not activated by the addition of β-ME. Furthermore, the distance between the two cysteines at position 40 and 40' in ISP from different monomers appears to be over 33 Å, as estimated from the distance between Ala⁶⁴ of one ISP monomer and Ala^{64'} in the symmetrically related monomer in the bovine *bc*₁ structure. Intermonomer disulfide bonding over such a long distance is impossible.

When the VQA-CQC and ADVQA-CDVQA mutant chromatophores, which have, respectively, 77 and 86% of the cytochrome *bc*₁ complex activity of the complement chromatophore, were treated with β-ME, the *bc*₁ activities were unchanged (Table II). Also, when β-ME-pretreated mutant chromatophores were reacted with NEM or PCMB, no change in activity was observed (Table II). These results proved that no disulfide bonds are formed between the cysteines at positions 44 and 46 or positions 42 and 46. The lack of

disulfide bond formation in the ISP neck region of these two mutant chromatophores is also supported by the bovine bc_1 crystal structure, which shows that the distances between C- β atoms of Val⁶⁸ and Ala⁷⁰ of ISP (Val⁴⁴ and Ala⁴⁶ in *R. sphaeroides*) and between C- atoms of Ala⁶⁶ and Ala⁷⁰ (Ala⁴² and Ala⁴⁶ in *R. sphaeroides*) are 7.35 and 12 Å, respectively. These exceed the distance that permits disulfide bond formation. Since no disulfide bond is formed, the flexibility of the ISP neck should not change in these mutant chromatophores. Thus, the decreased bc_1 activity in these two mutant chromatophores cannot be attributed to decreased mobility of the head domain of ISP.

The finding that the ADV-CDC mutant ICM has only 20% as much bc_1 complex activity as does its chromatophore membrane is rather surprising (Table I), because bc_1 complex activities in chromatophore and ICM are comparable in all of the other cysteine-substituted mutants and in complement cells (Table I). The addition of β -ME to ADV-CDC mutant membrane has no effect on bc_1 complex activity in chromatophores, while increasing the activity in ICM to the level observed in untreated chromatophores (Table II). The restored activity in the mutant ICM is diminished by removal of β -ME. The addition of 5-fold molar excess NEM or PCMB to the β -ME-treated mutant ICM preserves the restored activity in the membrane. These results indicate that the loss of bc_1 activity in the ADV-CDC mutant ICM, compared with that in its chromatophore, results from the decreased mobility of the head domain of ISP, due to formation of a disulfide bond between Cys42 and Cys44 in the neck region of ISP. However, a similar explanation does not account for the lower (32% less than complement) bc_1 complex activity in ADV-CDC mutant chromatophore or in β -ME-treated ICM, because neither contain disulfide bonds. Apparently, some other effect of cysteine substitution decreased the bc_1 activity.

It should be noted that the loss of bc_1 complex activity in the ADV-CDC mutant ICM is not due to the formation of an intermonomer disulfide bond, because the distance between potential cysteine pairs in the two monomers is over 30 Å. Recall that the bc_1 activity in the single cysteine substitution mutants A42C and V44C was not affected by the

addition of β -ME. In the bovine bc_1 complex structure, the distance between C- β atoms of Ala⁶⁶ and Val⁶⁸ (corresponding to residues Ala⁴² and Val⁴⁴ in *R. sphaeroides*) is 7 Å, and the orientations of the side chains are opposite each other. However, since the neck region is flexible, a different crystal form might result in a different conformation. This comparison is at the "noise" level of homologous sequence similarities, e.g. *bovine versus R. sphaeroides*. Therefore, formation of a disulfide bond between Cys⁴² and Cys⁴⁴ in ADV-CDC mutant ICM is not impossible.

Since disulfide bonds occur in ICM, but not in the chromatophore, of the ADV-CDC mutant, probably disulfide bond formation in this mutant ISP neck region depends on the oxygen supply in the cell culture and is related to the functionality of the bc_1 complex in the membranes. When these mutant cells are grown in the dark with an ample oxygen supply, no bc_1 activity is detected in the cytoplasmic membrane due to the formation of a disulfide bond in the ISP neck region. The addition of β -ME to the cytoplasmic membrane can restore bc_1 activity to the level observed in the chromatophore membrane. This is consistent with the fact that bc_1 complex is not required for dark aerobic growth of this organism because the cells can utilize quinol oxidases. When the O₂ supply is limited, the cells adjust their protein expression to prepare for photosynthetic growth, as indicated by the appearance of chlorophyll. The bc_1 activity in ICM increases slightly (0.3 μ mol of cytochrome *c* reduced per min per nmol of *b*; Table I), because either some part of the bc_1 complexes become active by disulfide bond cleavage or the newly synthesized complexes stay in a conformation that prevents disulfide bond formation between Cys⁴² and Cys⁴⁴. When oxygen is completely depleted from the culture, the cells undergo photosynthetic growth and require active bc_1 complex. Apparently, no disulfide bonds are formed in the mutant chromatophores, and bc_1 activity increases greatly (1.5 μ mol of cytochrome *c* reduced per min per nmol of *b*).

Effect of Mutation on Binding Affinity of the Iron-Sulfur Protein in the bc_1 Complex— Although chromatophores from mutants with a double cysteine mutation in the

ISP neck region (VQA-CQC, ADV-CDC, and ADVQA-CDVQC) have ISP amounts, EPR properties, and ISP neck flexibility similar to those in complement chromatophores, the bc_1 activities are 23, 32, and 14% less, respectively. Is this activity loss due to a decreased binding affinity of ISP to the whole complex? Assuming that ISP binding is sensitive to detergent treatment, any difference in subunit composition of purified His-tagged bc_1 complexes from mutant and complement strains will indicate detergent lability and binding affinity differences between normal and mutant ISPs.

When chromatophores from these three mutant cells, VQA-CQC, ADV-CDC, and ADVQA-CDVQC, at a cytochrome *b* concentration of 25 μ M were mixed with various amounts of dodecylmaltoside (up to 0.44 mg/nmol of cytochrome *b*), the cytochrome bc_1 complex activities decreased as the concentration of dodecylmaltoside (DM) increased (Fig. 3A). More than 95% of the bc_1 complex activity in all of these mutant chromatophores was inactivated by 0.44 mg of DM/nmol of cytochrome *b*. Under identical conditions, complement chromatophores did not lose activity (Fig. 3A), indicating that the mutant cytochrome bc_1 complexes (two-cysteine substitution) are more labile to detergent.

Since DM solubilizes the bc_1 complex from *R. sphaeroides* chromatophores, it is important to establish that DM denaturation of the bc_1 complex in mutant chromatophores is due to ISP dissociation from the complex and not due to a decreased affinity for membrane. This is done by centrifuging DM-treated chromatophores from mutants and complement cells at 100,000 X g for 30 min to separate the solubilized from the unsolubilized fractions and measuring cytochrome content, ISP amount, and bc_1 activity in both fractions. Since the amount of cytochrome bc_1 complex protein (cytochromes *b* and c_1 , ISP, and subunit IV) in the supernatant fractions of the three mutant chromatophores is comparable with that in the supernatant fraction from complement chromatophores at a given concentration of detergent, it is apparent that DM solubilization of the cytochrome bc_1 complex is not affected by mutation (data not shown). However, the specific activity of cytochrome bc_1 complex, based on *b* content in the supernatant fractions from mutant

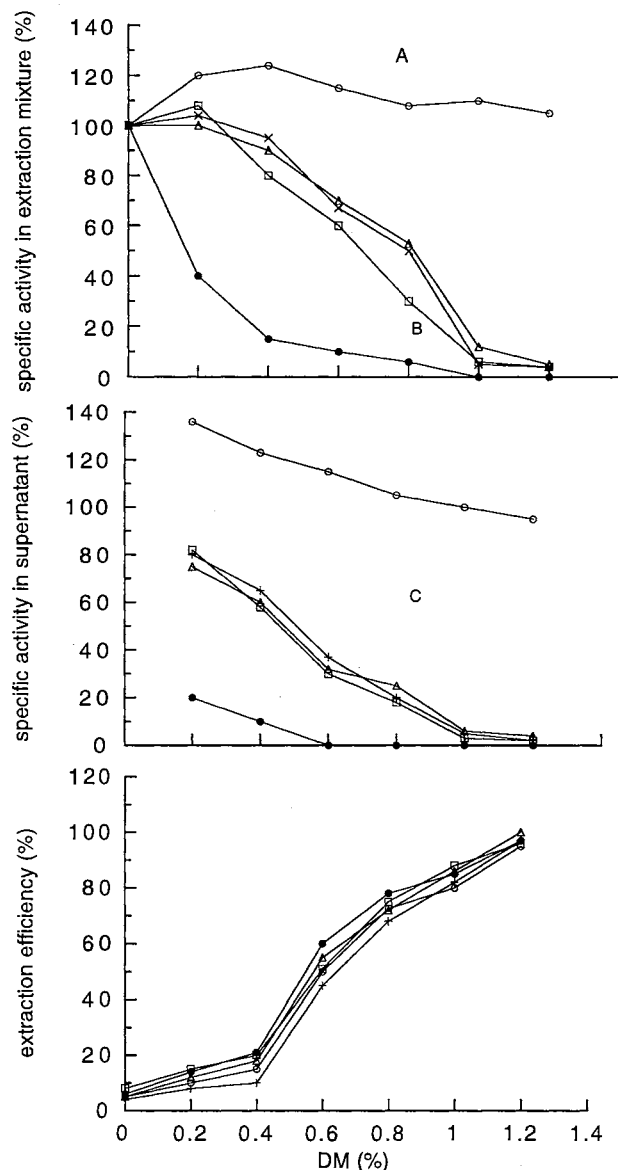


Figure 3. The effect of dodecylmaltoside concentration on the activity and the solubilization efficiency of bc_1 complex from membranes of the double cysteine-substituted mutants and the complement cells. The bc_1 complex activities in the extraction mixture (A) as well as in the supernatant fractions (B) obtained from membranes treated with various concentrations of dodecylmaltoside are expressed as the percentage of that of the untreated sample. Extraction efficiency (C) was calculated as the ratio of the cytochrome *b* present in the detergent-solubilized supernatant fraction to the total amount of cytochrome *b* in the extraction mixture. The β -ME -restored bc_1 activity in the PSA-CSC mutant ICM was used as 100% activity for this mutant membrane. Membranes from the complement (O), VQA-CQC (+), ADV-CDC (Δ), ADVQA-CDVQC (\square), and PSA-CSC (\bullet) cells were adjusted to 25 μ M cytochrome *b* with 50 mM Tris-Cl, pH 8.0, containing 20% glycerol. Dodecylmaltoside was added to give the final concentrations as indicated.

chromatophores, decreased as the detergent concentration increased (Fig. 3B). Under identical conditions, the bc_1 activity in supernatant fractions from complement chromatophores does not drastically decrease. The extraction efficiency, based on cytochrome b content, is the same for all mutants and complement membranes (Fig. 3C).

To confirm that the loss of bc_1 activity in the DM-solubilized fractions resulted from dissociation of ISP from the complex, the supernatant fractions, extracted by 0.5 or 1% of DM, were passed through a Ni^{2+} -NTA column. The column effluents and eluates were examined for bc_1 complex subunit composition. Two subunits, corresponding to cytochromes b and c_1 , were found in the Ni^{2+} -NTA column eluates (Fig. 4, lanes 5-7). ISP and subunit IV were detected in the column effluents by Western blot analysis (Fig. 1, lanes 9-11). On the other hand, four subunits (cytochrome b , cytochrome c_1 , ISP, and subunit IV) in unit stoichiometry are in the Ni^{2+} -NTA column eluates from detergent-solubilized complement chromatophores (Fig. 4, lane 2). These results indicate that a double cysteine substitution in the ISP neck region decreases the binding affinity of ISP for the bc_1 complex. Therefore, detergents dissociate ISP from the complex. Since no ISP is found in the Ni^{2+} -NTA column eluates from the DM (0.5%)-solubilized mutant chromatophore fractions having 40% of the untreated cytochrome bc_1 complex activity, the activity detected in this fraction reflects the ability of dissociated ISP to reconstitute into a functionally active bc_1 complex after dilution of detergent in the assay mixture. Perhaps the activity decrease in untreated mutant chromatophores indicates the extent of ISP dissociation from the complex. However, the 14% decrease in bc_1 complex activity in the A42C or V44C mutant chromatophores is probably due to a deviation in the activity assay and not to a mutational effect, since their activities are not labile to detergents. Indeed, all four subunits of the bc_1 complex are absorbed on the Ni^{2+} -NTA column after the detergent solubilization (Fig. 4, lanes 2 and 3). The purified complexes from these two mutants have specific activities comparable with that of the complement (Table I).

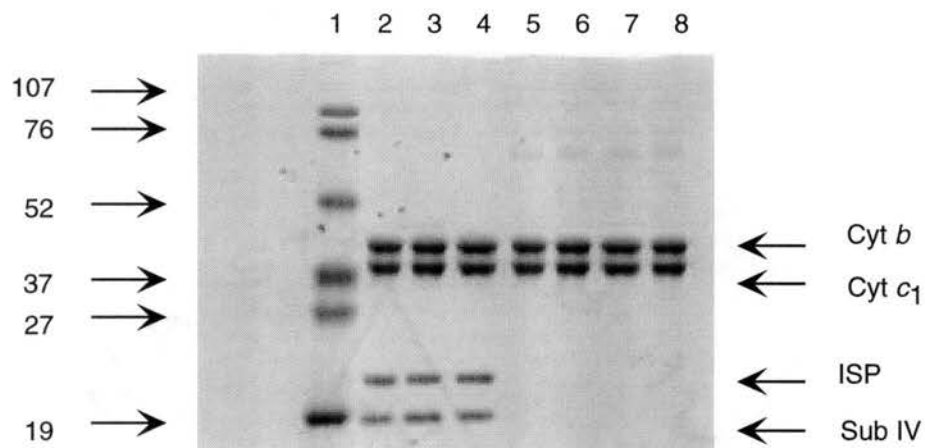


Figure 4. SDS-PAGE of purified His6-tagged *bc*₁ complexes. Aliquots of cytochrome *bc*₁ complexes (75 pmol of cytochrome *b*), recovered from the Ni²⁺-NTA column of DM-solubilized mutant and complement membrane fractions were loaded into each well of a SDS-PAGE gel. *Lane 1*, prestained molecular weight standards; *lane 2*, cytochrome *bc*₁ complex from the wild-type complement strain; *lanes 3-8*, the *bc*₁ complexes from mutants A42C, V44C, VQA-CQC, ADV-CDC, ADVQA-CDVQC, and PSA-CSC, respectively.

Although the restored bc_1 complex activity in the PSA-CSC mutant ICM treated with β -ME is more labile to DM treatment than are the bc_1 activities in VQA-CQC, ADV-CDC, and ADVQA-CDVQC mutant chromatophores (Fig. 3), the effectiveness of dodecylmaltoside in solubilizing bc_1 complex from PSA-CSC mutant ICM and the bc_1 complex subunit composition of the Ni^{2+} -NTA column effluents and eluates (Fig. 1, *lane 11*, and Fig. 4, *lane 8*) are the same as that for the three double cysteine-substituted mutant chromatophores. Probably the binding affinity of ISP for the bc_1 complex in PSA-CSC is weaker than in the other double cysteine mutant chromatophores. Thus, ISP is more easily dissociated from the complex by detergent. Since only 60% of the bc_1 activity found in complement chromatophore is restored to the PSA-CSC mutant ICM upon the addition of β -ME, it is likely that 40% of the ISP in this mutant ICM is dissociated from the bc_1 complex.

The ability of detergent-dissociated ISP to reconstitute into functionally active bc_1 complex depends on the detergent concentration in the reconstituting mixture (or in the assay mixture) and the status of the dissociated ISP. It has been reported (23) that including reducing reagents, such as dithiothreitol or β -ME, during isolation of ISP from the complex protects free ISP from oxidation by oxygen and that the addition of phospholipid to the detergent-containing solution reduces effective detergent concentration. Therefore, we examined the effect of β -ME and phospholipid on the reassociation of ISP into functionally active bc_1 complex in the DM-solubilized chromatophore fraction from the ADV-CDC mutant cells. As described above, β -ME has no effect on the bc_1 activity in this mutant chromatophore or on the solubilization efficiency of DM. β -ME preserves the activity of mutant ISP after its dissociation from bc_1 complex. In the presence of β -ME, when the mutant chromatophore is treated with 1.2% dodecylmaltoside, the cytochrome bc_1 complex activity in the supernatant fraction is 10-fold higher than that in the supernatant fraction obtained from mutant chromatophore without pretreatment with β -ME. The activity of the supernatant with β -ME is about 50% of that in the chromatophore before detergent

solubilization. When the detergent-solubilized fraction obtained from the β -ME -treated mutant chromatophore is incubated with phospholipid (10 mg/ml), the cytochrome bc_1 complex activity increases to 95% of that in the untreated chromatophore. Without prior addition of β -ME, the supernatant has minimal activity (2%), which only increases slightly after the addition of phospholipid. These results indicate that the addition of β -ME to the ADV-CDC chromatophore prior to detergent solubilization prevents denaturation of dissociated ISP and subunit IV and thus enables them to reconstitute with cytochromes b and c_1 to form functionally active bc_1 complex after excess detergent is removed by phospholipid and dilution with the assay mixture.

REFERENCES

1. Trumpower, B. L., and Gennis, R. B. (1994) *Annu. Rev. Biochem.* **63**, 675-716.
2. Mitchell, P. (1976) *J. Theor. Biol.* **62**, 327-367.
3. Yu, C-A., Kachurin, A. M., Yu, L., Xia, D., Kim, H., and Deisenhofer, J. (1996) *Biochim. Biophys. Acta* **1275**, 47-53.
4. Xia, D., Yu, C. A., Kim, H., Xia, J. Z., Kachurin, A. M., Zhang, L., Yu, L., and Deisenhofer, J. (1997) *Science* **277**, 60-66.
5. Kim, H., Xia, D., Deisenhofer, J., Yu, C. A., Kachurin, A., Zhang, L., and Yu, L. (1997) *FASEB J.* **11**, 1084.
6. Kim, H., Xia, D., Yu, C. A., Kachurin, A., Zhang, L., Yu, L., and Deisenhofer, J. (1998) *Proc. Natl. Acad. Sci. U. S. A.* **95**, 8026-8033.
7. Zhang, Z. L., Huang, L-S., Shulmeister, V. M., Chi, Y-I., Kim, K. K., Huang, L-W., Crofts, A. R., Berry, E. A., and Kim, S-H. (1998) *Nature* **392**, 677-684.
8. Yu, C. A., Xia, D., Kim, H., Deisenhofer, J., Zhang, L., Kachurin, A. M., and Yu, L. (1998) *Biochim. Biochem. Acta* **1365**, 151-158.

9. Iwata, S., Lee, J. W., Okada, K., Lee, J. K., Iwata, M., Rasmussen, B., Link, T. A., Ramaswamy, S., and Jap, B. K. (1998) *Science* 281, 64-71.
10. Crofts, A. R., and Meinhardt, S. W. (1982) *Biochem. Soc. Trans.* 10, 201-203.
11. Tsai, A. L., Olson, J. S., and Palmer, G. (1987) *J. Biol. Chem.* 262, 8677-8684.
12. Iwata, S., Saynovits, M., Link, T. A., and Michel, H. (1996) *Structure* 4, 567-579.
13. Link, T. A., Saynovits, M., Assmann, C., Iwata, S., Ohnishi, T., and Von Jagow, G. (1996) *Eur. J. Biochem.* 237, 71-75.
14. Tian, H., Yu, L., Mather, M., and Yu, C. A. (1998) *J. Biol. Chem.* 273, 27953-27959.
15. Khosravi, M., Ryan, W., Websger, D. A., and Stark, B. C. (1990) *Plasmid* 23, 138-143.
16. Siström, W. R. (1960) *J. Gen. Microbiol.* 22, 778-785.
17. Yu, L., and Yu, C. A. (1990) *Biochemistry* 30, 4934-4939.
18. Lowry, O. H., Rosebrough, N. J., Farr, A. L., and Randall, R. J. (1951) *J. Biol. Chem.* 193, 265-275.
19. Berden, J. A., and Slater, E. C. (1970) *Biochim. Biophys. Acta* 216, 237-249.
20. Yu, L., Dong, J. H., and Yu, C. A. (1986) *Biochim. Biophys. Acta* 852, 203-211.
21. Laemmli, U. K. (1970) *Nature* 227, 680-685.
22. Pemberton, J. M., and Bowen, A. R. S. G. (1981) *J. Bacteriol.* 147, 110-117.
23. Gonzalez-Halphen, D., Vazquez-Acecedo, M., and Garcia-Ponce, E. (1991) *J. Biol. Chem.* 266, 3870-3876.

CHAPTER V

DISCUSSION

I. General discussion.

II. The paradox about ISP interaction with Q_o pocket of cytochrome *b* and its position relative to *b* and c_1 subunit.

III. The paradox about stigmatellin induced redox potential increase of ISP.

IV. The paradox about the chemistry of quinol oxidation in the Q_o pocket.

V. Conclusion.

I. General discussion

The resolution of three-dimensional structure of cytochrome bc_1 complex has added a wealth of information to the already existing sophisticated body of knowledge, and further sharpened the available tools for studying the bc_1 complex in greater detail. The structural analysis has confirmed and consolidated many earlier findings, added atomic scale precision to our knowledge, and raised new and challenging issues on the mechanism of function and dynamic interactions between the subunits of the complex. Bifurcation of the electrons at Q_o site through ISP head domain movement within cytochrome bc_1 complex during catalysis is a striking step-forward. However, whether this movement is tethered diffusion, or is somehow triggered at the molecular level, and if so how, is yet to be determined.

Based on biochemistry and X-ray crystal structural studies, the following steps are proposed to make a mechanistic model of cytochrome bc_1 catalyzed reaction.

1. In the oxidized bc_1 complex, ISP may be loosely attached to cytochrome b at a so called “fixed position”, which is 27 Å to heme b_L and 31 Å to heme c_1 . The lower anomalous light scattering iron signal compared with that of heme indicates that ISP may oscillate around or distribute elsewhere randomly.

2. Substrate quinol comes in and binds near the opening of Q_o pocket. Inhibitor binding at this site is accompanied by slight conformational change around Q_o pocket, including the opening of the pocket to allow the inhibitor to interact with His161 (one of the ligands in [2Fe-2S] cluster). These changes may also happen after quinol binding. So far the poor densities of cd helices and ef loop have prevented us from predicting the exact conformational changes in those areas. Quinol binding in Q_o pocket would increase the “fixed” population of ISP. Such effect might be achieved through: (i) conformational changes in cytochrome b or ISP, although small but efficient enough to lock it up at “b-position”; (ii) direct interaction between quinol and His161 of ISP, or combination of both. It should be noted that no quinol binding at Q_o site is observed.

3. First proton leaving from QH_2 is facilitated by the positive charges in the environment, especially R282 and K288 which are located near the opening of Q_o pocket. QH^\cdot is subsequently stabilized by electrostatic interaction with those residues. The pathway leading proton to the aqueous phase is unclear at this moment. One of the attractive proton carriers is His161 of ISP. Isolated oxidized ISP has two pKa values (7.6 and 9), whereas reduced ISP has a pKa over 11. If one of the groups is His161, protonation and reduction of ISP will be coupled tightly because extra electron uptake by Fe in the cluster will be stabilized through binding of a proton nearby. After reduction, hydrogen bond formation between ISP and QH^\cdot is not favored due to slight conformational change in ISP part. QH^\cdot moves deeper into the Q_o pocket, where it is stabilized by weak hydrophobic interaction with the environment. Compared with semiquinone generated at Q_i site, QH^\cdot at P2 site is not stabilized by a positive charge. Dissociation of second proton is facilitated by a positive charge in heme b_L as well as the polar residues clustered at the bottom of Q_o pocket. Electron transferring from Q^\cdot to heme b_L leads to a change of conformation in cytochrome b , which unlocks ISP from the fixed position. In chicken $P2_12_12_1$ native crystal, ISP is at c_1 position; ef loop holds ISP and cytochrome c_1 together in the right orientation and distance for electron transfer (Figure 1B). The extrinsic domains of cytochrome c_1 and ISP sit on the first half (residues 246-261) and the second half (residues 262-268) of ef loop respectively. In stigmatellin cocrystal, the tip of ISP is underneath part of ef loop and is held in b-position by cooperative interaction of cd helices, ef loop and gh loop of cytochrome b (figure 1A). The most profound conformational change other than Q_o pocket between these two positions is confined in the ef loop. The average displacement of the loop is ca 2 Å with the largest deviation observed for residues 262-265. Therefore, the unlocking of ISP may be achieved by moving ef loop out of the way to allow ISP to get closer to cytochrome c_1 . Movement of ef loop may result from: (i) the binding of QH^\cdot at P2 site. Expansion of PEWY in the ef loop is observed as a result of MOA-stilbene binding which may in turn

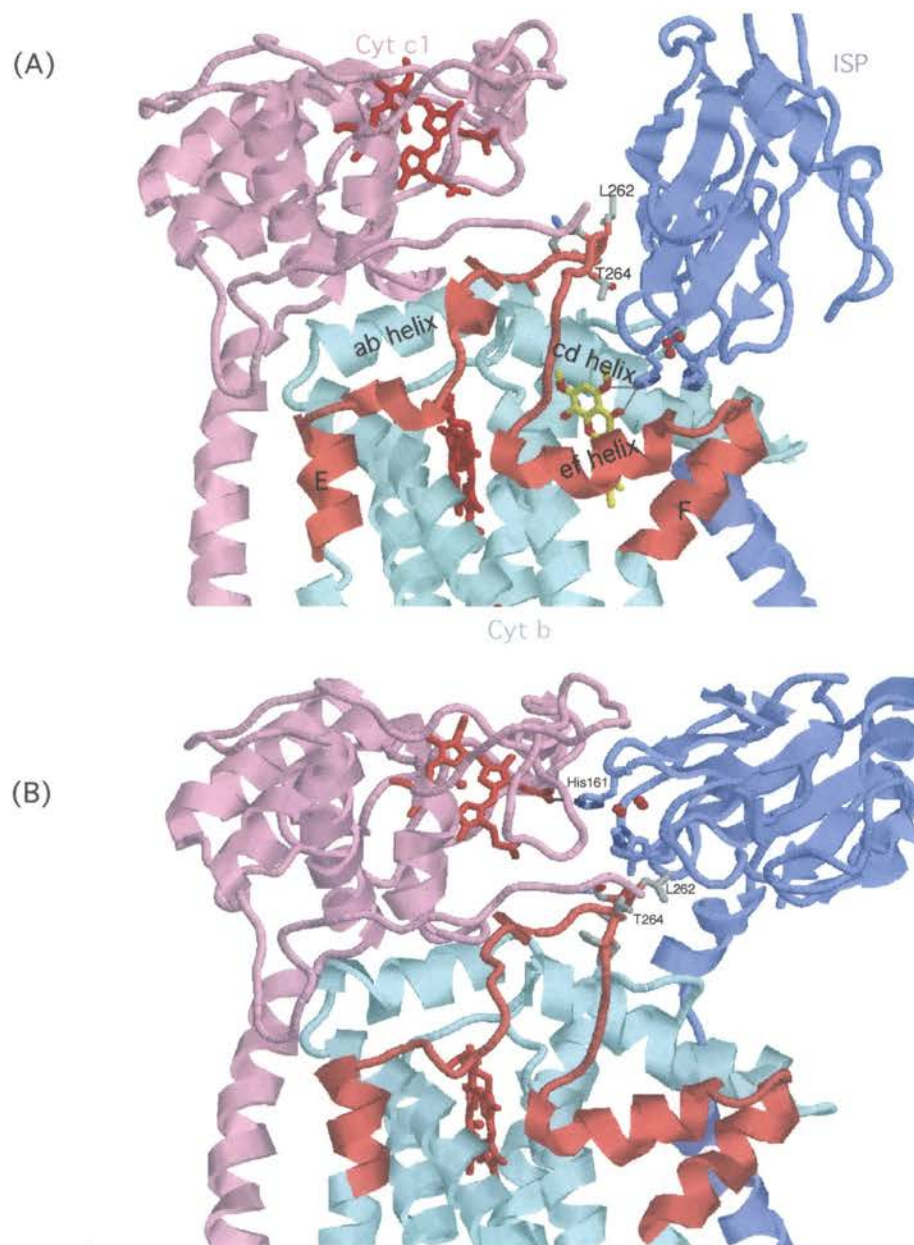


Figure 1. The architecture of ef loop of cytochrome *b*: staging area of ISP and cytochrome *c*₁. (A) The interaction between ISP and cytochrome *b* in stigmatellin (yellow) loaded crystal. NεH of His161 (blue stick) in ISP is within hydrogen-bonding distance of carbonyl and methoxy oxygens (red stick) of stigmatellin. (B) Interaction between ISP and Cyt *c*₁ in bovine *p*6₅22 crystal form. Hydrogen bond is formed between His161 of ISP and D propionate of heme *c*₁. Helix E, F and connecting ef loop are lighted in pink.

change the whole conformation of ef loop; (ii) conformational changes of transmembrane helices of cytochrome *b*.

4. Reduced ISP has higher affinity for oxidized cytochrome c_1 subunit. This affinity is related to the conformation of reduced ISP and oxidized c_1 , or hydrogen bonding. Unlocked ISP will diffuse to c_1 position. This diffusion could be further facilitated or triggered again by ef loop conformational change that is induced by electron transferring from heme b_L to b_H . Such hypothesis is based on the observation that cytochrome *b* reduction occurs before cytochrome c_1 reduction in stop-flow kinetic studies (1). It is possible that the energy released during electron transfer from b_L and b_H is transformed into conformational change in cytochrome *b*. The ef loop comes back near the original position, sitting inbetween c_1 and cytochrome *b* Q_o pocket and holding reduced ISP and c_1 together.

5. In the c_1 form, the [2Fe-2S] cluster of ISP is very close to heme c_1 . The [2Fe-2S] cluster is only 15 Å away from the Fe atom of heme c_1 . The head domain of ISP interacts with residues of the cytochrome c_1 subunit as well as the ef loop. Most of these interactions are van der Waals contacts and only two clear hydrogen bonds are observed in bovine *P6₅22* crystal form in which the crystal contact occurs on the ISP head domain. One of hydrogen bonds formed between His 161 of ISP and the D propionate (figure 1B) could be an artifact of the crystal packing since the enzymatic turn-over requires fast on and off rate between ISP and c_1 . A hydrogen bond between ISP and c_1 at c_1 -position will inevitable slow down the dissociation of ISP and cytochrome c_1 . Since the redox potential difference between ISP and c_1 is very small at physiological condition, electron equilibrates between these two centers easily.

6. With the help of acidic residues located around 70 and 167 in cytochrome c_1 , cytochrome *c* gains access to the exposed C corner of heme c_1 , where electron transfer is expected to occur. The C corner is facing intermembrane space region and is not involved with binding of ISP. After electron is carried away by cytochrome *c*, oxidized

ISP takes a conformation that disfavors the tight interaction with oxidized cytochrome c_1 , therefore, the repulsive force may cause slight disorientation of ef loop. Part of the oxidized ISP comes back and loosely interacts with cytochrome b at b position. It should be noted that the resolution of ef loop in oxidized protein is not as good as the transmembrane helix part, suggesting slight flexible nature of that region. Furthermore, point mutation on T265M abolished bc_1 activity without changing EPR signal and ISP incorporation. T265 is located right at the turn of ef loop, the highest point from the membrane in cytochrome b . One explanation is the movement of the ISP is hindered by introducing a bulky methionine side-chain at a critical spot of the cytochrome b surface.

7. Electron transfer from b_H to quinone at Q_i site could happen simultaneously with cytochrome c reduction. The edge to edge distance between heme b_H and the bound quinone is less than 5 Å. Therefore, electron transfer between Q and heme b_H should take place at a high rate. The product $Q^{\cdot-}$ is then stabilized by positive charge in the environment such as K227. There are several residues close by, including H201 and D228 which may serve as proton donor. The proton can be easily replenished by water since the Q_i site is located near the aqueous interface, and there are obvious openings or channels in the van der Waals surface of the matrix side of these transmembrane helices.

Since the crystal structure only catches the static state of the protein, the proposed conformational changes during catalysis remain to be confirmed, either by crystallizing bc_1 at different redox state or by other indirect methods, such as NMR, EPR and FTIR. In the above hypothesis, movement of ISP is viewed as a triggered motion coupled with the redox states of cytochrome b . The tethered diffusion of ISP is also possible because the calculated energy input for ISP travelling from b to c_1 position is only 1.4 Kcal mol⁻¹, which allows the electron delivery to cytochrome c_1 within the time scale of turnover of the bc_1 complex. Generally, a regulated and controlled process is more favorable in the biological system. The conformational changes linked in particular to the redox state of

the iron-sulfur cluster were also demonstrated by significant body of experimental evidence.

II. The paradox about the interaction of the head domain of ISP with Q_o site of cytochrome *b* and its position relative to *b* and *c*₁ subunits

The lack of quinone density in the Q_o pocket present a great obstacle in proposing the nature of quinol binding in the Q_o pocket as well as the paths of electrons and protons. The combination of the inhibitor binding studies and EPR spectral analysis of reduced ISP leads to the above single Q occupancy model in which Q changes its binding sites in the Q_o pocket after one electron is transferred to ISP. Double Q occupancy (2), proton gated affinity change (3) and proton gated charge transfer (4) models were also proposed to explain the bifurcated quinol oxidation. These models all assumed that two Q molecules bind simultaneously in the Q_o pocket. The double Q occupancy model was first proposed by Ding et al (2) based on the empirical observations of the effect of quinone concentration on the EPR spectral g_x signal line shape of reduced [2Fe-2S]. When the Q pool is oxidized, a prominent signal at $g_x=1.8$ is observed: partial extraction of Q results in the broadening and an upfield shift of the g_x resonance to 1.783. When Q-pool was reduced, or Q completely extracted, or myxothiazol bound at the Q_o site, the g_x line shape becomes further broadened and centered near 1.77. In Ding and Dutton's work, the $g_x=1.8$ signal was attributed to a weak binding Q_{ow} and $g_x=1.783$ to a strong binding Q_{os}, a species that binds 30-fold more tightly than Q_{ow}. The Q_{os} was also expected to bind about 20-fold tighter than Q at Q_i site, based on the chromatophore Q-extraction EPR analysis. Although center P is rather a spacious pocket that could accommodate two Q headgroups, none of the structures reported show a density in the pocket expected for a tightly bound quinone species. Instead, a well defined negative Q density was observed in the Q_i site, indicating that the binding at the Q_i site is stronger than at the Q_o site. Therefore, the reported cytochrome *bc*₁ structure does not support the double Q-occupancy. The low quinone content in all the crystalline *bc*₁ complex

indicates the weak binding of quinone at Q_o pocket. It should be noted that all the EPR spectral studies that lead to the double Q occupancy model were carried out in the chromatophore level which is naturally rich of quinone/quinol. After bacterial bc_1 complex was purified by traditional iron-exchange or the newly developed histidine affinity chromatography, at least 2-3 Q per bc_1 complex remained in the preparation. The EPR spectrum is essentially the same as what is recorded in the chromatophore. Slight variation among batches was observed. In some batches, g_x at 1.8 is followed by a broad signal at 1.78. Addition of stigmatellin, UHDBT or MOAS shifts the g_x resonance to 1.785, 1.775 and 1.783, respectively. Binding of myxothiazol leads to a broad g_x signal at 1.77, similar to that of ISF. In crystalline Q deficient (0.7Q/ bc_1) bovine bc_1 complex, the g_x resonance at 1.8 is replaced by a broad signal at 1.77. Addition of stigmatellin and UHDBT still results in the generation of a sharp signal at 1.783 and 1.775, respectively. However, no difference in EPR spectral line shape is observed after MOAS and myxothiazol binding (4). These results indicated the direct interaction between stigmatellin or UHDBT with [2Fe-2S] cluster, which is not affected by Q_o pocket occupancy of quinone. As long as the inhibitors can bind to the pocket, the signal at 1.785 and 1.775 arises. The close contact between stigmatellin and UHDBT with reduced ISP is also supported by crystal structure analysis. In the fully oxidized enzyme, these inhibitors bind very close to His161 of ISP. The binding affinity decreases drastically after removal of ISP from bc_1 complex. The lack of direct contact between MOA type inhibitors with [2Fe-2S] cluster histidine ligands suggested an indirect effect on the EPR spectra. Compared with myxothiazol, MOAS binding site is deeper in the Q_o pocket, farther separated from ISP. Extensive kinetic investigation of Q_o site inhibition by MOAS implies that it is behaving as a non-competitive inhibitor of the cytochrome bc_1 complex function (5). Brandt and coworkers (5) have shown that ubiquinone was still present in the MOAS inhibited Q_o site on the basis of the inhibition pattern. Therefore we can explain that the EPR spectrum change in the naturally Q rich bc_1 preparations

after MOAS binding is originated from its interaction with a loosely bound quinone at P1 site. After Q is removed from Q_o pocket through crystalline bc_1 preparation methods, There is no more molecule to tie down reduced ISP to the Q_o site. A “free” form of ISP is indicated by EPR spectrum, in which g_x signal of 1.77 is observed. Myxothiazol’s binding site partially overlaps with that of stigmatellin and UHDBT in the crystal structure. Binding of myxothiazol may replace any endogenous quinone without direct interaction with ISP, thus ISP favors the “free” position in both Q-rich and Q-deficient preparations.

It is indicated by the EPR spectral analysis that the equilibrium position for reduced ISP is at “b-position”(6), which can explain why the g_x signal is extremely sensitive to the changes on the docking interface between ISP and surface of cytochrome $b Q_o$ pocket, as well as the occupancy in the Q_o pocket. Unless the EPR g_x data can be proven to arise from other sources, the best model to interpret the difference of EPR data between crystalline bc_1 and quinone rich bc_1 preparation is that one quinone occupying the Q_o pocket can tie down reduced ISP to give a distinct g_x resonance at 1.8. On the other hand, a slight trough around $g=1.77$ is observed in many cases, such as in ISF, no inhibitory mutation, and buffer containing ethanol or glycerol. Therefore it is somewhat uncertain to assign the $g_x=1.77$ signal observed in Q-deficient preparation, or MOAS or myxothiazol inhibited sample to the “free” form of ISP. The exact position and orientation of ISP in those cases remains to be verified by other approaches.

One question arises directly from the above analyses is whether movement of ISP is under redox control, in other words, whether the position of ISP is redox dependent? Traditional EPR is not the best tool to investigate this as only the reduced form of ISP can be probed, meanwhile, both ISP and cytochrome c_1 are also reduced in EPR study which does not exist under the normal physiological conditions. Crystallizing bc_1 complex under the different redox states of ISP is a straightforward approach to visualize the exact location of ISP. A method has been developed to crystallize partially or totally

reduced bc_1 complex. The result will be forthcoming. However, the lack of quinone in the preparation may be the excuse for the EPR specialist not to correlate the crystal structures with the previously obtained vast volume of information related to EPR studies in the chromatophore level. A noncrystallographic technique for evaluating the orientation of the ISP has been developed in the direction-dependence of the EPR signal from the [2Fe-2S] cluster in oriented bilayer (7,8). The preliminary data suggest that the structural heterogeneity might account for the different orientation of Rieske g tensor. According to these data, a large fraction of [2Fe-2S] cluster points their g_y and g_x orientations parallel and perpendicular, respectively, to the membrane. However, a broad additional maximum in the polar plot of g_y was observed at high angles with respect to the membrane, indicating a second conformation of ISP may exist with respect to the membrane (7). It should be noted that the oriented multilayer chromatophore membrane is dried on mylar sheet and reduced with gamma irradiation of the reaction centers. The signals detected can actually reflect the conformation of the oxidized state of ISP. The heterogeneity of ISP conformation indicated by this approach is also observed in the oxidized different crystal forms of bc_1 complex. The next step is to freeze ISP at different redox state and reduce it using gamma irradiation. EPR spectrum will be taken at two different angles (magnetic field is perpendicular or parallel to the membrane). The EPR g tensor change with respect to the membrane will then reflect the position change of ISP.

The position of ISP relative to c_1 and cytochrome b in partially reduced complex is obtained indirectly through studying the electron transfer between ISP and c_1 induced by (1) pH change and (2) laser flash photolysis. In the pH induced study, cytochrome c_1 partially reduced cytochrome bc_1 complex is used. It is known that ISP redox potential is pH dependent with a slope of -60mV/pH unit in the pH range of 6 to 9, while that of c_1 is not. At pH 8.0, the redox potentials of ISP and cytochrome c_1 are the same. Increasing the pH by mixing enzyme solution with a buffer of higher pH results in further reduction

of cytochrome c_1 at the expense of the oxidation of ISP. Likewise, dropping pH leads to reduction of ISP at the expense of the oxidation of c_1 . The pH induced electron transfer rate between c_1 and ISP is too fast to be determined accurately by the conventional stop-flow apparatus, indicating that ISP stays close to c_1 (“c-position”) when one of the two redox centers is in the reduced state. When ISP is fixed at “b position” by inhibitor stigmatellin, reduction of cytochrome c_1 is extremely slow ($t_{1/2}$ is one minute) after pH is adjusted from 7 to 9 (9). However, a much faster rate is observed for UHDBT-treated complex ($t_{1/2}$ is one second). The faster rate is due to the dissociation of UHDBT from the complex at higher pH (10). One can assume from this experimental observation that the fast diffusion of ISP from b - to c_1 -position is possible. The dissociation constant of UHDBT at higher pH remains to be determined, so far there is no straightforward method to measure the diffusion rate of ISP. These results also indicate that reduced ISP would favor c_1 position. In the laser photolysis experiment, reduced bacteria bc_1 complex is used. Laser flash induces reduction of ruthenium, which in turn leads to oxidation of cytochrome c_1 . Oxidized c_1 is soon reduced by ISP. The observed rate constant for rereduction of c_1 by ISP is only 3000 s^{-1} , which indicates ISP stays close to b -position when both redox centers are reduced. In conclusion, these studies suggested ISP is close to c_1 when either redox center is reduced. Hence this result seems consistent to the traditional EPR studies, which suggest the close interaction between ISP and cytochrome b Q_o pocket when both ISP and c_1 are reduced. In the end, we still need direct evidence to show the distinct location of ISP under different redox states by crystallizing of bc_1 complex at different redox states.

III. The paradox about stigmatellin induced redox potential increase of ISP

Binding of stigmatellin to cytochrome b results in more than 200 mV potential increase in ISP. In the Q_o pocket, carbonyl and methoxy oxygens of stigmatellin can be modeled as being within hydrogen-bonding distance of NεH of His 161 of the ISP in the stigmatellin loaded bc_1 crystal (11). Based on the Em change, Ohnishi and Link et al.

proposed that stigmatellin binds 5 orders of magnitude more tightly when the cluster is reduced (12, 13). Although the binding site for stigmatellin is mostly confined in cytochrome *b* subunit, stigmatellin binding does require ISP because the binding affinity decreased more than three order of magnitude after removal of ISP from the bc_1 complex, as indicated by the cytochrome *b* spectrum redshift studies. However there is no direct evidence to support that stigmatellin binding affinity is dependent on the redox state of ISP. The competitive fluorescent quenching titration of MOA type inhibitors suggested that stigmatellin effectively prevented binding of MOA-stilbene even when all the redox centers of the enzyme were oxidized(14). Obviously the dissociation constant for stigmatellin is low enough in all the redox states to abolish binding of a tight Q_o inhibitor MOA-stilbene completely (14). The poor correlation between E_m shift and binding affinity was also observed for hydroxyquinone type of inhibitor UHNQ (14). It is not appropriate to correlate the binding affinity with the E_m change solely based on the calculation, as the E_m values obtained by equilibrium titration of EPR g_y may reflect only a specific state of ISP. In this case, the most likely position for ISP during equilibrium titration is in c_1 position(14). It is tempting to speculate that the redox potential may be much higher when ISP switches back to *b* position, even in the absence of an inhibitor. Daldal and coworkers (15) have observed an 120 mV potential increase of [2Fe-2S] cluster when ISP was fixed at *b*-position by two alanine insertion in the neck region.

The most obvious parameter affecting the midpoint potential of [2Fe-2S] cluster is the electronic environment surrounding the redox active iron. The crystal structure indicates an extensive hydrogen bond network linking the iron-sulfur cluster to the surrounding protein. Breaking down the hydrogen bonds to the sulfur atoms inevitably increases the negative charge density around it and decreases iron-sulfur cluster potential. However, the increase of redox potential after stigmatellin binding can not simply be explained as the result of the hydrogen bonding between NεH His 161 in ISP to carbonyl and methoxy oxygens of stigmatellin (in this form of hydrogen bond, stigmatellin acts as

electron rich partner to stabilize the protonated Nε of His 161, then protonated NεH drags electron further away from the iron atoms which in turn leads to the increased redox potential). It is difficult to define the exact orientation of chromone ring of stigmatellin at current level of resolution. The hydrogen bond between deprotonated Nε and hydroxy group in stigmatellin is also possible when the chromone ring is flipped over 180 degree. The later case is more like the interaction between substrate quinol and ISP. However, Stigmatellin does not bind to ISF. The redox potential of ISF and EPR spectrum is unchanged in the excess amount of stigmatellin. Therefore the potential change induced by stigmatellin has to be achieved through cytochrome *b* in a rather indirect manner.

Crystal structure shows that binding of stigmatellin at Q_o pocket distal end pulls down ISP to *b* position. The compact docking contact between ISP and cytochrome *b* may be partially responsible for the redox potential change. Similar results (15) are obtained by the ISP neck insertion mutants. Significant redox potential increase is observed when ISP is locked at *b*-position. Mutations that change the interactions between the Rieske protein and cytochrome *b* are likely to affect the midpoint potential of stigmatellin inhibited [2Fe-2S] cluster. Such mutations need not be at the interacting interfaces between proteins; since mutation induced structural changes can be transmitted significant distances through proteins. This phenomenon was observed in the stigmatellin induced electron transfer between cytochrome *c*₁ and ISP subunits. In the *c*₁ partially reduced *bc*₁ complex, stigmatellin binding induces rapid oxidation of *c*₁ through increasing the high redox potential of ISP, suggesting that stigmatellin binding causes potential increase without or before docking of ISP to *b*-position. If the high redox potential of ISP can only be achieved through the docking between ISP head tip and cytochrome *b* Q_o pocket, then the rapid oxidation of *c*₁ is not going to happen since the distance between *c*₁ and ISP is over 31 Å under this circumstance. Therefore the redox potential increase has to happen when ISP is still close to *c*₁ which is the equilibrium position when one of the redox centers is reduced. Binding of stigmatellin induces

conformational changes in cytochrome *b*, which are in turn transmitted to ISP at a relatively higher speed than the tying down effect on ISP after inhibitor binding. In other words, after stigmatellin binding, ISP prefers the *b* position. The transition from c_1 to *b* is expected to be slow compared with intramolecular electron transfer. The neck region of ISP may be on the transmission pathway. It was reported that the presence of stigmatellin, but not that of antimycin or myxothiazol, blocks the proteolytic cleavage of ISP at its neck region by thermolysin, inferring that the conformation of this region must be modified under this condition (16). Such conformational change has been seen in the chicken mitochondria bc_1 structure obtained in the presence of stigmatellin; the neck region undergoes extension in the stigmatellin bound form. Furthermore, non-inhibitory mutations located in *R. capsulatus* ISP neck region V44F, V44L and A46T raised the potential of ISP by about 70 mV (17). Therefore changes in the neck region do have indirect effect on the midpoint potential of ISP.

Even though we proposed that QH₂ binding at Q_o pocket would have similar fixation effect on ISP as stigmatellin, one should realize the structural difference between them. The binding of QH₂ can be easily replaced by the inhibitor. The very tight interaction between ISP and cytochrome *b* in the presence of stigmatellin can restore the distorted chromatophore EPR signal caused by ethanol or glycerol (18). Somehow, binding of stigmatellin to ISP depleted complex can recruit ISF from the solvent and restore the typical g_x signal at 1.78 (19). No change was observed when Q_o pocket is occupied by QH₂. Therefore stigmatellin binding changes the conformation of cytochrome *b* to a configuration that will dock very well with ISP head domain. We should not expect similar tight docking between ISP and cytochrome *b* to occur when Q_o pocket is occupied by QH₂, because ISP depleted bc_1 complex does not have any activity when the complex is mixed with ISF in the presence of QH₂.

IV. The paradox about the chemistry of quinol oxidation at the Q_o pocket

Although the crystal structure and biochemistry studies on ISP suggested the possible movement of ISP head domain and its role in the bifurcated quinol oxidation, the chemical basis for obligatory bifurcation of electron flow remains unsolved. The current focus of interest is on two closely related questions linked to the mechanism of quinol oxidation: (1) what are the individual steps of quinol oxidation? (2) What is the energetics of the intermediates? In particular, how stable is semiquinone?

The original idea from Q cycle hypothesis is that the high redox potential of ISP drives reduction of heme b_L , sometimes called the “redox seesaw” (20). In other words, the thermodynamically unfavorable reduction of heme b_L ($E_m = -20\text{mV}$) by quinol ($E_m = +90\text{mV}$) is coupled to the energetically favorable oxidation of quinol by ISP ($E_m = +290\text{mV}$). The first electron must go to ISP in order for heme b_L to become reduced. However, the redox potential for one electron reduction of $\text{QH}_2/\text{QH}_2^{\cdot-}$ is near $+850\text{mV}$. This potential is too positive for electron transfer to any of the bc_1 redox centers. Deprotonation and subsequent formation of the semiquinone ($\text{QH}^{\cdot}/\text{Q}^{\cdot-}$) has an $E_m = +190\text{mV}$. Therefore it is generally acknowledged that for thermodynamic reasons a deprotonation step has to precede oxidation of quinol. The first pK_a value of ubiquinol in 80% ethanol is 11.2. Such high value leads Brandt to propose that this step makes most of the activation energy barrier for the overall bc_1 complex catalyzed reaction (3), based on the assumption that the electrostatic environment of quinol bound at Q_o pocket is similar to that in 80% ethanol. The standard free energy change for deprotonation at $\text{pH}7$ is 24kJ/mol , which is in desirable range of activation energy barrier of bc_1 complex determined experimentally. However, this value could be quite different when quinol is in the bound state. It has been calculated, on the basis of the high-resolution structure of the bacterial reaction center, that the effect of a charge on a bound quinone on the electrostatic potential of the surrounding protein can vary considerably. The above proposal only works when there is no strong base nearby in the Q_o pocket to facilitate protonation and to stabilize the quinol anion by a positive charge (3), otherwise the

thermodynamic barrier will be easily abolished. Although the detailed structural information about binding of quinol at Q_o pocket is not available, a positive charge R282 is located near the P1 site, the putative QH_2 binding site. Mutagenesis study suggested that R282 is critical for activity as mutant R282M only maintained 20% wild type activity. The possible role for this residue would be to lower the effective pKa of QH_2 and transiently stabilize QH^- . This observation basically undermines Brandt's proposal. The identity of the signal that triggers quinol deprotonation is still not known, but it must be an "oxidant-induced deprotonation". In other words, it is triggered by binding of oxidized ISP to the P1 site. The His161 in ISP then serves as a carrier to move the first proton to aqueous phase through domain movement. The proximity of His 161 to P1 site is indicated by the crystal structure. At this position, ISP could influence the environment of the P1 site, with the help of R282, leading to the first deprotonation, and electron transfer from QH to ISP occurs efficiently. If deprotonation of QH_2 occurs before ISP binding at P1 site, the product QH^- has to be stabilized substantially by the environment until the first electron transfer can occur. Then the redox potential for $QH^-/Q\cdot$ will be too high to allow its oxidation by ISP.

There are two points of view concerning the lifetime of intermediate semiquinone. It is either very unstable and immediately removed by transferring electron to heme b_L , or is stabilized by forming a tight complex with ISP His161. Both cases would result in no detectable semiquinone signal at center P in the EPR spectrum (4). In the first hypothesis, the immediate removal of semiquinone by reduction of heme b_L lowers redox potential of the QH/QH^\cdot sufficiently to allow the otherwise not very favorable electron transfer to occur between ISP and QH^\cdot . It should be mentioned that even though the redox potential of QH/QH^\cdot is near 200mV in 80% ethanol, the actual value for this pair in the protein is still unknown since the stability of the product QH^\cdot would drastically affect the equilibrium. No Q_o inhibitor sensitive semiquinone signal was detected by

EPR, even in the “oxidant-induced reduction” experiment, a condition previously believed lead to accumulation of semiquinone (21). Therefore this semiquinone never accumulates to significant amount to be detected. The “intermediate-controlled bifurcation mechanism” proposed by Junemann and Rich et al (21) could explain how antimycin inhibits oxidation of ubiquinol, even though the ISP is oxidized by electron transfer through the cytochrome c and oxidase. When heme b_L is trapped in the reduced state in the oxidant induced reduction experiment by addition of antimycin A, the unstable semiquinone generated at P1 site can not be removed, and the high potential of QH/QH^{\cdot} could prevent the reduction of ISP. The elaborate kinetic control of quinol oxidation is a step forward toward better understanding of the reaction mechanism at center P. In the second hypothesis, semiquinone is stabilized by binding to ISP after the first electron transfer. This hypothesis is based on the interaction between stigmatellin and His161 of ISP. Link proposed that stigmatellin is a mimic of semiquinone. The inhibitor induced redox potential increase is also applied to semiquinone binding. As a result, the high redox potential of ISP prevents the reduction of heme c_1 until heme b_L oxidizes the semiquinone (4). The fact this species can not be observed by EPR spectroscopy could be explained by tight magnetic coupling between the semiquinone radical and the reduced [2Fe-2S] cluster. However, this hypothesis still requires an alternative spectroscopic technique to resolve the issue. It has been reported that changes in catalytic rate caused by point mutations of ISP in *Saccharomyces cerevisiae* correlated very well with a corresponding shift of the redox midpoint potential (22). A 2.5 fold activity decrease per 60 mV potential decrease (22) is consistent with the Marcus theory, when electron transfer occurs between a donor and acceptor of similar midpoint potential. This phenomenon is not expected when semiquinone is stabilized by ISP because the redox potential between donor and acceptor is too great to be affected by a small

potential change of ISP (23). Thus, it is not necessary to postulate stabilization of the semiquinone at center P.

The immediate transfer of the second electron from semiquinone generated at P1 site to heme b_L may be achieved through: (1) directly through-space and five covalent bonds. Cramer and coworkers suggested that the attenuation factor, $(TDA)^2$ is in the range of the factors calculated for the transfers between hemes b (20). However, the actual value of semiquinone potential is unknown, and this will affect the rate through the Franck-Condon term ($\Delta G^\ddagger = (\Delta G^0 + \lambda)^2/4\lambda KT$). (2) movement of semiquinone to P2 site, where it is closer to heme b_L to allow the fast electron transfer. Such movement could be induced by reduction of ISP. However semiquinone is not going to be stabilized at P2 site substantially, otherwise one should be able to detect semiquinone signal. Furthermore, the movement of semiquinone may be accompanied by deprotonation of second proton. Oxidized heme b_L facilitates movement by lowering the effective pKa of semiquinone. When heme b_L is trapped in reduced state, movement of QH \cdot is prevented since P2 site has little affinity for this species, then oxidation of QH $_2$ is prohibited due to the increase potential of QH $_2$ /QH \cdot . (3) another weakly bound quinone at P2 site, which shortens the distance for electron transfer from P1 to heme b_L , making it more efficient. The involvement of a second Q is more likely to be the case for bacteria bc_1 complex than for bovine enzyme since the quinone content in bacteria bc_1 preparation is always 3-2Q/ bc_1 . In general, the issue concerning the second electron transfer and deprotonation remains controversial and no experimental evidence has been presented so far to resolve it.

V. Conclusion:

This dissertation briefly described straightforward chemical modifications to explore the topology of membrane protein. The functional evidences for the ISP domain movement obtained by generation and characterization of *Rhodobacter sphaeroides* strains expressing cytochrome bc_1 complexes with altered ISP neck regions were also

described in details in Chapter 3 and 4. There still is a long way to go toward the complete understanding of the molecular mechanism of bc_1 complex working as a redox-driven pump and ultimately use this understanding to design “green” pesticides. Large-scale commercial application has been frustrated by the rather general range of lethality of the inhibitors. A detailed understanding of the molecular basis of inhibitor selectivity would allow rational design of more specific reagents. Hopefully cytochrome bc_1 crystals from other organisms will be available soon to speed up this process. There are still many controversial issues regarding the delicate kinetic control of quinol oxidation at center P. Further experimental evidence and better crystals are needed to settle the debates about how many quinones in center P and how the movement of ISP is triggered. The interactions between subunits remain to be discovered, especially in the light of their dynamic behavior during catalysis. The complex interplay between the neck regions of ISP, the disulfide-bridged peptide loops around the [2Fe-2S] cluster and the cd and ef loops of cytochrome b are only now emerging, and need to be defined at the atomic scale. Although such a road currently seems to be tortuous and distant, yet it is clear that bacterial models, in particular that from *Rhodobacter* species, will continue to be of choice for multidisciplinary studies on the structure, function, regulation and biogenesis of the bc complexes.

VI. References:

1. King, T. E., Yu, C. A. Yu, L. and Chiang, Y. L. (1975) An examination of components, sequence, mechanisms and their uncertainties involved in mitochondrial electron transfer from succinate to cytochrome *c*. In *Electron Transfer Chains and Oxidative phosphorylation* (Quagliariello, T., Papa, S., Palmieri, F., Slater, E. C., Siliprandi, N. eds), North-Holland publishing company-Amsterdam, pp. 105-118.
2. Ding, H., Robertson, D. E., Daldal, F. and Dutton, P. L. (1992) Cytochrome *bc*₁ complex [2Fe-2S] cluster and its interaction with ubiquinone and ubihydroquinone at the Q_o site: a double-occupancy Q_o site model. *Biochemistry* **31**, 3144-3158.
3. Brandt, U. (1996) Energy conservation by bifurcated electron-transfer in the cytochrome *bc*₁ complex. *Biochim. Biophys. Acta* **1275**, 41-46.
4. Link, T. A. (1997) The role of the 'Rieske' iron sulfur protein in the hydroquinone oxidation (Q(P)) site of the cytochrome *bc*₁ complex. The 'proton-gated affinity change' mechanism. *FEBS Lett.* **412**, 257-264.
5. Kachurin, A. M. unpublished data.
6. Brandt, U. Schägger, H and von Jagow, G. (1988) Characterization of binding of methoxyacrylate inhibitors to mitochondrial cytochrome *c* reductase. *Eur. J. Biochem.* **173** 499-506.
6. Sharp. R. E., Moser, C. C., Gibney, B. R. and Dutton, P. L. (1999) Primary steps in the energy conversion reaction of the cytochrome *bc*₁ complex Q_o site. *J. Bioenerg. Biomembr.* In press.
7. Brugna, M., Albouy, D, and Nitschke, W. (1998) Diversity of cytochrome *bc* complexes: example of the Rieske protein in green sulfur bacteria. *J. Bacteriol* **80**, 3719-3723.

8. Schoepp, B., Brugna, M., Riedel, A., Nitschke, W, and Kramer, D.M. (1999) The Qo-site inhibitor DBMIB favours the proximal position of the chloroplast Rieske protein and induces a pK-shift of the redox-linked proton. *FEBS Lett.* **450**, 245-250.
9. Zhang, L., Snyder, C., Trumpower, B. L., Yu, L. and Yu, C. A. (1999) *Biophysical J.* **76**, 255a.
10. Zhang, L., Tai, CH., Yu, L. and Yu, C. A. (1999) *Biophysical J.* **76**, 255a
11. Zhang Z. L., Huang, L., Shulmeister, V. M., Chi, Y-I., Kim, K. K., Hung L-W., Crofts, A. R., Berry, E. A. and Kim, S. H. (1998) Electron transfer by domain movement in cytochrome *bc*₁. *Nature* **392** 677-684.
12. von Jagow, G. and Ohnishi, T. (1985) The chromone inhibitor stigmatellin--binding to the ubiquinol oxidation center at the C-side of the mitochondrial membrane. *FEBS Lett.* **185**, 311-315.
13. Link, T.A. (1997) The role of the 'Rieske' iron sulfur protein in the hydroquinone oxidation (Q(P)) site of the cytochrome *bc*₁ complex. The 'proton-gated affinity change' mechanism. *FEBS Lett.* **412**, 257-264.
14. Brandt, U. and von Jagow, G. (1991) Analysis of inhibitor binding to the mitochondrial cytochrome c reductase by fluorescence quench titration. *Eur. J. Biochem.* **195**, 163-170.
15. Darrouzet, E., Valkova-Valchanova, M., Ohnishi, T. and Daldal, F. (1999) Structure and function of the bacterial *bc*₁ complex: domain movement, subunits interaction, and emerging rationale engineering attempts. *J. Bioenerg. Biomembr.* In press.
16. Darrouzet, E., Valkova-Valchanova, M., and Daldal, F. Proceeding of the XIth congress on photosynthesis, 1998, in press.
17. Brasseur, G., Sled, V., Liebl, U., Ohnishi, T. and Daldal, F. (1997) The amino-terminal portion of the Rieske iron-sulfur protein contributes to the ubihydroquinone oxidation site catalysis of the *Rhodobacter capsulatus* *bc*₁ complex. *Biochemistry* **36**, 11685-11696.

18. Sharp, R. E., Palmitessa, A., Gibney, B. R., Moser, C. C., Daldal, F. and Dutton, P. L. (1998) Non-inhibiting perturbation of the primary energy conversion site (Q_o site) in *Rhodobacter capsulatus* ubihydroquinone: cytochrome *c* oxidoreductase (cytochrome bc_1 complex). *FEBS Lett.* **431**, 423-426.
19. Valkova-Valchanova, M., Saribas, A. S., Gibney, B. R., Dutton, P. L. and Daldal, F. (1998) Isolation and characterization of a two-subunit cytochrome $b-c_1$ subcomplex from *Rhodobacter capsulatus* and reconstitution of its ubihydroquinone oxidation (Q_o) site with purified Fe-S protein subunit. *Biochemistry* **37**, 10242-10251.
20. Soriano, G. M., Ponamarev, M. V., Carrell, C. J. Xia, D., Smith, J. L. and Cramer, W. A. (1999) Comparison of the cytochrome bc_1 complex with the anticipated structure of cytochrome b_f . *J. Bioenerg. Biomembr.* In press.
21. Jünemann, S., Heath cote, P. and Rich, P. R. (1998) On the mechanism of quinol oxidation in the bc_1 complex. *J. Biol. Chem* **273**, 21603-21607
22. Denke, E., Merbitz-Zahradnik, T., Hatzfeld, O.M., Snyder, C.H., Link, T.A. and Trumppower, B.L. (1998) Alteration of the midpoint potential and catalytic activity of the rieske iron-sulfur protein by changes of amino acids forming hydrogen bonds to the iron-sulfur cluster. *J. Biol. Chem.* **273**, 9085-9093.
23. Brandt, U. (1999) Control of ubiquinol oxidation at center P (Q_o) of the cytochrome bc_1 complex. *J. Bioenerg. Biomembr.* In press.

VITA

Hua Tian

Candidate for the Degree of

Doctor of Philosophy

Thesis: STRUCTURAL AND FUNCTIONAL STUDIES OF CYTOCHROME *bc*₁
COMPLEX FROM *RHODOBACTER SPHAEROIDES*

Major Field: Biochemistry

Biographical:

Personal Data: Born in Beijing, China, on October 23, 1971, the daughter of
Guangxin Tian and Daijia Li.

Education: Graduated from the first High of Dagang, Tianjing, China in July
1989; received Bachelor of Science degree in Biochemistry from Nankai
University, Tianjin, China in July 1993. Completed requirements for the
Doctor of Philosophy degree with a major in Biochemistry and
Molecular Biology at Oklahoma State University in December, 1999.

Professional Memberships: American Association for the Advancement of Science;
American Biophysical Society.